Journal of Oncology

Molecular Imaging in Breast Cancer

Guest Editors: Alvaro Ruibal, José María Benlloch, Renato Valdés Olmos, and Bengt Langstrom

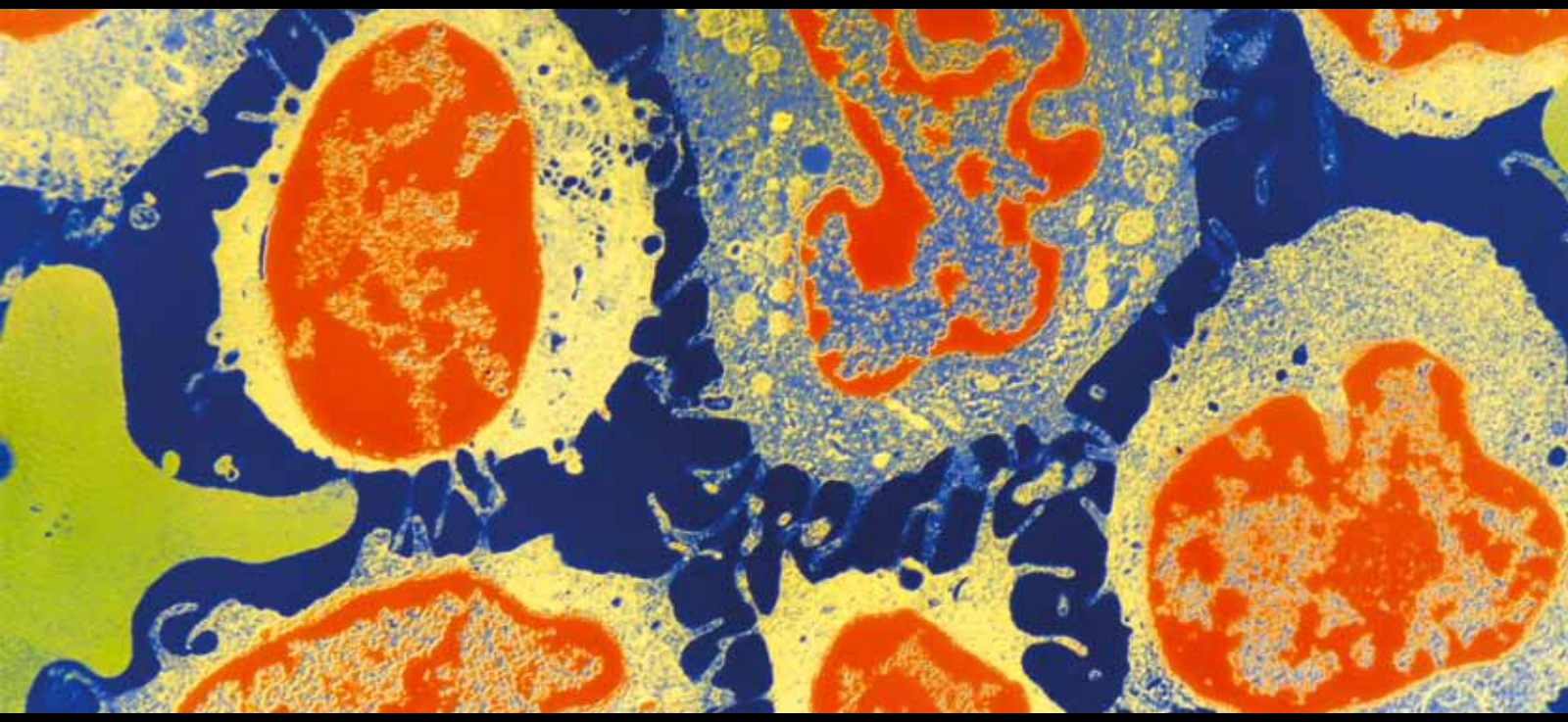

Molecular Imaging in Breast Cancer

Journal of Oncology

Molecular Imaging in Breast Cancer

Guest Editors: Alvaro Ruibal, José María Benlloch, Renato Valdés Olmos, and Bengt Langstrom

Copyright © 2012 Hindawi Publishing Corporation. All rights reserved.

This is a special issue published in "Journal of Oncology." All articles are open access articles distributed under the Creative Commons Attribution License, which permits unrestricted use, distribution, and reproduction in any medium, provided the original work is properly cited.

Editorial Board

Thomas E. Adrian, UAE
Massimo Aglietta, Italy
Bruce Baguley, New Zealand
A. J. M. Balm, The Netherlands
F. Barr, USA
Søren M. Bentzen, USA
Rolf Bjerkvig, Norway
P. Black, USA
Susana M. Campos, USA
Michael Carducci, USA
Stefano Cascinu, Italy
Soonmee Cha, USA
Susan Chang, USA
Thomas R. Chauncey, USA
Srikumar P. Chellappan, USA
Dennis S. Chi, USA
Edward A. Copelan, USA
Richard Crevenna, Austria
Massimo Cristofanilli, USA
Christos G. Dervenis, Greece
Andreas Dietz, Germany
Frederick E. Domann, USA
Avraham Eisbruch, USA
Joann G. Elmore, USA
Thomas J. Fahey, UK
Dominic Fan, USA
Phillip G. Febbo, USA
Douglas L. Fraker, USA
H. S. Friedman, USA
Hani Gabra, UK
Cicek Gercel-Taylor, USA
William J. Gradishar, USA
Akira Hara, Japan
Robert M. Hermann, Germany
Mario A. Hermsen, Spain
Fred H. Hochberg, USA
William J. Hoskins, USA
Toshiyuki Ishiwata, Japan
Andreas H. Jacobs, Germany
Ismail Jatoi, USA
Ozkan Kanat, Turkey
Gertjan Kaspers, The Netherlands
Michael J. Kerin, Ireland
Türker Kiliç, Turkey
Timothy J. Kinsella, USA
Jorg Kleeff, Germany
George O. Klein, Sweden
Mark J. Krasna, USA
M. Kudo, Japan
Robert Langley, USA
A. Lipton, USA
J. S. Loeffler, USA
Dario Marchetti, USA
S. Masood, USA
Keisuke Masuyama, Japan
Ian E. McCutcheon, USA
Raju Mehta, USA
Minesh P. Mehta, USA
Sofia D. Merajver, USA
Bradley J. Monk, USA
Yoshihiro Moriya, Japan
Satoru Motoyama, Japan
James L. Mulshine, USA
Arya Nabavi, Germany
P. Neven, Belgium
Christophe Nicot, USA
Felix Niggli, Switzerland
Patrizia Olmi, Italy
Jan I. Olofsson, Norway
Frédérique Penault-Llorca, France
Richard T. Penson, USA
Michael C. Perry, USA
Joseph M. Piepmeier, USA
M. Steven Piver, USA
Alfredo Quinones-Hinojosa, USA
Janet S. Rader, USA
Dirk Rades, Germany
Zvi Ram, Israel
Dirk Reinhardt, Germany
Paul G. Richardson, USA
Michel Rigaud, France
Jörg Ritter, Germany
M. Roach, USA
Bernd F. M. Romeike, Germany
Volker Rudat, Saudi Arabia
Thomas Rutherford, USA
Siham Sabri, Canada
Aysegula A. Sahin, USA
Giovanni Scambia, Italy
Paul M. Schneider, Switzerland
Peter E. Schwartz, USA
Jalid Sehouli, Germany
Edgar Selzer, Austria
Francis Seow-Choen, Singapore
Dong Moon Shin, USA
Keshav K. Singh, USA
Judith A. Smith, USA
Lawrence J. Solin, USA
Luis Souhami, Canada
Alphonse G. Taghian, USA
Hiromitsu Takeyama, Japan
Nelson N. H. Teng, USA
Chris Terhaard, The Netherlands
D. S. Tyler, USA
Raul A. Urrutia, USA
V. Valentini, Italy
Daniel Vallböhmer, Germany
Michiel van den Brekel, The Netherlands
J. R. Van Nagell, USA
Bruno Vincenzi, Italy
J. A. Werner, Germany

Contents

Hindawi Publishing Corporation
Journal of Oncology
Volume 2012, Article ID 426260, 3 pages
doi:10.1155/2012/426260

Editorial

Molecular Imaging in Breast Cancer

Alvaro Ruibal,[1] José María Benlloch,[2] Renato Valdés Olmos,[3] and Bengt Langstrom[4]

[1] *IDIS, Complejo Hospitalario Universitario, Universidade de Santiago de Compostela, 15706 Santiago de Compostela, Spain*
[2] *Instituto de Instrumentación para Imagen Molecular, Universidad Politécnica de Valencia (UPV) and Consejo Superior de Investigaciones Científicas (CSIC), 46022 València, Spain*
[3] *Nuclear Medicine Department, The Netherlands Cancer Institute-Antoni van Leeuwenhoek Hospital, 1066 CX Amsterdam, The Netherlands*
[4] *Physical Organic Chemistry, Department of Chemistry (BMC), Uppsala University, 75123 Uppsala, Sweden*

Correspondence should be addressed to Alvaro Ruibal, alvaro.ruibal.morell@sergas.es

Received 24 September 2012; Accepted 24 September 2012

Copyright © 2012 Alvaro Ruibal et al. This is an open access article distributed under the Creative Commons Attribution License, which permits unrestricted use, distribution, and reproduction in any medium, provided the original work is properly cited.

1. Breast Cancer: Challenges in Diagnosis and Characterization Using Molecular Imaging Techniques

At the present time, *breast cancer (BC)* is one of the most frequently diagnosed cancers and the leading cause of cancer death in females worldwide. Breast cancer is a heterogeneous disease including different groups of illnesses in relation to presentation, biology, clinical behavior, and response to therapy. Thus, nowadays, knowledge of their biology is imposed in daily practice. Likewise, we know that tumor biology can also affect significantly the efficacy of the different modern techniques of molecular imaging.

While many breast cancers are not associated with known risk factors, others do, highlighting with a relative risk [(RR) > 4] the following: *females; age:* >65 *versus* <65 years; *gene mutations* (BRCA1 and BRCA2); *two or more first degree relatives with BC in early ages; personal history of BC*; *high breast tissue density and biopsy-confirmed atypical hyperplasia (Breast Cancer Facts & Figures 2009-2010)*. In relation with secondary prevention, we know that aspirin and other nonsteroidal anti-inflammatory drugs (NSAIDs) inhibit production of prostaglandins and cyclooxygenase 2, and they are potential agents for chemoprevention of breast cancer. A meta-analysis indicates that regular use of aspirin may be associated with reduced risk of breast cancer (OR: 0.86) [1].

With advances in the sensitivity of mammographic screening and the broader population of women screened via national programs in different countries, the diagnosis of breast tumors has changed considerably. As an example, more than 50% of all invasive breast cancers in the UK are screen-detected and 52.3% of all invasive breast cancers measured 15 mm or less in diameter and were deemed clinically nonpalpable [2]. Likewise, about 20–30% of the new breast cancers are in situ carcinomas, and 60–80% of all invasive breast cancers have no axillary lymph node involvement (N), so we need to have new prognostic factors other than classics ones (size, N, and distant metastases (M)). *Screening-detected breast cancer* is associated with older age, smaller tumor size, more hormone receptor positiveness, less lymph node involvement, earlier stage, and reduced mortality compared with symptomatic breast cancer. According to the molecular subtype, luminal A is the most common (63.6%) and acts as an independent prognostic factor itself. Another aspect of practical interest is interval cancers, those detected between two screening scans. *Interval cancer* represents between 12% and 28% of all cancers diagnosed in a screening program, especially in women below 50 years, and have a higher percentage of nonductal histology. Likewise, they often overexpressed epidermal growth factor receptor (EGFR) and were more frequently estrogen receptor negative and triple negative, with a poorer prognosis. This observation provides new data indicating that EGFR may be important in the etiology of interval cancer.

The standard imaging techniques for the diagnosis of this malignant tumor includes compression and magnification

mammography (digital or not), breast ultrasounds (USs), and MRI. Although PET/CT is not included in initial explorations of breast cancer, it is known to be useful in detecting distant metastasis (7-8% of patients who are not suspected) and to improve the prediction of neoadjuvant therapy response. Recently, tomosynthesis and PEM (positron emission mammography) have been included as diagnostic tools in a reduced number of medical centers.

The problem of imaging techniques focused on the important number of false positive results obtained with mammography, so reduction of false positive risk and associated factors is, nowadays, the major goal of breast cancer screening. Tomosynthesis has improved the diagnostic efficacy, and MRI can play an important role in preoperative planning if used in selected patients with high risk of multifocal/multicentric lesions. Also it is very useful in young women or with dense breast and in BRCA1/2 mutation carriers. However, the histological confirmation of all suspicious findings detected by MRI is compulsory prior to definitive surgery [3].

2. Which Problems We Find?

In daily practice, we find the following situations that require an effort from the image scans to be solved.

2.1. Mammograms Doses of Radiation. This technique requires very small doses of radiation (2–4 mGy; 200–400 mRad). The risk is slight, but repeated X-rays have the potential to cause cancer, but this is very rare. However, we know the mechanisms of DNA repair after ionizing radiation and many of the genes involved are altered in certain subpopulations that we need to keep in mind. These patients show a greater sensitivity to ionizing radiation and the continued use of this imaging technique can be harmful.

Special interest have patients with mutations in BRCA1and/or BRCA2 genes and ataxia telangiectasia (ATM) gene, as well as certain genes of Fanconi anemia and those related to the normal functioning of the cell cycle. Another aspect of great value is the absorbed dose by the mammary glands of girls and young women during radiological examinations of other sites of their bodies. As an example, the chest CT and abdominal CT scan radiate between 3 and 30 times the dose of a mammogram. We need to take into account the future consequences of these "unnecessary" radiations.

2.2. Occult Breast Cancer Presenting with an Axillary Metastasis. Occult breast cancer incidence is decreasing, because more primary breast cancers can be detected with the introduction of more advanced techniques. Breast MRI can identify the primary tumor in approximately two thirds of this population, but, due to the low specificity, lesions need to be histologically confirmed. Other recent imaging techniques can be useful also. The immunohistochemical study of the lymph node using certain breast cyst fluid proteins (alpha-2-glycoprotein 1, zinc-binding, apolipoprotein D, GCDFP15, etc.) may be of great diagnostic value.

2.3. Nonpalpable Breast Cancer. This is a situation of great practical interest, and its location is a routine necessity. There are many techniques for identification, and we know that US-guided BCS (breast conserving surgery) could be more accurate than wire-guide localization (WL) and ROLL-guided surgery because it optimized the surgeon's ability to obtain adequate margins. However, other authors consider that the radioguided localization surgery determines lower positive margins rates and fewer reoperations.

2.4. Ductal Carcinoma In Situ in Younger Women. Ductal carcinomas in situ (DCIS) are a heterogeneous entity and early and accurate diagnosis is a necessity, since they are often tumors in women under 40 years. Likewise, high recurrence rates (mainly invasive: 62%; in situ: 38%) after breast conservative treatment have been observed in young women with this tumor.

2.5. Sentinel Node (SLNB). At present, their detection and analysis is a mandatory practice in the breast cancer surgery. The use of radioguided methods for lymphatic mapping and SLNB localization has represented a breakthrough. There are several nomograms for predicting the nonsentinel lymph node metastases after a positive sentinel lymph node biopsy and also we know that lymphoedema occurs in 21% of patients who undergo axillary lymph node dissection (ALND) versus 7% of patients who undergo SLNB. Optical scans seem to be reliable and effective to detect this lymph node when located in level one of the axilla. The clinical significance of micrometastases continues to be a subject of controversy, even though now some groups consider that they do not influence tumor outcome.

2.6. Evaluation of Axillary Lymph Node Metastases. The accurate diagnosis of axillary nodal involvement using imaging methods is of great practical usefulness. SLNB remains the standard of care to stage the axilla. MRI could be the most cost-effective strategy to replace SLNB. However, further large studies are required to obtain more accurate data on the sensitivity and specificity of this technique [4]. Gadolinium-enhanced MRI has a sensitivity of 88% and a specificity of 100%, and ultrasmall superparamagnetic iron oxide-(USPIO-) enhanced MRI has 98% and 96% respectively. However, it does not appear that currently can replace SLNB. Axillary ultrasound fine needle aspiration has a sensitivity of 63.4% and a specificity of 100%, while intraoperative frozen section analysis of the sentinel node has a sensitivity of 76.5% and a specificity of 100%. Sensitivity of both procedures together is 91.4%. In patients with stage II and III breast cancer, high-resolution FDG PET/CT has reached a sensitivity of 82% and a specificity of 92% in detecting axillary metastases, and due to its high predictive value (98%), if positive, SLNB may be omitted [5].

2.7. Locoregional Breast Cancer Recurrence (LRR). Luminal tumors exhibit the lowest rates of locoregional recurrence while patients with triple negative and HER2 overexpression have an increased risk of developing LRR following surgery

and other associated treatments. In this clinical situation, FDG-PET/CT can be a good choice, with a sensitivity, specificity, accuracy, and positive and negative predictive values of 97%, 92%, 95%, and 94% and 96%, respectively. Also, this technique can change the clinical management in almost half of the patients. The use of new PET tracers opens a new point of view giving us more physiopathological information. Also the "classic" imaging techniques (mammography US), MRI, and PEM can play an important role is this clinical situation.

2.8. Identification of Residual Breast Tumor Localization after Neoadjuvant Chemotherapy. It is an increasing clinical situation due to the enhancing of conservative surgery. Besides the current imaging techniques, recently has been introduced in clinical practice the use of 125I seed and its injection into the tumor area before chemotherapy with very good results, due to the half time of 125I (60 days).

3. Challenges

The first challenge posed is to diagnose and establish the stage of breast cancer in its earliest stages and as safely as possible. Also the study of premalignant lesions will be crucial in the near future. We must focus our efforts in these different areas to make no delay diagnosis. In relation with this, in Sweden, the delay in diagnosis occurs in about 1/1000 new patients and the delay was considered to have an impact on the magnitude of therapeutic measures in almost 25% of the women. Economic compensation for the patient's injuries was given in 90% of the cases [6]. *The second challenge* is the detection of a recurrence prior to the development of symptoms, which can improve overall survival. *The third challenge* will be to study how the biology of the tumor is capable of influence imaging techniques, especially the molecular imagines, and how we define those targets that allow us the biological characterization of an injury through an image. The use of modern laboratory techniques (stem cells, proteomics, epigenetic, etc.) will be mandatory. The use of advance imaging technology is a necessity and a reality, but, as Panageas et al. write [7], a question arises in some situations: "*It is not clear whether if early detection of distant recurrence leads to a survival benefit improvement or whether it simply increases the amount of time women spend living with the knowledge that their disease has recurred.*"

Finally, we thank the different authors for their hard work and excellent papers that allowed the elaboration of this special issue. Our main goal was to show different aspects of breast cancer related to biology and molecular imaging as well as their clinical usefulness.

Alvaro Ruibal
José María Benlloch
Renato Valdés Olmos
Bengt Langstrom

References

[1] T. Luo, H.-M. Yan, P. He, Y. Luo, Y.-F. Yang, and H. Zheng, "Aspirin use and breast cancer risk: a meta-analysis," *Breast Cancer Research and Treatment*, vol. 131, no. 2, pp. 581–587, 2012.

[2] S. M. Dua, R. J. Gray, and M. Keshtgar, "Strategies for localisation of impalpable breast lesions," *Breast*, vol. 20, no. 3, pp. 246–253, 2011.

[3] N. Biglia, V. E. Bounous, L. Martincich et al., "Role of MRI (magnetic resonance imaging) versus conventional imaging for breast cancer presurgical staging in young women or with dense breast," *European Journal of Surgical Oncology*, vol. 37, no. 3, pp. 199–204, 2011.

[4] Y. Meng, S. Ward, K. Cooper, S. Harnan, and L. Wyld, "Cost-effectiveness of MRI and PET imaging for the evaluation of axillary lymph node metastases in early stage breast cancer," *European Journal of Surgical Oncology*, vol. 37, no. 1, pp. 40–46, 2011.

[5] B. B. Koolen, R. A. ValdésOlmos, P. H. M. Elkhuizen et al., "Locoregional lymph node involvement on 18F-FDG-PET/CT in breast cancer scheduled for noeadjuvant chemotherapy," *Breast Cancer Research and Treatment*. In press.

[6] L. Hafström, H. Johansson, and J. Ahlberg, "Diagnostic delay of breast cancer—an analysis of claims to Swedish Board of Malpractice (LÖF)," *Breast*, vol. 20, pp. 539–542, 2011.

[7] K. S. Panageas, C. S. Sima, L. Liberman, and D. Schrag, "Use of high technology imaging for surveillance of early stage breast cancer," *Breast Cancer Research and Treatment*, vol. 131, no. 2, pp. 663–670, 2012.

Hindawi Publishing Corporation
Journal of Oncology
Volume 2012, Article ID 680262, 6 pages
doi:10.1155/2012/680262

Review Article

Recent Design Development in Molecular Imaging for Breast Cancer Detection Using Nanometer CMOS Based Sensors

Dung C. Nguyen,[1] Dongsheng (Brian) Ma,[2] and Janet M. W. Roveda[1]

[1] *BIO 5 Institute, Department of Electrical and Computer Engineering, University of Arizona, Tucson, AZ 85721, USA*
[2] *Department of Electrical and Computer Engineering, The University of Texas at Dallas, 800 W Campbell Road, EC33, Richardson, TX 75080-3021, USA*

Correspondence should be addressed to Janet M. W. Roveda, wml@ece.arizona.edu

Received 21 April 2012; Accepted 22 September 2012

Academic Editor: José María Benlloch

Copyright © 2012 Dung C. Nguyen et al. This is an open access article distributed under the Creative Commons Attribution License, which permits unrestricted use, distribution, and reproduction in any medium, provided the original work is properly cited.

As one of the key clinical imaging methods, the computed X-ray tomography can be further improved using new nanometer CMOS sensors. This will enhance the current technique's ability in terms of cancer detection size, position, and detection accuracy on the anatomical structures. The current paper reviewed designs of SOI-based CMOS sensors and their architectural design in mammography systems. Based on the existing experimental results, using the SOI technology can provide a low-noise (SNR around 87.8 db) and high-gain (30 v/v) CMOS imager. It is also expected that, together with the fast data acquisition designs, the new type of imagers may play important roles in the near-future high-dimensional images in additional to today's 2D imagers.

1. Introduction

Today, the mainstay of clinical imaging still vastly depends on traditional anatomical imaging methods such as ultrasound (US), computed X-ray tomography (CT), and magnetic resonance imaging (MRI). With the uprising genomic and proteomic technologies, cancer detection is no longer just detecting tumor position and size, it also involves more precise understanding of anatomical structures of cells that would lead to different treatment in managing cancer clinically. The center of this new transformation is molecular imaging, a new technique that allows one to combine molecular information with physiological study. It is believed by many researchers that this new development will detect molecular alterations related to cancer, will help evaluate existing cancer treatment in real time, and will eventually reshape the cancer medicine delivering process in the near future [1–3]. Here, "real-time" refers to treatment followups, information sharing, and collaborations among physicians and patients at the same time. Two key trends of molecular imaging techniques include magnetic resonance imaging (MRI) and optical imaging. However, high cost and possible invasive penetrations are the major road blocks. For example, it has been estimated that the MRI may cost each patient from $2000 up to $3800 for each visit [4], while optical probes require prescreening using traditional anatomical imaging approaches to first locate problematic areas and then penetrate through skin/muscles to the questionable locations. Such techniques would not be suitable for real-time tracking of cancer development and detection.

Over the last several years, a lot of effort has been focused on how to improve the mainstream techniques to improve cancer detection rate without increasing the cost and additional biopsy-type penetrations. One trend is to improve the existing X-ray techniques. In this paper, we intend to review our recent progress in X-ray-based breast cancer detection system design. We focus on the device, the circuit, and the embedded software and hardware perspectives to reveal the potential of the future mammographic system design considering the new development in the nanometer CMOS technologies.

It is worth mentioning that the current film screen-based mammography is very mature and successful. Yet this popular technique still misses as many as 20% of cancer cases [5] due to the anatomical noise. This type of noise is caused by the overlap of normal structures within breast tissues. Very

common in a standard two-dimensional mammogram is that tissue structures tend to superimpose on each other. One approach to reduce the anatomical noise is tomosynthesis. Researchers [6, 7] have reported that tomosynthesis may increase cancer detection rate by 16% and decrease false positive cases by 85% compared with the film-based mammography. However, the design of such a system to support tomosynthesis is tricky. This is because tomosynthesis algorithm requires multiple images of the imaged breast. Thus, it also demands multiple image acquisitions. On the other side, we would like to limit to a comparable amount of radiation dose. That is, if we wish to read out 10 to 15 images, each image should only use 1/10 to 1/15 of the single image radiation dose without tomosynthesis algorithm. However, such a low X-ray dose would lead to high level of noise in the current mammographic designs. How to design a system that overcomes these contradicting requirements is the main focus of this paper.

For the rest of this article, we first discuss the potential of Silicon-On-Insulator device for the new pixel sensor and its design. Then, we introduce the current research in fast data acquisition and high dynamic range design and their contribution to the CMOS based molecular imager. Finally, we review the upcoming new generation of X-ray generators and their potentials in discovering pathological development of cancer cells.

2. Nanometer CMOS-Based Molecular Imaging with Silicon on Insulator

Together with Bioptics Inc., we were among the first ones that designed the architecture using Silicon-On-Insulator (SOI) and the back-side illumination etched substrate. This new architecture makes it possible to increase the fill factor (up to 100%) and to separate the photodiodes from the rest of the device electronics to reduce coupling noises [8].

The standard bulk CMOS technology-based imager faces two roadblocks: the short depth of n-well and the high parasitic capacitance. It is well known that high-resolution requirement demands long exposure time. The shorter the well, the less the exposure time we can have. Together with the impact from parasitic capacitance, the speed and performance of the CMOS imager are both limited. One advantage of the SOI technology is its low parasitic capacitance which leads to high speed and the potential to extract images with less exposure time. Currently, the main-stream SOI techniques include two types of technologies: fully depleted SOI (FD-SOI) and partially depleted SOI (PD-SOI), while in the manufacture process, PD-SOI is less expensive but suffers from kink effect (different slope rate in the saturation region in the I-V curve) which will affect the SNR ratio of the imager [9]. This is the reason why we choose FD-SOI instead of PD-SOI. Figure 1 demonstrates the device cross-section. Figures 2 and 3 display the design architecture and the test structure of the new SOI-based molecular imager, respectively.

To fully utilize the advantage of SOI technique, we also developed a new hybrid architecture to design sensors and its auxiliary circuitry. This is different from the monolithic architecture where we need to integrate detectors and read-out circuitry in a high-resistivity silicon substrate [10].

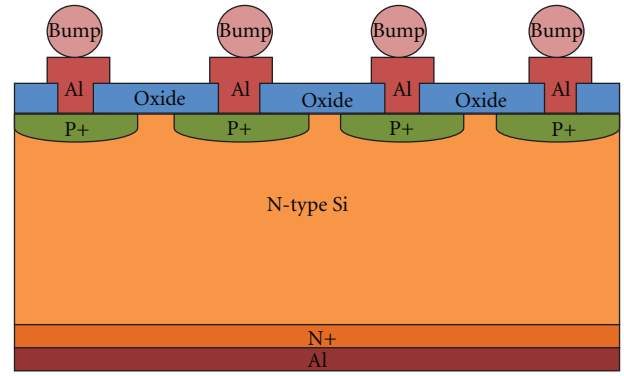

Figure 1: The cross-section of the newly proposed device and its design [7].

In general, this requires two-sided wafer process. In the hybrid pixel architecture, the read-out integrated circuit connects with the detector material by solder bumps [11, 12]. Compared with the monolithic technique, the hybrid technology is able to integrate different detector platforms with the same read-out circuitry. The hybrid technique also reduces the design cost as it simplifies the design process of the read-out circuitry which can be optimized independently from the detector. The test architecture (Figure 3) includes a charge sensitive amplifier (CSA), a discriminator, a sigma-delta analog digital converter [13], and a 14-bit counter/shift register. The last two test modules are a complete 128 × 128 photon counting array and a 128 × 128 in pixel analog-to-digital array [8]. Table 1 recorded the read-out noises for the 128 × 128 array in Figure 3. Two different ways to store the output signals of photons include counting approach and the integrating method. The later one sums up all the input signals including noise which causes low signal-to-noise ratio, short dynamic range, and a redistribution of photons with different energy level. Photons of higher energy level store more charges in the detector and will generate a higher voltage or current. Note that even though the higher-energy-level X-rays can pass through the patient breast easily, they do not necessarily carry more useful information than the lower-energy ones. On the other hand, these higher-energy ones may also defer photon integration time. In the photon counting method, the input signal height from a photon is compared to an energy window threshold set in a comparator. If the signal is within the energy window threshold range, the value of a counter is incremented. Each photon within this window threshold has the same value. Thus, the photon counting approach has the ability to set an appropriate threshold to remove the background noise, which in turn improves the signal-to-noise ratio and the dynamic range [8, 14]. Preliminary Silvaco/Atlas P-i-N photodiode Detective Quantum Efficiency (DQE) simulation results at 50 V is in Figure 4(a). The estimate dose efficiency for the proposed device can be found in Figure 4(b), where q_{CsI} = photon absorption efficiency of CsI(Tl) at 30 keV, g_{CsI} = the CsI(Tl)

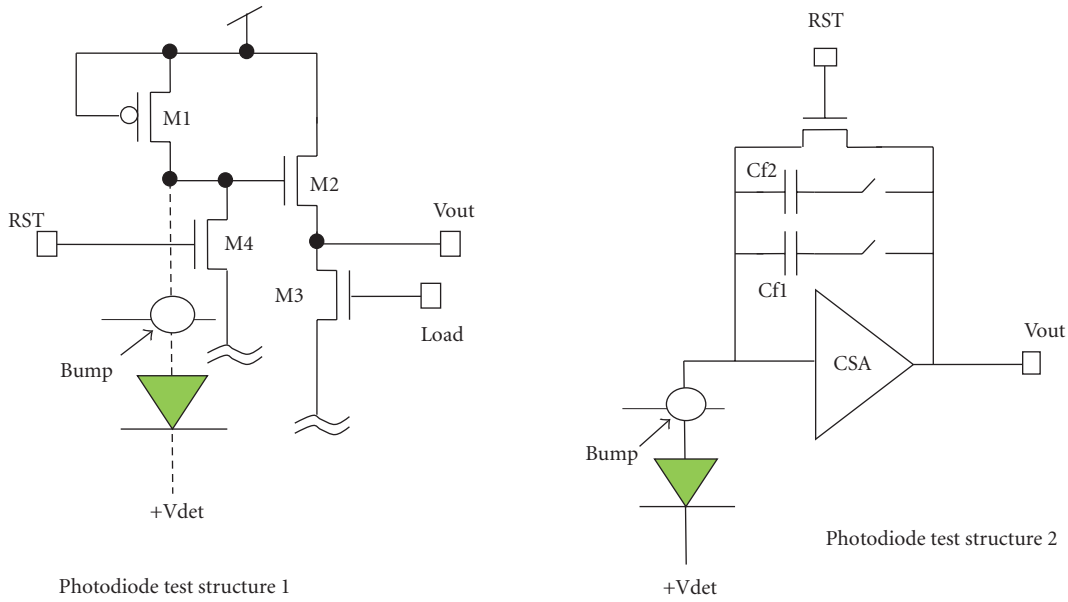

Figure 2: The test circuits of the proposed SOI sensors [7].

light gain, $O_{\text{CsI\_fiber}}$ = the optical coupling between CsI(Tl) and the fiber faceplate, and q_{Si} = the silicon quantum efficiency.

3. 3D Imaging versus 2D Imaging to Improve Diagnostic Rate

One effective way to avoid anatomical noises is by using higher-dimensional approaches, that is, 3D and 4D breast computed tomography (Breast CT) [15] and tomosynthesis. Still, the major challenge is the dramatic increase in the data volume: for 3D tomosynthesis, 15 frames of images are required comparing with 2 frames for the traditional 2D ones. This is equivalent to a 7x increase in the data volume (i.e., for cone-beam CT; this is about 300 projections) [16]. In addition, there will be an increase in the X-ray dose as well. For the "average" breast (compressed thickness of 5.0 cm and a 50% glandular fraction), a digital breast tomosynthesis (DBT) acquisition results in an 8% increase in the X-ray dose comparing with 2D ones. For high-density breasts, the increased amount can be as high as 83% [17, 18].

Over the past several years, great efforts have been invested into analog-to-information converter (AIC) [19] to acquire raw sample at a low rate while accurately reconstructing the compressed signals. The key components under investigations were analog-to-digital converters, random filtering and demodulations. Authors from [20] were the first ones that applied compressive sensing into pixel array data acquisition systems. Instead of directly extracting pixel array data to column buffers and then processing with A/D converters, the authors used random selection measurement matrix to regroup the pixel data. And then, the data are fed into A/D at a much lower sample rate than the original design. By doing this, they implemented the random selection measurements and multipliers using analog components. Such designs choose "heavy" analog front end to reduce the sample rate and data amount at A/D. For example, in the traditional signal/data flow, the A/D converter is placed right after pixel array. That is, the pixel data are directly digitized at the Nyquist sample rate with compressive sensing where the A/D converter is placed after random selection/demodulation. The sample rate is a lot lower. Even though compressive sensing algorithms helped us to reduce the sample rate of A/D converter, it comes with a price. It requires analog front end to achieve randomized measurements which in turn lead to large analog computing units at the front end. These components are cumbersome and slow. For example, an analog multiplier works at 10 MHz with over 200 ns set-up time. Not to mention that most elements in the front end use 0.25 um technology node, some exploit 0.5 um technology node (i.e., floating gate technology to store random selection coefficients). While compressive sensing algorithms provide a promising future to reduce data, how to effectively implement such a scheme on hardware is still an open question.

High-dynamic-range imaging is an emerging field that has the potential to cause a great scientific and technological impact in the near future. In this paper, we aim at covering the field of high-dynamic-range imaging and its applications in extending the imager dynamic range and the impact on X-ray dose reduction for medical imaging application. A typical pixel cycle in an integrating-type image sensor receiving a constant light intensity is shown in Figure 3. An initial reset cycle zeroes the intensity signal, which later increases linearly throughout the integration time. The illumination signal is thus limited by fabrication process parameters, system factors, and circuit implementation regardless of the type of pixel used. Additionally, the noise of the pixel read-out circuitry and other noise sources overwhelm the illumination signal in low light situations. The ratio between the illumination that saturates the pixel and the minimum detectable illumination is the dynamic range (DR) of the image sensor.

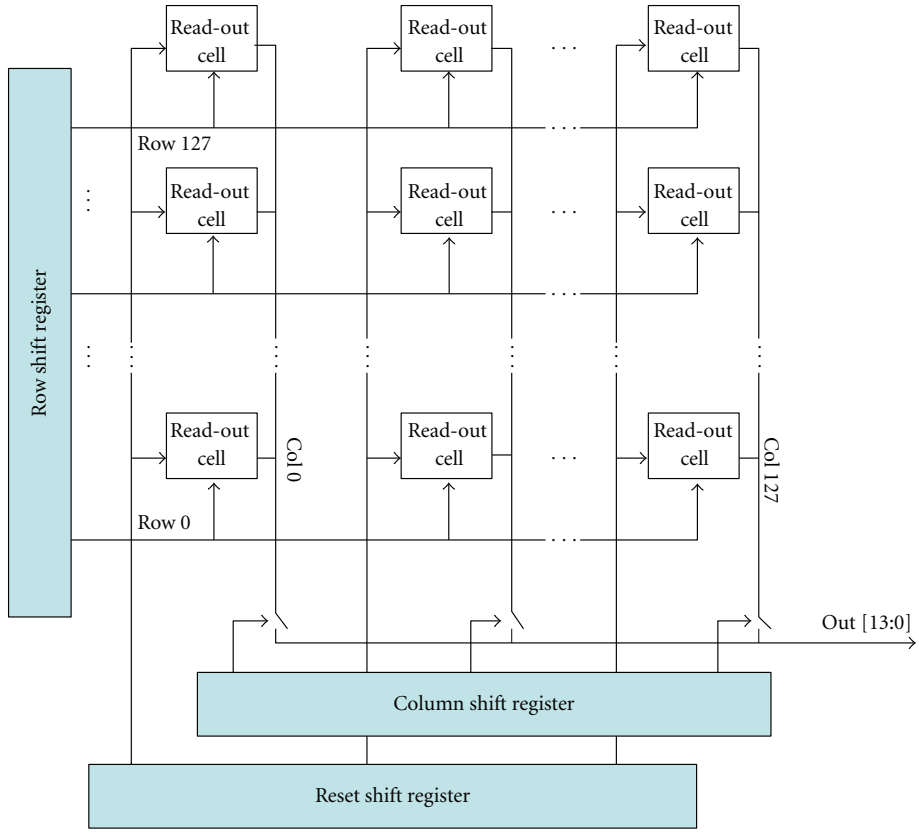

Figure 3: The test architecture for the pixel array [8].

Table 1: Read-out noise estimation (worst case).

Simulate read-out noise	Description	Value	Unit
Electronic gain		29.6	electron/ADU
Dark rate	30.6 ADU/sec ∗29.6 electron/ADU	906	electron/pixel/sec
Dark current noise	sqrt(dark rate $*t$)		
Read-out noise	Gain × std_dev(offset)/sqrt(2)		
	29.6 ∗ 3.27/1.414	69	electron/pixel (for 500 kHz rate)
SNR	Full well potential/read-out noise		
	20∗ log10(1700000/69)	87.8	dB

Low-noise circuitry, careful engineering of the photodiode reverse saturation current, and other improvements can help lower the noise floor, and has been previously attempted by several techniques. Previous efforts to increase the DR of a CMOS imager have introduced various image-acquiring schemes including logarithmic, a combination of linear and logarithmic, well-capacitance adjusting, dual or multiple sampling, and multiple integrations [21–23].

4. Conclusion and Future Work

Based on our experience [8, 24] and existing research works [5, 7, 17, 25], it is apparent that the new technologies in CMOS image sensor designs have great potential in improving the current mammographic breast cancer detection. To be more specific, using SOI technology can provide low-noise (SNR around 87.8 db) and high-gain (30 v/v) CMOS imager. This type of imagers together with fast data acquisition designs may play important roles in the near future high-dimensional images. It is also worth mentioning the new X-ray-free electron laser technique [25–27]. Comparing with the molecular imager reviewed in the paper (we can have images that reveal cells of size of tens of micrometers), this new technique can take a snapshot of molecule size object in femtosecond (fs). This is the first time we can monitor proteins and chromosomes in real time. It is believed that this new technique can reveal the relationship of genomic and proteomic technologies and cancer growth. Its promises to the breast cancer detection yet needs to be

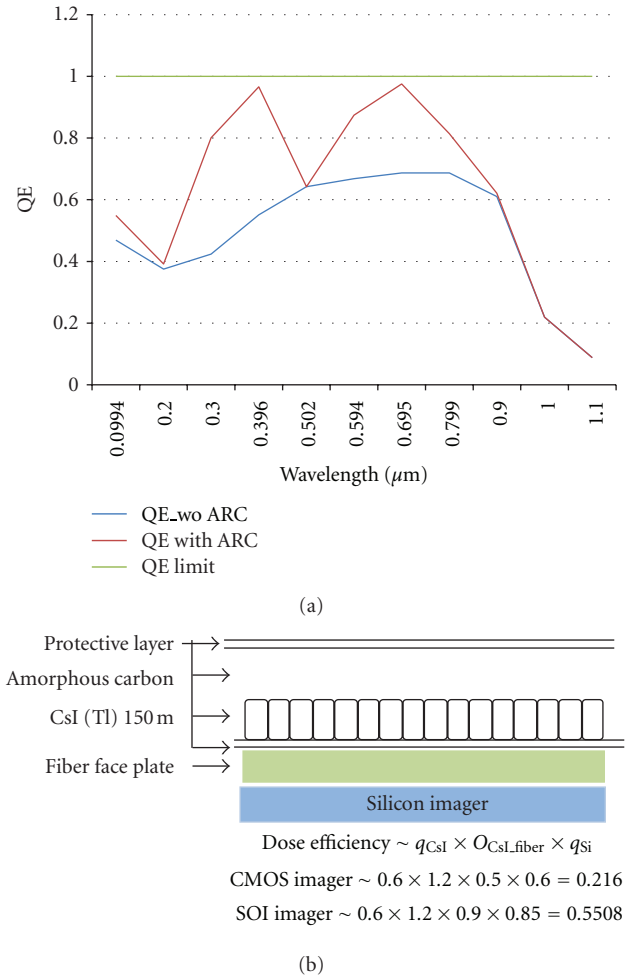

Figure 4: (a) DOE simulation results for structure 1 and structure 2 in Figure 2 at different optical wavelengths. (b) The cross-section structure of optical architecture.

further confirmed and calls for strong collaborations among scientists and researchers from different disciplines including radiology, pathology, device designers, and circuit and system designers.

References

[1] R. Weissleder, "Molecular imaging in cancer," *Science*, vol. 312, no. 5777, pp. 1168–1171, 2006.

[2] W. A. Hendrickson, "X rays in molecular biophysics," *Physics Today*, vol. 48, no. 11, pp. 42–48, 1995.

[3] H. Varmus, "The new era in cancer research," *Science*, vol. 312, no. 5777, pp. 1162–1165, 2006.

[4] http://community.breastcancer.org/forum/83/topic/758058.

[5] S. Hoff, A.-L Abrahamsen, J. H. Samset, E. Vigeland, O. Kelpp, and S. Hofvind, "Breast cancer: missed interval and screening-detected cancer at full-field digital mammography and screen-film mammography-results from a retrospective review," *Radiology*, vol. 264, no. 2, pp. 378–386, 2012.

[6] E. Rafferty, "Tomosynthesis: new weapon in breast cancer fight," Guest editorial in Decisions in Imaging Economics, The Journal of Imaging Technology Management, April 2004.

[7] S. P. Poplack, T. D. Tosteson, C. A. Kogel, and H. M. Nagy, "Digital breast tomosynthesis: initial experience in 98 women with abnormal digital screening mammography," *American Journal of Roentgenology*, vol. 189, no. 3, pp. 616–623, 2007.

[8] D. Nguyen, H. Cormican, A. Baysal, C. Wiswall, J. M. Wang, and D. Ma, "A mammography imaging hybrid pixel sensor test chip with low noise CMOS readout IC on fully depleted silicon-on-insulator design feasibility and trade off study," in *Proceedings of the 9th International Conference on Applications of Nuclear Techniques*, Crete, Greece, 2008.

[9] O. Faynot, "Mechanisms in PDSOI and FDSOI devices," presentation, international Summer School on Advanced Microelectronics, MIGAS, 2009, http://www.eurosoi.org/public/MIGAS09_3_1_Faynot.pdf.

[10] KEK Detector Technology Project, http://rd.kek.jp/index_e.html.

[11] W. Kucewicz, Fully Depleted Monolithic Active Pixel Detector in SOI Technology, Seminar at the University of Bonn, Bonn, Germany, 2005.

[12] G. Hulsen, E. F. Eikenberry, R. Horisberger et al., "Pixel detectors for diffraction experiments at the swiss light source," in *Proceedings of the 8th International Conference on Synchrotron Radiation Instrumentation*, vol. 705 of *AIP Conference Proceedings*, pp. 1009–1012, San Francisco, Calif, USA, August 2003.

[13] Sunetra Kanchana Mendis, *CMOS active pixel image sensor with on chip Analog-to-Digital conversion [Ph.D. thesis]*, Columbia University, 1995.

[14] http://medipix.web.cern.ch/MEDIPIX.

[15] http://www.ucdmc.ucdavis.edu/radiology/research/boone3.html.

[16] A. O'Connell, D. L. Conover, and Y. Zhang, "Cone-beam CT for breast imaging: radiation dose, breast coverage, and image quality," *American Journal of Roentgenology*, vol. 195, no. 2, pp. 496–509, 2010.

[17] J. S. The, K. J. Schilling, J. W. Hoffmeister et al., "Detection of breast cancer with full-field digital mammography and computer-aided detection," *American journal of roentgenology*, vol. 192, no. 2, pp. 337–340, 2008.

[18] S. S. Feng and I. Sechopoulos, "Clinical digital breast tomosynthesis system: dosimetric characterization," *Radiology*, vol. 263, no. 1, pp. 35–42, 2012.

[19] N. G. Prelcic, "State of the art of Analog to Information Converters," Invited Talk, at Stanford, 2010.

[20] A. Bandyopadhyay, J. Lee, R. W. Robucci, and P. Hasler, "MATIA: a programmable 80 μW/frame CMOS block Matrix Transform Imager Architecture," *IEEE Journal of Solid-State Circuits*, vol. 41, no. 3, pp. 663–671, 2006.

[21] O. Yadld-Pecht, "Wide-dynamic-range sensors," *Optical Engineering*, vol. 38, no. 10, pp. 1650–1660, 1999.

[22] R. Gonzalez and R. Woods, *Digital Image Processing*, Addison Wesley Publishing Company, Reading, Mass, USA, 3rd edition.

[23] A. El Gamal, "High dynamic range image sensors," in *IEEE International Solid State Circuit Conference Tutorial*, San Francisco, Calif, USA, February 2002.

[24] J. M. Wang, D. Nguyen et al., "Low power design for biomedical image using compressed sensor theory," in *BME Workshop*, San Jose, Calif, USA, 2010.

[25] S. S. Feng and I. Sechopoulos, "Clinical digital breast tomosynthesis system: dosimetric characterization," *Radiology*, vol. 263, no. 1, pp. 35–42, 2012.

[26] C. Pellegrini and J. Stöhr, "X-ray free-electron lasers—principles, properties and applications," *Nuclear Instruments and*

Methods in Physics Research A, vol. 500, no. 1–3, pp. 33–40, 2003.

[27] K. J. Gaffney and H. N. Chapman, "Imaging atomic structure and dynamics with ultrafast X-ray scattering," *Science*, vol. 316, no. 5830, pp. 1444–1448, 2007.

Hindawi Publishing Corporation
Journal of Oncology
Volume 2012, Article ID 863747, 10 pages
doi:10.1155/2012/863747

Review Article

Optical Imaging in Breast Cancer Diagnosis: The Next Evolution

Michel Herranz[1] and Alvaro Ruibal[2]

[1] *Molecular Imaging Program, PET Radiopharmacy Unit, Molecular Imaging Group, IDIS, GALARIA-SERGAS, University Hospital Complex, Travesía de Choupana s/n., 15706 Santiago de Compostela, Spain*
[2] *Nuclear Medicine Service, Medicine Faculty, Molecular Imaging Group, IDIS, University Hospital Complex, Travesía de Choupana s/n., 15706 Santiago de Compostela, Spain*

Correspondence should be addressed to Michel Herranz, michel.herranz.carnero@sergas.es

Received 21 June 2012; Accepted 28 August 2012

Academic Editor: José María Benlloch

Copyright © 2012 M. Herranz and A. Ruibal. This is an open access article distributed under the Creative Commons Attribution License, which permits unrestricted use, distribution, and reproduction in any medium, provided the original work is properly cited.

Breast cancer is one of the most common cancers among the population of the Western world. Diagnostic methods include mammography, ultrasound, and magnetic resonance; meanwhile, nuclear medicine techniques have a secondary role, being useful in regional assessment and therapy followup. Optical imaging is a very promising imaging technique that uses near-infrared light to assess optical properties of tissues and is expected to play an important role in breast cancer detection. Optical breast imaging can be performed by intrinsic breast tissue contrast alone (hemoglobin, water, and lipid content) or with the use of exogenous fluorescent probes that target specific molecules for breast cancer. Major advantages of optical imaging are that it does not use any radioactive components, very high sensitivity, relatively inexpensive, easily accessible, and the potential to be combined in a multimodal approach with other technologies such as mammography, ultrasound, MRI, and positron emission tomography. Moreover, optical imaging agents could, potentially, be used as "theranostics," combining the process of diagnosis and therapy.

1. Introduction

Breast cancer is a major global health problem. In 2007, an estimated 1.3 million new cases of invasive breast cancer will be diagnosed and about 465,000 women are expected to die from this disease worldwide [1]. Approximately one in nine women will develop breast cancer in their lifetime, and of these cancers, approximately 30% will be lethal [2].

Breast cancer is one clear example of excellent survival statistics when early-stage disease is treated using current therapies. Currently, numerous clinical methods are used in breast cancer screening and diagnosis [3]. The most effective screening technique at this time is X-ray mammography. The overall sensitivity of X-ray mammography for breast cancer detection is moderate (75%), and even more reduced in women with dense breasts: 62% [4, 5]. X-ray mammography has a 22% false positive rate in women under 50 [6]. The method cannot accurately distinguish between benign and malignant tumors [7].

Techniques such as magnetic resonance imaging (MRI) and ultrasound are sometimes used in addition to X-ray mammography, but have limitations such as high cost, low throughput, limited specificity (MRI), and low sensitivity (ultrasound). Thus, there is still a need to detect cancers earlier for treatment [4, 5], missed by mammography [8], and to add specificity to the procedures, since the majority of invasive follow-up procedures (e.g., surgical biopsies) are performed on normal or benign tissue.

New methods are being investigated to bridge the current gap in clinical utility. Examples of such experimental techniques are elastography, tomosynthesis, dedicated computed tomography (CT) and positron emission tomography (PET), photoacoustic (or optoacoustic) imaging, and optical imaging.

2. Breast Cancer Imaging

Breast imaging is largely indicated for detection, diagnosis, and clinical management of breast cancer. Commonly used imaging modalities include mammography, ultrasonography, magnetic resonance imaging (MRI), scintimammography, single photon emission computed tomography (SPECT) and positron emission tomography (PET).

2.1. Mammography. Mammography is, essentially, the only widely used Imaging modality for breast cancer screening. Several large randomized clinical trials have shown that mammography reduces mortality from breast cancer [9–12]. Extensive investigations on radiation dose to the breast and its dependence on breast composition, breast thickness, and X-ray spectral characteristics have been documented [13, 14]. Calcifications, or soft-tissue hardening with calcium deposits, are especially important. They are often an early sign of breast cancer, especially if the calcifications are small (microcalcifications) or irregularly shaped. The study does have some limitations. Imaging is more difficult with breasts that are dense or breasts in younger women. Breasts with implants or significant surgical scars are also difficult to visualize on mammography.

2.2. Ultrasonography. The role of ultrasound in breast imaging has been largely limited to applications such as distinguishing between cystic versus solid masses, evaluation of palpable masses, and for needle core biopsy. In recent years, the number of indications has been greatly expanded and breast ultrasonography is now an essential modality in breast imaging. Colour Doppler and more recently sensitive power Doppler ultrasound has been used for further evaluation of the breast. In 2002, Kolb et al. published a fundamental article that showed improved sensitivity (97% versus 74%) when adjunctively used with mammography compared to physical examination with mammography [15]. However, there was also a substantial decrease in positive predictive value with mammography plus ultrasound (11.2%) compared to mammography (22.6%) alone. Ultrasound has become a valuable tool to use with mammograms because it is widely available, noninvasive, and less costs than other options. But, ultrasound test value depends on the operator's level of skill and experience.

2.3. Magnetic Resonance Imaging. Independent clinical trials for women at high risk of hereditary breast cancer indicate increased sensitivity with breast MRI than mammography but with variable specificity. Dynamic contrast enhanced MRI (DCE-MRI) is a very important tool for detection, diagnosis, and clinical management of breast cancer. However, it requires intravenous injection of Gadolinium-contrast agent that entails some elevated risk [16]. Breast MRI is frequently used in the management of breast cancer, especially to determine disease extent in the breast and to direct local therapy. Another promising technique that has garnered substantial interest recently is proton magnetic resonance spectroscopy (1H-MRS). This technique allows quantitative characterization of total or composite choline concentration that has been shown to be elevated in malignant tumors compared to normal breast tissue [17]. Breast MRI will play a role, perhaps complementary to mammography, in screening for high-risk patients. The development of newer and, possibly, more targeted MRI contrast agents may expand the capabilities of breast MRI.

2.4. Radionuclide Imaging. Radionuclide-based imaging techniques such as scintimammography, single-photon emission computed tomography (SPECT), positron emission mammography (PEM), and positron emission tomography (PET) are additional imaging techniques that provide for physiologic information. Scintimammography and SPECT typically use 99mTc-Sestamibi or 99mTc-Tetrofosmin for breast-cancer imaging. Scintimammography is used for imaging mostly palpable lesions that were occult or indeterminate from other imaging modalities. Radionuclide imaging has long been used in breast cancer management, primarily in the form of bone scintigraphy ("bone scan") to detect bone metastases.

18F-fluorodeoxyglucose (FDG) PET is increasingly used in staging advanced or recurrent breast cancer and in monitoring response to therapy; in fact, has received approval for Medicare reimbursement for these clinical indications. For detection of primary tumors, 18F-FDG-PET has been reported to have similar sensitivity as SPECT [18]. A meta-analysis of whole body 18F-FDG-PET that included 13 studies indicated an overall sensitivity of 89% and specificity of 80% [19]. To overcome the limited sensitivity and spatial resolution of whole-body PET systems, a PEM system was developed [20]. The biochemical information provided by radiotracer imaging provides an early window to identify response to systemic therapy and may provide a quantitative endpoint for both clinical practice and clinical trials.

2.5. Other Modalities

2.5.1. Volumetric X-Ray Imaging Techniques. There is a need to develop techniques that provide depth information in breast X-ray imaging. Currently, stereoscopic digital mammography (SDM), digital breast tomosynthesis (DBT), and dedicated breast computed tomography (BCT) are three modalities that are being actively investigated.

2.5.2. Stereoscopic Digital Mammography. In stereoscopic digital mammography, two projection images, spaced a few degrees apart, are acquired with a digital mammography system. A dedicated stereoscopic workstation displays orthogonally polarized images and are viewed by the observer using passive cross-polarized glasses, so that each eye visualizes one image to provide depth perception.

2.5.3. Optical Imaging. Optical imaging techniques of the breast such as diffuse optical tomography (DOT), diffuse optical imaging, and diffuse optical spectroscopy are being investigated as an adjunct technique. Electrical impedance spectroscopy (EIS) and microwave imaging spectroscopy (MIS) are also being explored for potential use in breast cancer detection.

3. Optical Imaging

Optical characterization of the breast has been attempted since 1929 [21] when the term diaphanography was applied to shadowgraphs of breast tissue: "*...a simple procedure and a valuable aid in the interpretation of pathological conditions in the mammary gland. Its use is recommended in the routine examination of the breast...*" [21]. Cutler hoped to distinguish between solid tumors and cysts in the breast, but

found it difficult to produce the necessary light intensity for diaphanography without exposing the patient's skin to extreme heat. Although large, highly vascular, malignant lesions could be detected, the method did not achieve sufficient sensitivity and specificity to be used in clinical practice at the time. Transillumination proved largely inadequate for clinical use because it was too difficult to separate the effects of absorption and scattering within the tissue and because the two-dimensional data was poorly suited for image reconstruction.

Optical imaging as an adjunct device to mammography or ultrasound imaging is a natural choice, because the information gained with the optical signal is markedly different from that of the clinical imaging information. As a result of numerous scientific and technological advances in tissue optics since 1990, optical mammography now appears feasible with levels of specificity and resolution superior to early developments.

Optical breast imaging is a novel imaging technique that uses near-infrared (NIR) light to assess optical properties of tissues, and is expected to play an important role in breast cancer detection. When fluorescent probes are excited by NIR light, they emit photons at predefined wavelength ranges, detectable by an optical imaging system.

Until now, studies have focused on using the intrinsic optical properties of the breast to visualize lesions without the use of fluorescent contrast agents. These studies described higher absorption for carcinomas than for the surrounding parenchyma due to increased blood content associated with angiogenesis [22–25]. However, intrinsic contrast alone is probably not sensitive enough for (early) lesion detection [26]. Optical breast imaging using a fluorescent contrast agent may improve lesion contrast and can potentially detect changes in breast tissue earlier. The fluorescent probes can either binds specifically to certain targets associated with cancer or can nonspecifically accumulate at the tumor site, mostly by extravasations through leaky vessels (Figure 1).

Clinical optical imaging diagnosis started with the development of clinical optical breast imaging systems (Figure 2). Companies and academia put a lot of effort in this task; some systems are commercially available at the moment. The computed tomography laser mammography system CTLM, developed by Imaging Diagnostic Systems Inc., is a fully tomographic system and generates volumetric images of the breast. Poellinger et al. [27] and Floery et al. [28] concluded that CTLM could be used for the delineation of malignant tissue. The ComfortScan system, distributed by Danum International Ltd., is a transillumination system that requires breast compression to generate 2D images. Fournier and colleagues concluded that the system had the potential to distinguish benign from malignant lesions assuming a higher number of false-positive results compared to conventional mammography [29]. The SoftScan system by Advanced Research Technologies Inc., is a system that requires slight breast compression but is able to generate tomographic images of the breast. Using this system, van de Ven concluded that the use of such contrast agents, at least in addition to a targeting ligand, would have a great potential in future optical breast cancer diagnosis [30].

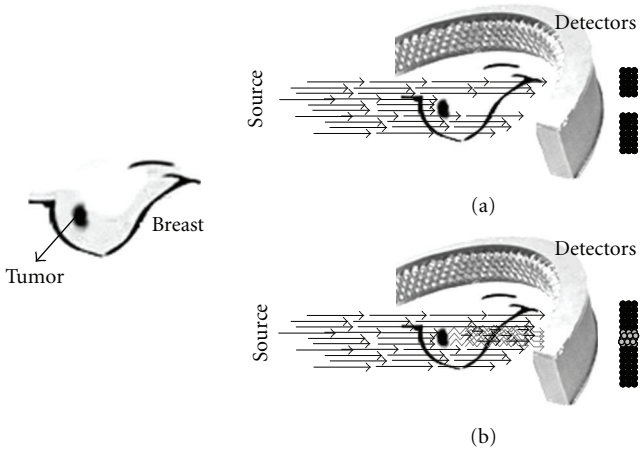

Figure 1: Optical breast-imaging basis. (a) Optical imaging without contrast agent where absorption results in decreased light intensity. (b) Optical imaging with contrast agent where a fluorescent probe emits light at a higher wavelength.

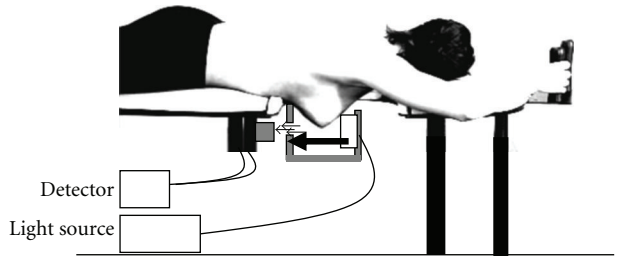

Figure 2: Breast optical imaging prototype. Patient lies in prone position. Soft compression in a plane and detection in the opposite one.

Major advantages of optical imaging are that it does not use any radioactive components (as in PET and SPECT), which can result in repeated use even in young women, and that its sensitivity is very high (nanomolar to picomolar concentration range) compared to MRI, it is relatively inexpensive, and is easily accessible. However, this technique is still in a very early phase of development.

4. Basic Concepts of Optical Breast Imaging

Optical imaging uses light propagation through tissue to assess its optical properties. In general, optical imaging devices transmit light through the breast, where it is both absorbed and scattered by the tissue components present. The light used in optical imaging is commonly monochromic and in the near-infrared (NIR) range permitting imaging up to several centimeters deep in soft tissue. Different tissue components have unique scattering and absorption characteristics for each wavelength. NIR in the wavelength range of 600–1000 nm is used to allow for sufficient tissue penetration. After passing through the breast, the remaining

light is registered by detectors and advanced computer algorithms are used to reconstruct the images [31, 32].

All optical imaging systems, in general, use three different illumination methods: continuous wave (CW), time-domain photon migration (TDPM), and frequency-domain photon migration (FDPM).

4.1. Continuous-Wave (CW) Imaging. Continuous-wave systems emit light at constant intensity or modulated at low frequencies (0.1–100 kilohertz) [33]. The constant intensity source is focused on the tissue, surface, and the tissue volume is illuminated with light whose intensity becomes exponentially attenuated with distance form the surface. It is a straightforward technique, which basically measures the attenuation of light transmitted between two points on the breast surface. Because of its simplicity, continuous-wave equipment is cheap and image acquisition fast.

4.2. Time-Domain Photon Migration (TDPM) Imaging. The time domain technique uses short (50–400 picoseconds) light pulses to assess the temporal distribution of photons [34]. Because scattering increases the times of flight spent by photons migrating in tissues, the photons that arrive earliest at the detector have encountered the fewest scattering events. Consequently, a spatial intensity image of early-arriving photons can conceivably be used to detect tissue regions of high absorbance based on their attenuation.

4.3. Frequency-Domain Photon Migration (FDPM) Imaging. Frequency domain devices modulate the amplitude of the light that is continuously transmitted at high frequencies (10 MHz–1 GHz). Measuring photons phase-shifts and their amplitude decay (compared to a reference signal), information on optical properties of tissue is acquired and scattering and absorption can be distinguished. When photon density waves encounter tissue regions of varying optical properties, they refract, scatter, and interfere. The result is a "perturbation" whose magnitude is dependent on the location, size, and optical contrast of variations within a tissue volume.

During the last decade, progress in source and detector technology, light-propagation modeling, and potential fluorescent contrast agents, has resulted in a renewed interest in optical imaging [35].

4.4. Light Sources. Three types of light sources are used for optical imaging applications: white light, light-emitting diodes (LED), and laser diodes. The spectrum of most white light sources extends over the visible range and into the near-infrared. In light-emitting diodes, free electrons move across a diode junction. In this process, photons are generated. The photon energy is set by the energy drop between the conduction band and the valence band. In laser diodes (or diode lasers), a population inversion is induced. Laser diodes are used widely for optical imaging applications.

4.5. Detectors. Photodiode is a robust and inexpensive detector for relatively high light levels. Light with energy greater than band-gap energy hits the photodiode, excites electrons into the conduction band, and creates a hole in the valence band. *Avalanche photodiode (APD)* is a high-speed, high-sensitive photodiode with an internal gain mechanism through a reverse-bias voltage. The electron-hole pairs are generated from exposure to light with higher photon energy than band-gap energy. *Photomultiplier tube (PMT)* is a sensitive detector which amplifies the input light signal 105 to 106 times with almost no additional noise. It is usually selected for high-speed or low-light level detection. It is suitable for single-photon counting applications when the rate photons striking the photocathode are below 100 MHz. *Charge-coupled device (CCD)* is a solid-state sensor with a wafer of silicon crystal. When the silicon is exposed to light, the photoelectric effect generates electrons from the silicon bonds. These free electrons are collected by CCD electrodes at the interface created by positive surface potential to form an extremely thin, but very dense, inversion layer. *Image intensifier* is a vacuum tube device consisting of a photocathode input, microchannel plate, and the phosphor screen. The electrons due to photoelectric effect are accelerated and multiplied through microchannel plate (MCP) via mechanism analogous to photomultiplier, to the phosphor screen where the light is released upon striking the coating.

Optical breast imaging can be performed (1) relying on intrinsic breast tissue contrast alone (mapping hemoglobin, water, and lipid content (Figure 3)); or (2) with the use of exogenous fluorescent probes that target molecules specific for breast cancer (Figure 1). The use of fluorescent probes has great potential in early breast cancer detection, since in vivo imaging of molecular changes associated with breast cancer formation is technically feasible.

5. Optical Breast Imaging without Contrast Agent

Optical breast imaging uses NIR light to assess the optical properties of breast tissue. Light absorption at these wavelengths is minimal, allowing for sufficient tissue penetration (up to 15 cm). The main components of the breast all have specific absorption characteristics as a function of the wavelength. Imaging of scattering may be associated with structural characteristics and the concentrations of organelles. By combining images acquired at various wavelengths (spectroscopy) concentrations of oxy- and deoxy-hemoglobin, water, and lipid can be determined. In a malignant tumor, hemoglobin concentration is directly related to angiogenesis, the key factor required for tumor growth and metastases [36]. In addition, the proportions of oxy- and deoxy-hemoglobin change in such a tumor due to its metabolism [37]. By measuring concentrations of the breast components, discrimination of benign and malignant tumors may be possible with diffuse optical imaging. More importantly, imaging of the absorption coefficient, at appropriately selected wavelengths, can quantify the concentrations of water and oxy- and deoxy-hemoglobin of breast tumors, and obtain measures of hemoglobin concentration and hypoxia.

The scattering properties of tissues also contain important information for lesion diagnosis. The scattering coefficients are related to the tissue structure properties and

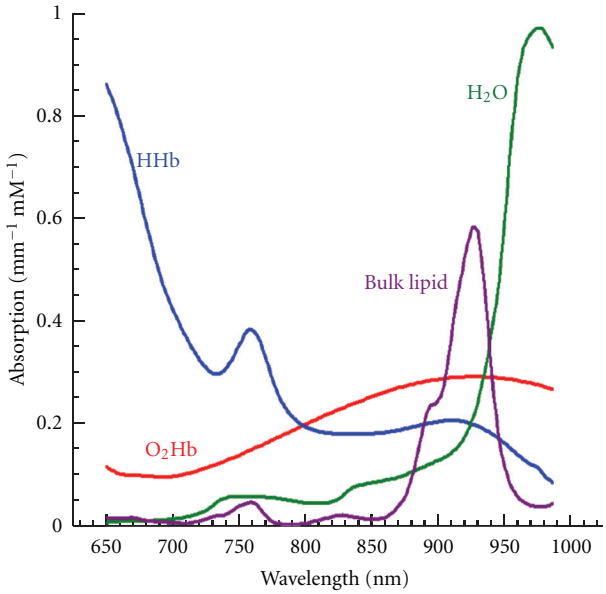

Figure 3: Endogenous absorption related to wavelength. HHb. Hemoglobin. O_2Hb: Oxigenated Hemoglobin.

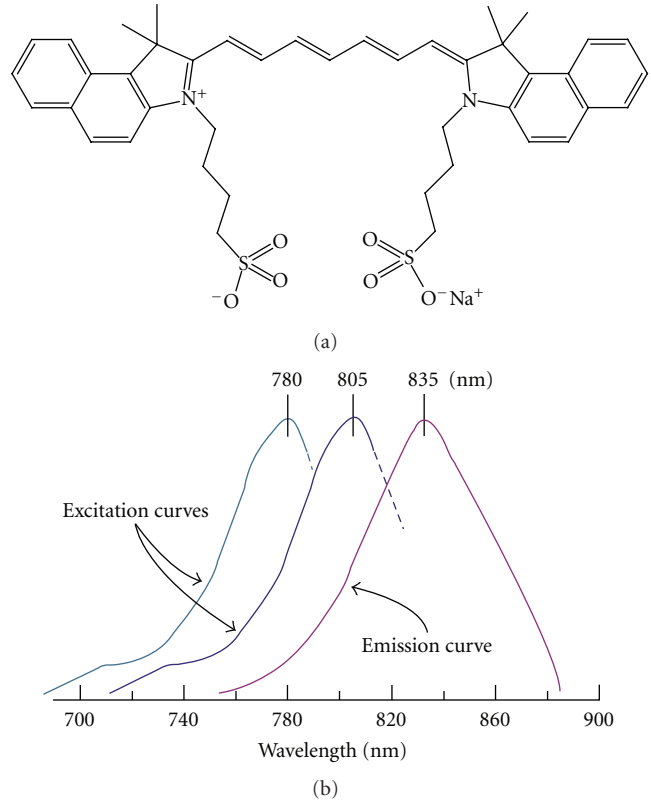

Figure 4: (a) Estructure of ICG. (b) Absorption/fluorescene spectrum of ICG.

the concentration or size of organelles. The *in vivo* measurements show that scattering coefficients are wavelength-dependent. While *ex vivo* studies suggest that the scattering coefficients alone do not provide sufficient information to discriminate the small breast tumors from normal breast tissue (Figure 1).

Detection rates for the transillumination approach range from 0.58 to 0.94 [34, 38]. With tomography, carcinomas were detected between 50% and 74% [39]. Detection rates of benign lesions vary between 0.04 and 0.94 [34, 38, 39]. Benign cysts were detected with tomography in 83% [40]. Malignant lesions were detected by their higher optical attenuation compared to the surrounding tissue, mainly related to increased light absorption by their higher hemoglobin content [41]. Solid benign lesions were more difficult to detect, but sometimes showed increased attenuation, although to a lesser extent than malignant lesions [34, 38–41].

Optical imaging can probe the concentrations of those chromophores, especially the oxygenated and deoxygenated hemoglobin. Hence, it can provide the biochemical specificity in breast cancer diagnosis. Typically, two important parameters are given by optical spectroscopy and imaging, the blood volume (the sum of the oxygenated and deoxygenated hemoglobin concentration) and the oxygen saturation (the ratio of oxygenated hemoglobin to the blood volume). Statistical data indicate that there are two-to fourfolds of contrast between normal and tumor structures for the blood volume, and the oxygen saturation in the tumor is also less than normal.

6. Optical Breast Imaging with Contrast Agent

A novel element that can enhance the potential applications of optical imaging is the use of contrast agents. In optical breast imaging with contrast agent, fluorescent probes are used that emit photons at predefined wavelengths after excitation by laser light. These photons are detected while the light of the excitation wavelength is filtered (Figure 1). Fluorescent probes that target molecules specific for breast cancer are currently being developed and validated in preclinical animal studies [42–45]. New "Smart" optical probes to target proteases are being analyzed [42, 43]. These probes are nonfluorescent in their native state, but convert to a highly fluorescent active state when their backbone is cleaved by cathepsins.

Like other imaging modalities, contrast enhancement through contrast agents, either for absorption or fluorescence, have shown great promise for improving the sensitivity and specificity of breast cancer detection [46].

6.1. Nonspecific Contrast Agents. The most commonly used contrast agent in the NIR spectral window is Indocyanine Green (ICG) (Figure 4).

ICG is a nonspecific blood pool agent that is both absorbing and fluorescent in the NIR range. It is used clinically, mainly for retinal angiography and liver function tests. Both studies observed differences in ICG pharmacokinetics between malignant and benign lesions on the optical images.

Important advantages of optical imaging with contrast agent are that it does not use any radioactive components (as in PET and SPECT), and that its sensitivity for probe detection is very high (possibly in the nanomolar to the 100 picomolar concentration range) as compared

to MRI (micromolar to millimolar range). Moreover, optical imaging uses no ionizing radiation and can thus be used repeatedly, also in younger women. Similar to nuclear imaging, however, the optical method generally can detect very small concentrations of chromophores or fluorophores, but without using ionizing radiation and at a reduced cost.

Few studies reported on optical breast imaging with the use of a fluorescent contrast agent. Two case reports described their experiences using the nonspecific agent Indocyanine Green (ICG), the only fluorescente agent approved for use in humans today [46–48]. Both groups observed a marked absorption increase in the malignant tumors due to accumulation of ICG. In the study by Corlu et al. it was shown that the use of ICG is feasible for fluorescence Diffuse Optical Tomography (DOT). This was the first, and thus far the only, study to demonstrate fluorescence DOT in vivo in three women with breast cancer [49] (Table 1).

6.2. Molecular Specific Contrast Agents. Cancer cells overexpress certain receptors, and increase the uptake of the corresponding ligands. This process will result in the accumulation of those ligands in a certain type of cells, thus providing high detection specificity. Conjugation of a fluorophore to those ligands can provide high fluorescent contrast for tumor versus normal cells.

Breast cancer (BC) is a heterogeneous class of disease exhibiting a variety of phenotypes and molecular profiles. For selection of the most promising therapy, with regard to the molecular profile of a cancer lesion, immunohistochemistry (e.g., biopsies) is performed. In this context, identification of for example, hormone receptor positive (estrogens, ER+, progesterone PR+) or human epidermal growth factor receptor 2 positive (HER-2+) cancers are important and significant points to be addressed.

A new advance that holds great promise for breast cancer research is the recent development of optical probes for molecular imaging, specifically in the NIR range. Fluorescent dyes that target specific tumor receptors [50], or that are activated (fluoresce) by tumor-associated enzymes (such as cathepsins and matrix metalloproteases) [51], have been shown to identify their molecular targets *in vivo*.

Using this technology, appropriately engineered fluorescent probes can be selectively activated by endogenous or transferred gene expression. The combination of such probes with optical imaging may yield a unique, highly sensitive technology for *in vivo* and real-time imaging of the expression patterns for various enzymes, which are crucially involved in tumor formation and metastasis.

Therefore, the impact of developing molecular-optical imaging, and in particular molecular-DOT, of the breast is potentially enormous. First, selected molecular activity can be achieved with high sensitivity. Second, cancers could be detected at their molecular onset, before anatomic changes become apparent. Therefore, therapies can be initiated at a very early stage. Third, specific cancer parameters such as growth kinetics, angiogenesis growth factors, tumor cell markers, and genetic alterations could be studied without perturbing the tumor environment. Finally, those points are important in the development of novel targeted drugs and therapies.

7. Multimodality Imaging

Another exciting application of optical technology is the combination of optical imaging with other imaging modalities. Light guidance using optical fibers makes optical imaging compatible with many other radiologic methods [52], such as mammography, ultrasound, MRI, and positron emission tomography, among others. The development of hybrid modalities offers the potential of simultaneously scanning of the breast, under identical physiologic conditions. The optical method offers several complementary features to those of established medical imaging methods, mainly through targeting oxy- and deoxy-hemoglobin (Figure 3), but also through the study of molecular events and gene expression. This can produce an increased number of features that may augment the diagnostic value of any single technique alone.

8. Optical-Imaging-Guided Surgery

The only two imaging techniques used, even occasionally, during oncologic surgery are X-ray fluoroscopy (for angiography) and US (for mass detection). However, the former exposes patients and professionals to ionizing radiation, and, the latter requires direct contact with tissue, and neither can be used with targeted contrast agents. Optical imaging, that exploits invisible NIR fluorescent light (700 to 900 nm), offers several advantages for image-guided surgery, including low inherent autofluorescence background, highly sensitive and specific detection of tumors up to millimetres deep in scattering tissue, and real-time imaging (reviewed in Frangioni [53]). Intraoperative imaging systems developed also provide simultaneous acquisition of surgical anatomy (colour video) and function (NIR fluorescence) [54]. Innovative work from other groups has extended depth penetration to several centimetres using frequency domain photon migration techniques. Currently, the only clinically available NIR fluorophore is indocyanine green (Figure 4, Table 1), which is a nontargeted extracellular fluid agent approved for nonfluorescence indications. ICG can be used for NIR fluorescent sentinel lymph node mapping of virtually any tissue or organ [54–56]. Many investigators are also developing NIR fluorophores targeted specifically to human cancer and normal structures [57, 58]. If translated to the clinic, these targeted NIR fluorescent contrast agents would permit the oncologic surgeon to resect malignant cells under direct visualization, while actively avoiding critical structures such as vessels and nerves.

9. Conclusions

Optical imaging is a very promising imaging technique. Optical imaging systems can detect imaging agents in picomolar to nanomolar concentration ranges, whereas, for instance, magnetic resonance imaging (MRI) needs larger molecular masses before probe detection is possible (at least micromolar concentrations). In contrast to X-ray, computed

Table 1: Devices used for clinical trials of ICG Fluorescence imaging. adapted from: Marshal et al. ; The Open Surgical Oncology Journal, 2010, 2, 12–25.

Device	Excitation source	Fluorescence collection	Detector	Working distance	Field of view	Depth of penetration	Integration time or frames per Sec (FPS)
Photodynamic Eye (PDE) Hamamatsu	Laser-emitting diodes (LEDs) centered at 760 nm, incident power not specified	Bandpass filter > 820 nm	CCD	20 cm	Not given, but limited	2 cm	Not specified
SPY (Novadaq)	Laser-emitting at 806 nm, 2.0–2.7 W, incident power not specified	835 nm "camera," not specified	CCD	30 cm	56 cm^2	1 mm DOP	30 fps
FDPM imager (Texas)	Laser diode, 785 ± 10 nm. <1.9 mW/cm^2	Notch filters at 785 nm, and at 830 nm	Gen III intensifier coupled to CCD, gain modulatable for tomography	Variable, but reported <76.2 cm	Max reported FOV 900 cm^2	Estimated to be 4 cm	50–800 msec
IC-View (Pulsion Medical)	Laser diode 780 nm (0.16 W), incident power not specified	Not specified	CCD	Not specified	Not specified	Not specified	Not specified
FLARE (Israel Beth Deaconess Hospital)	LEDs emitting 745–779 nm, 14 mW/cm^2	Bandpass filter 800–848 nm	CCD	45 cm	3.7 cm^2–169.5 cm^2	Not specified	200 msec
Custom system (Kochi Medical School)	LEDs emitting light centered at 760 nm, incident power not specified	840 nm cut-on filter	Color CCD	~50 cm	78.5 cm^2	Not specified	Not specified

tomography (CT) and positron emission tomography (PET), optical imaging uses no ionizing radiation. Repeated imaging is therefore possible without radiation risks. Moreover, optical imaging is relatively cheap, and imaging agents are easy to generate and have long half-lives, particularly compared to PET tracers.

Main challenges in optical imaging are depth penetration, signal quantification, and development, validation and approval of relevant imaging agents for human use. Light penetration in tissue is limited, but with the use of near-infrared light, and the development of more sensitive detection equipment, penetration in human tissue is now possible up to 15 centimeters deep.

Another way to deal with the lower spatial resolution is a multimodality approach. Optical imaging could be fused with other anatomical imaging techniques, such as ultrasound (photoacoustic imaging) or MRI, similar to nuclear imaging techniques as PET/CT.

The other key challenge in clinical translation of optical imaging is the development of relevant imaging agents. Crucial for this step is the full understanding of the molecular biology of breast cancer to identify potential targets. Biologic processes to study for target identification include, for example, tumor metabolism, angiogenesis, proliferation, apoptosis, and hypoxia.

When clinical translation of appropriate optical imaging agents will be successful, optical breast imaging could improve early detection of breast cancer; for example, in women with dense breasts who are at increased risk for breast cancer. X-ray mammographic screening has very limited sensitivity in these women due to the tumor-hiding projection of the dense glandular tissue [59, 60], while near-infrared light is far less hindered by dense breast tissue. Optical breast imaging could also have a role in the selection of appropriate adjuvant treatment, the evaluation of response to treatment, and the fine-tuning of treatment strategy in the individual breast cancer patient. Moreover, optical imaging agents could, potentially, be used as "theranostics", combining the process of diagnosis and (local) therapy [61].

References

[1] M. Garcia, A. Jemal, E. M. Ward et al., *Global Cancer Facts & Figures 2007*, American Cancer Society, Atlanta, Ga, USA, 2007.

[2] American cancer Society, Statistics for 2004: Cancer facts & figures, 2004, http://www.cancer.org/research/cancerfactsfigures/cancerfactsfigures/index.

[3] S. A. Feig, "Decreased breast cancer mortality through mammographic screening: results of clinical trials," *Radiology*, vol. 167, no. 3, pp. 659–665, 1988.

[4] "Breast cancer. Early detection and prompt treatment are critical," *Mayo Clinic Health Letter*, supplement 1–8, 2001.

[5] S. L. Jacques, "Time resolved propagation of ultrashort laser pulses within turbid tissues," *Applied Optics*, vol. 28, no. 12, pp. 2223–2229, 1989.

[6] K. Kerlikowske, J. Barclay, D. Grady, E. A. Sickles, and V. Ernster, "Comparison of risk factors for ductal carcinoma in situ and invasive breast cancer," *Journal of the National Cancer Institute*, vol. 89, no. 1, pp. 77–82, 1997.

[7] M. J. Homer, "Breast imaging: pitfalls, controversies, and some practical thoughts," *Radiologic Clinics of North America*, vol. 23, no. 3, pp. 459–472, 1985.

[8] J. Wang, T. T. F. Shih, J. C. Y. Hsu, and Y. W. Li, "The evaluation of false negative mammography from malignant and benign breast lesions," *Clinical Imaging*, vol. 24, no. 2, pp. 96–103, 2000.

[9] S. Shapiro, P. Strax, and L. Venet, "Periodic breast cancer screening in reducing mortality from breast cancer," *Journal of the American Medical Association*, vol. 215, no. 11, pp. 1777–1785, 1971.

[10] E. L. Thurfjell and J. A. Lindgren, "Breast cancer survival rates with mammographic screening: similar favorable survival rates for women younger and those older than 50 years," *Radiology*, vol. 201, no. 2, pp. 421–426, 1996.

[11] R. E. Hendrick, R. A. Smith, J. H. Rutledge III, and C. R. Smart, "Benefit of screening mammography in women aged 40–49: a new meta-analysis of randomized controlled trials," *Journal of the National Cancer Institute Monographs*, no. 22, pp. 87–92, 1997.

[12] L. Tabar, B. Vitak, H. H. Chen, M. F. Yen, S. W. Duffy, and R. A. Smith, "Beyond randomized controlled trials: organized mammographic screening substantially reduces breast carcinoma mortality," *Cancer*, vol. 91, no. 9, pp. 1724–1731, 2001.

[13] J. M. Boone, "Normalized glandular dose (DgN) coefficients for arbitrary x-ray spectra in mammography: computer-fit values of Monte Carlo derived data," *Medical Physics*, vol. 29, no. 5, pp. 869–875, 2002.

[14] G. R. Hammsterstein, D. W. Miller, and D. R. White, "Absorbed radiation dose in mammography," *Radiology*, vol. 130, no. 2, pp. 485–491, 1979.

[15] T. M. Kolb, J. Lichy, and J. H. Newhouse, "Comparison of the performance of screening mammography, physical examination, and breast US and evaluation of factors that influence them: an analysis of 27,825 patient evaluations," *Radiology*, vol. 225, no. 1, pp. 165–175, 2002.

[16] FDA, US Public Health Advisory: Update on Magnetic Resonance Imaging (MRI) Contrast Agents Containing Gadolinium and Nephrogenic Fibrosing Dermopathy, 2006, http://www.fda.gov/Cder/Drug/advisory/gadolinium(agents)2006-1222.htm.

[17] I. S. Gribbestad, B. Sitter, S. Lundgren, J. Krane, and D. Axelson, "Metabolite composition in breast tumors examined by proton nuclear magnetic resonance spectroscopy," *Anticancer Research*, vol. 19, no. 3, pp. 1737–1746, 1999.

[18] K. Yutani, E. Shiba, H. Kusuoka et al., "Comparison of FDG-PET with MIBI-SPECT in the detection of breast cancer and axillary lymph node metastasis," *Journal of Computer Assisted Tomography*, vol. 24, no. 2, pp. 274–280, 2000.

[19] M. F. Smith, S. Majewski, A. G. Weisenberger, D. A. Kieper, R. R. Raylman, and T. G. Turkington, "Analysis of factors affecting positron emission mammography (PEM) image formation," *IEEE Transactions on Nuclear Science*, vol. 50, no. 1, pp. 53–59, 2003.

[20] C. J. Thompson, K. Murthy, I. N. Weinberg, and F. Mako, "Feasibility study for positron emission mammography," *Medical Physics*, vol. 21, no. 4, pp. 529–538, 1994.

[21] M. Cutler, "Transillumination of the breast," *Surgery, Gynecology & Obstetrics*, vol. 48, pp. 721–727, 1929.

[22] D. Floery, T. H. Helbich, C. C. Riedl et al., "Characterization of benign and malignant breast lesions with computed tomography laser mammography (CTLM): initial experience," *Investigative Radiology*, vol. 40, no. 6, pp. 328–335, 2005.

[23] V. Ntziachristos, A. G. Yodh, M. D. Schnall, and B. Chance, "MRI-guided diffuse optical spectroscopy of malignant and benign breast lesions," *Neoplasia*, vol. 4, no. 4, pp. 347–354, 2002.

[24] B. J. Tromberg, A. Cerussi, N. Shah et al., "Diffuse optics in breast cancer: detecting tumors in pre-menopausal women and monitoring neoadjuvant chemotherapy," *Breast Cancer Research*, vol. 7, no. 6, pp. 279–285, 2005.

[25] Q. Zhu, E. B. Cronin, A. A. Currier et al., "Benign versus malignant breast masses: optical differentiation with US-guided optical imaging reconstruction," *Radiology*, vol. 237, no. 1, pp. 57–66, 2005.

[26] D. R. Leff, O. J. Warren, L. C. Enfield et al., "Diffuse optical imaging of the healthy and diseased breast: a systematic review," *Breast Cancer Research and Treatment*, vol. 108, no. 1, pp. 9–22, 2008.

[27] A. Poellinger, J. C. Martin, S. L. Ponder et al., "Near-infrared laser computed tomography of the breast. First clinical experience," *Academic Radiology*, vol. 15, no. 12, pp. 1545–1553, 2008.

[28] D. Floery, T. H. Helbich, C. C. Riedl et al., "Characterization of benign and malignant breast lesions with computed tomography laser mammography (CTLM): initial experience," *Investigative Radiology*, vol. 40, no. 6, pp. 328–335, 2005.

[29] L. S. Fournier, D. Vanel, A. Athanasiou et al., "Dynamic optical breast imaging: a novel technique to detect and characterize tumor vessels," *European Journal of Radiology*, vol. 69, no. 1, pp. 43–49, 2009.

[30] S. M. W. Y. Van De Ven, N. Mincu, J. Brunette et al., "Molecular imaging using light-absorbing imaging agents and a clinical optical breast imaging system—a phantom study," *Molecular Imaging and Biology*, vol. 13, no. 2, pp. 232–238, 2011.

[31] S. R. Arridge and M. Schweiger, "Image reconstruction in optical tomography," *Philosophical Transactions of the Royal Society B*, vol. 352, no. 1354, pp. 717–726, 1997.

[32] M. Schweiger, I. Nissilä, D. A. Boas, and S. R. Arridge, "Image reconstruction in optical tomography in the presence of coupling errors," *Applied Optics*, vol. 46, no. 14, pp. 2743–2756, 2007.

[33] A. M. Siegel, J. J. A. Marota, and D. A. Boas, "Design and evaluation of a continuous-wave diffuse optical tomography system," *Optics Express*, vol. 4, no. 8, pp. 287–298, 1999.

[34] P. Taroni, A. Torricelli, L. Spinelli et al., "Time-resolved optical mammography between 637 and 985 nm: clinical study on the detection and identification of breast lesions," *Physics in Medicine and Biology*, vol. 50, no. 11, pp. 2469–2488, 2005.

[35] A. P. Gibson, J. C. Hebden, and S. R. Arridge, "Recent advances in diffuse optical imaging," *Physics in Medicine and Biology*, vol. 50, no. 4, pp. R1–R43, 2005.

[36] A. Rice and C. M. Quinn, "Angiogenesis, thrombospondin, and ductal carcinoma in situ of the breast," *Journal of Clinical Pathology*, vol. 55, no. 8, pp. 569–574, 2002.

[37] P. Vaupel and L. Harrison, "Tumor hypoxia: causative factors, compensatory mechanisms, and cellular response," *Oncologist*, vol. 9, no. 5, pp. 4–9, 2004.

[38] L. Gotz, S. H. Heywang-Kobrunner, O. Schutz, and H. Siebold, "Optical mammography on preoperative patients," *Aktuelle Radiologie*, vol. 8, no. 1, pp. 31–33, 1998.

[39] D. Floery, T. H. Helbich, C. C. Riedl et al., "Characterization of benign and malignant breast lesions with computed tomography laser mammography (CTLM): initial experience," *Investigative Radiology*, vol. 40, no. 6, pp. 328–335, 2005.

[40] X. Gu, Q. Zhang, M. Bartlett, L. Schutz, L. L. Fajardo, and H. Jiang, "Differentiation of cysts from solid tumors in the breast with diffuse optical tomography," *Academic Radiology*, vol. 11, no. 1, pp. 53–60, 2004.

[41] Q. Zhu, E. B. Cronin, A. A. Currier et al., "Benign versus malignant breast masses: optical differentiation with US-guided optical imaging reconstruction," *Radiology*, vol. 237, no. 1, pp. 57–66, 2005.

[42] C. Bremer, V. Ntziachristos, B. Weitkamp, G. Theilmeier, W. Heindel, and R. Weissleder, "Optical imaging of spontaneous breast tumors using protease sensing 'smart' optical probes," *Investigative Radiology*, vol. 40, no. 6, pp. 321–327, 2005.

[43] C. Bremer, C. H. Tung, A. Bogdanov, and R. Weissleder, "Imaging of differential protease expression in breast cancers for detection of aggressive tumor phenotypes," *Radiology*, vol. 222, no. 3, pp. 814–818, 2002.

[44] I. Hilger, Y. Leistner, A. Berndt et al., "Near-infrared fluorescence imaging of HER-2 protein over-expression in tumour cells," *European Radiology*, vol. 14, no. 6, pp. 1124–1129, 2004.

[45] S. Ke, X. Wen, M. Gurfinkel et al., "Near-infrared optical imaging of epidermal growth factor receptor in breast cancer xenografts," *Cancer Research*, vol. 63, no. 22, pp. 7870–7875, 2003.

[46] V. Ntziachristos, A. G. Yodh, M. Schnall, and B. Chance, "Concurrent MRI and diffuse optical tomography of breast after indocyanine green enhancement," *Proceedings of the National Academy of Sciences of the United States of America*, vol. 97, no. 6, pp. 2767–2772, 2000.

[47] K. Licha, B. Riefke, V. Ntziachristos, A. Becker, B. Chance, and W. Semmler, "Hydrophilic cyanine dyes as contrast agents for near-infrared tumor imaging: synthesis, photophysical properties and spectroscopic in vivo characterization," *Photochemistry and Photobiology*, vol. 72, pp. 392–398, 2000.

[48] V. Ntziachristos, A. G. Yodh, M. Schnall, and B. Chance, "Concurrent MRI and diffuse optical tomography of breast after indocyanine green enhancement," *Proceedings of the National Academy of Sciences of the United States of America*, vol. 97, no. 6, pp. 2767–2772, 2000.

[49] A. Corlu, R. Choe, T. Durduran et al., "Three-dimensional in vivo fluorescence diffuse optical tomography of breast cancer in humans," *Optics Express*, vol. 15, no. 11, pp. 6696–6716, 2007.

[50] S. Achilefu, R. B. Dorshow, J. E. Bugaj, and R. Rajagopalan, "Novel receptor-targeted fluorescent contrast agents for in vivo tumor imaging," *Investigative Radiology*, vol. 35, no. 8, pp. 479–485, 2000.

[51] R. Weissleder, C. H. Tung, U. Mahmood, and A. Bogdanov, "In vivo imaging of tumors with protease-activated near-infrared fluorescent probes," *Nature Biotechnology*, vol. 17, no. 4, pp. 375–378, 1999.

[52] T. A. Giambernardi, G. M. Grant, G. P. Taylor et al., "Overview of matrix metalloproteinase expression in cultured human cells," *Matrix Biology*, vol. 16, no. 8, pp. 483–496, 1998.

[53] J. V. Frangioni, "In vivo near-infrared fluorescence imaging," *Current Opinion in Chemical Biology*, vol. 7, no. 5, pp. 626–634, 2003.

[54] E. Tanaka, H. S. Choi, H. Fujii, M. G. Bawendi, and J. V. Frangioni, "Image-guided oncologic surgery using invisible light: completed pre-clinical development for sentinel lymph node mapping," *Annals of Surgical Oncology*, vol. 13, no. 12, pp. 1671–1681, 2006.

[55] D. W. Knapp, L. G. Adams, A. M. DeGrand et al., "Sentinel lymph node mapping of invasive urinary bladder cancer in animal models using invisible light," *European Urology*, vol. 52, no. 6, pp. 1700–1708, 2007.

[56] C. P. Parungo, D. I. Soybel, Y. L. Colson et al., "Lymphatic drainage of the peritoneal space: a pattern dependent on bowel lymphatics," *Annals of Surgical Oncology*, vol. 14, no. 2, pp. 286–298, 2007.

[57] J. L. Figueiredo, H. Alencar, R. Weissleder, and U. Mahmood, "Near infrared thoracoscopy of tumoral protease activity for improved detection of peripheral lung cancer," *International Journal of Cancer*, vol. 118, no. 11, pp. 2672–2677, 2006.

[58] E. Tanaka, S. Ohnishi, R. G. Laurence, H. S. Choi, V. Humblet, and J. V. Frangioni, "Real-time intraoperative ureteral guidance using invisible near-infrared fluorescence," *Journal of Urology*, vol. 178, no. 5, pp. 2197–2202, 2007.

[59] P. A. Carney, D. L. Miglioretti, B. C. Yankaskas et al., "Individual and combined effects of age, breast density, and hormone replacement therapy use on the accuracy of screening mammography," *Annals of Internal Medicine*, vol. 138, pp. 168–175, 2003.

[60] N. F. Boyd, H. Guo, L. J. Martin et al., "Mammographic density and the risk and detection of breast cancer," *New England Journal of Medicine*, vol. 356, no. 3, pp. 227–236, 2007.

[61] P. Debbage and W. Jaschke, "Molecular imaging with nanoparticles: giant roles for dwarf actors," *Histochemistry and Cell Biology*, vol. 130, no. 5, pp. 845–875, 2008.

Hindawi Publishing Corporation
Journal of Oncology
Volume 2012, Article ID 291898, 10 pages
doi:10.1155/2012/291898

Research Article

Rapid Stereomicroscopic Imaging of HER2 Overexpression in *Ex Vivo* Breast Tissue Using Topically Applied Silica-Based Gold Nanoshells

Lissett R. Bickford,[1,2,3] Robert J. Langsner,[1] Joseph Chang,[4] Laura C. Kennedy,[1,5] Germaine D. Agollah,[6] and Rebekah Drezek[1,7]

[1] *Department of Bioengineering, Rice University, 6100 Main Street, MS 142, Houston, TX 77005, USA*
[2] *School of Biomedical Engineering and Sciences, Virginia Polytechnic Institute and State University, Blacksburg, VA 24061, USA*
[3] *Department of Mechanical Engineering, Virginia Polytechnic Institute and State University, Blacksburg, VA 24061, USA*
[4] *School of Medicine, University of California San Francisco, San Francisco, CA 94143, USA*
[5] *School of Medicine, Baylor College of Medicine, Houston, TX 77030, USA*
[6] *Department of Chemistry and Process Development, Nanospectra Biosciences, Inc., Houston, TX 77054, USA*
[7] *Department of Electrical and Computer Engineering, Rice University, Houston, TX 77005, USA*

Correspondence should be addressed to Rebekah Drezek, drezek@rice.edu

Received 5 April 2012; Accepted 11 September 2012

Academic Editor: José María Benlloch

Copyright © 2012 Lissett R. Bickford et al. This is an open access article distributed under the Creative Commons Attribution License, which permits unrestricted use, distribution, and reproduction in any medium, provided the original work is properly cited.

Tumor margin detection for patients undergoing breast conservation surgery primarily occurs postoperatively. Previously, we demonstrated that gold nanoshells rapidly enhance contrast of HER2 overexpression in *ex vivo* tissue sections. Our ultimate objective, however, is to discern HER2 overexpressing tissue from normal tissue in whole, nonsectioned, specimens to facilitate rapid diagnoses. Here, we use targeted nanoshells to quickly and effectively visualize HER2 receptor expression in intact *ex vivo* human breast tissue specimens. Punch biopsies of human breast tissue were analyzed after a brief 5-minute incubation with and without HER2-targeted silica-gold nanoshells using two-photon microscopy and stereomicroscopy. Labeling was subsequently verified using reflectance confocal microscopy, darkfield hyperspectral imaging, and immunohistochemistry to confirm levels of HER2 expression. Our results suggest that anti-HER2 nanoshells used in tandem with a near-infrared reflectance confocal microscope and a standard stereomicroscope may potentially be used to discern HER2-overexpressing cancerous tissue from normal tissue in near real time and offer a rapid supplement to current diagnostic techniques.

1. Introduction

Currently, breast cancer is the second leading cause of cancer-related deaths in women, and it accounts for approximately one-third of all cancers diagnosed in women in the United States [1]. To reduce cancer recurrence and progression, cancerous tissue must be completely eliminated, regardless of grade [2]. Surgical breast cancer therapy focuses on removing the primary tumor and identifying the possibility of metastatic disease from the evaluation of sentinel lymph nodes. Although some patients may require modified radical mastectomy, many patients with less-advanced breast cancer elect breast-conserving surgery. The presence of a positive surgical margin during these surgeries has been associated with lower rates of patient survival [3]. Due to residual cancer cells being left in many patients that undergo breast conservation therapy, as many as 40% of patients have experienced local breast cancer recurrence near the site of the original tumor [4]. Intraoperative treatment decisions are, therefore, absolutely critical.

Presently, intraoperative tumor margin detection occurs primarily in specialized tertiary centers, such as The University of Texas M.D. Anderson Cancer Center (MDACC). In these centers, the resected tissue receives a preliminary evaluation by a pathologist while the patient remains in the operating room; if necessary, additional tissue can be

removed until the pathologist determines that the tumor margins are negative. In community hospitals, however, pathologic analysis of excised tissue only occurs postoperatively [5]. Patients who consequently have positive tumor margins must return for surgical reexcision and receive increased doses of adjuvant radiation therapy [6, 7]. Thus, the existence of positive tumor margins portends additional risks and costs to the patient. Due to the existing limitations of current intraoperative tumor margin detection, there is an opportunity to develop superior diagnostic tools to assist in reducing the recurrence and progression of cancer due to inadequate tissue removal during primary surgery.

While histologic analysis remains the gold standard for tumor margin assessment, the macroscopic evaluation of whole, nonsectioned tissue specimens may also be used to provide an intraoperative estimate of tumor margin status prior to subsequent processing. This would be an invaluable tool in hospitals without onsite pathology suites. Macroscopic visualization of questionable tissue is attractive for enhancing the sensitivity and specificity of tumor margin delineation: if the number of suspicious regions that require further microscopic processing can be reduced, surgeons and pathologists can focus their attention and resources on areas that remain inconclusive. Currently, macroscopic evaluation only occurs for breast cancer specimens that involve microcalcifications or nonpalpable masses and does not occur for palpable breast masses [8]. For nonpalpable masses that have been resected, radiographic images are used to determine the extent of the breast disease and the proximity to the resected margins. Although specimen radiography appears to increase the accuracy of tumor margin detection, limitations have been noted. For instance, microcalcifications that appear as tumor on radiographic images may actually be areas of lymphocytic accumulation [9]. The use of contrast agents targeted to specific biomarkers associated with disease may present an opportunity to increase the sensitivity and specificity of macroscopic evaluations.

In preceding studies, we confirmed that silica-based gold nanoshells targeted to the Human Epidermal growth factor Receptor 2 (HER2) could be used for the rapid contrast enhancement of both cells [10] and tissue sections [11] which overexpress HER2 biomarkers. While gold nanoshells can be conjugated to a variety of biomarkers [12, 13], we have selected HER2 due to its association with increased cancer aggression, recurrence, and progression when amplified [14, 15]. Amplification of this cell-surface bound tyrosine kinase receptor occurs in up to a quarter of all human breast cancer cases [16]. Importantly, using biomarkers for tumor margin detection has recently been shown to better identify patients at high risk of cancer recurrence over standard histological analysis [17].

To facilitate prompt tumor margin detection intraoperatively, the ability to assess tumor margins without physical sectioning is highly desirable as sectioning may incur significant time to the surgical procedure [5]. Thus, in this study, we advance our previous findings by examining the ability to rapidly target HER2 receptors in intact *ex vivo* human breast tissue specimens without sectioning. We first confirm the predominance of the surface targeting needed to identify the tumor margins and preferential labeling of HER2-positive tissue using two photon and hyperspectral imaging. Then, we demonstrate that anti-HER2-targeted gold nanoshells can be used as rapid diagnostic imaging agents for HER2 overexpression in intact breast tissue specimens using a standard stereomicroscope and confirm these results through reflectance confocal microscopy and immunohistochemistry.

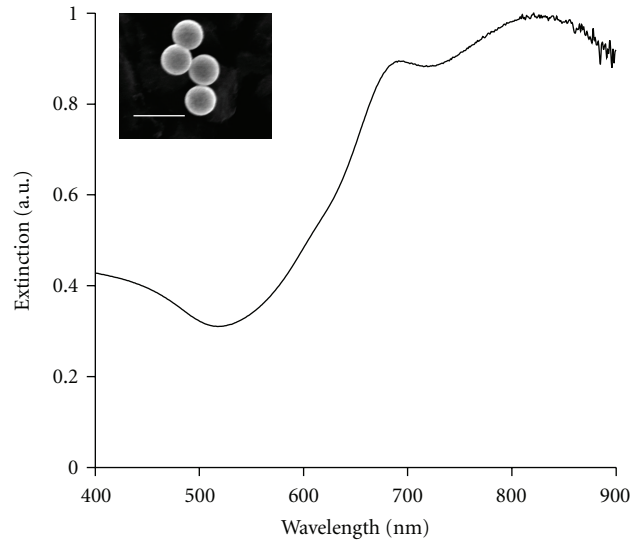

Figure 1: Measured extinction spectra of nanoshells with an average core diameter of 276 nm and average shell thickness of 19 nm. Insert depicts corresponding image from scanning electron microscopy. Scale bar represents 500 nm.

2. Materials and Methods

2.1. Nanoshell Fabrication and Antibody Conjugation. Nanoshells were fabricated as formerly described [18–20], and only a brief summary will be provided here. Silica cores were made using the Stöber method [21], in which tetraethyl orthosilicate was reduced in the presence of ammonium hydroxide dissolved in 200 proof ethanol. The surfaces of the cores were then modified by reaction with aminopropyltriethoxysilane (APTES) to functionalize reactive amine groups on the surface. The final particles were measured by dynamic light scattering (DLS) to have an average diameter of 276 nm. Next, gold colloid (~1–3 nm diameter) was fabricated and adsorbed onto the surface of the silica cores via the amine groups to form gold nucleation sites [22]. To fully cover the surface of the silica cores, additional gold was added to these nucleation sites via a reduction reaction in which hydrogen tetrachloroaurate trihydrate ($HAuCl_4 3H_2O$) was dissolved in potassium carbonate and then added with formaldehyde to help reduce the gold. After the gold layer over the silica cores was formed, the spectrum of the final nanoshell solution was visualized using a UV-VIS spectrophotometer (Varian Cary 300) (Figure 1).

To determine the concentration of nanoshells in solution, the absorption, scattering, and extinction coefficients were

determined using Mie theory. The average nanoshell diameter, as validated by scanning electron microscopy (SEM), was 314 nm with a peak surface plasmon resonance at 840 nm. The concentration of the working nanoshell solution was approximately 2.0×10^9 particles/mL.

Nanoshells were targeted to biological HER2 antigens by linking the surfaces of the nanoshells to anti-HER2 antibodies using previously described methods [18]. Prior to beginning experimental studies, nanoshells were incubated with an anti-HER2-linker cocktail [18] for 2 hours at 4°C. To ensure nanoparticle stabilization in biological media, the nanoshells were next incubated with a 1 mM polyethylene glycolthiol solution (PEG-SH, MW = 5 kD, Nektar) for 12–16 hours at 4°C. Next, unbound antibodies and excess PEG-SH were removed from the nanoshells by centrifugation. Prior to experimental studies, the nanoshells were resuspended in antibody diluent (IHC World, pH 7.4) by gentle pipetting to a final volume of 165 μL.

2.2. Ex Vivo Human Breast Tissue Specimens. Normal and cancerous (HER2-negative and HER2-positive) breast tissue specimens were supplied by the Cooperative Human Tissue Network (CHTN) through a protocol approved by the Institutional Review Board (IRB). Tissues were designated as normal or cancerous by pathologists at the medical centers where the tissue samples were obtained. Additionally, HER2 status was previously determined by pathologists at the respective medical centers prior to the patients undergoing any form of medical treatment.

Before use, samples were thawed briefly in a 37°C water bath and cut on a disposable cutting board using a 5 mm punch biopsy to maintain size consistency. At least two punch biopsies were taken from each specimen for control and experimental conditions. Each cut specimen used was 5 mm in diameter with an average thickness of 1 mm. Tissue samples were subsequently incubated in prewarmed antibody diluent for 1 minute at room temperature with gentle agitation in a 24-well plate. After prerinsing, the samples were incubated in either antibody diluent or the aforementioned targeted-nanoshell cocktail in polyethylene sample vials (Sigma Aldrich). The vials were placed on a nutator in an incubator at 37°C for 5 minutes. After incubation, the tissue samples were removed from the vials and rinsed 3 times in 1x PBS briefly in a 24-well plate. Samples were moved to a clean well of 1x PBS prior to imaging.

2.3. Two-Photon Imaging of Human Breast Tissue Specimens. Both HER2-positive and HER2-negative cancerous samples were evaluated for surface labeling of HER2-targeted nanoshells by employing two-photon imaging of intact breast tissue specimens. Samples were placed directly on a glass coverslip (Fisher Scientific), and an additional coverslip was placed on top of the tissue in order to facilitate moderate tissue compression. For image acquisition, a Zeiss multiphoton confocal microscope (LSM 510 META NLO) was used in tandem with a Coherent Chameleon femtosecond-pulsed, mode-locked Ti: sapphire laser. This system was set to operate as formerly described [23]. Specifically, an excitation wavelength of 780 nm and a power setting of 10% maximum excitation power were used. The collected emission wavelength range was 451–697 nm. Images were collected at a magnification of 20x and a z-stack (depth) increment of 5 μm. In order to calculate the percentage of area covered by nanoshells, ImageJ imaging software was implemented after image acquisition. Recent research has shown that ImageJ can be used to analyze signal intensity of silica-gold nanoshells under different imaging systems [11, 24]. Each pixel in the images had an intensity value in the range of 0–255. To determine the nanoshell level in each image, an intensity threshold of 30 was used to separate areas that did not have nanoshells ($\leq$30) from those that did have nanoshells (>30). The value of 30 was chosen because images of negative controls were found to have a maximum intensity of 30. The number of pixels that were above the threshold value was then used to calculate the area of each image that contained nanoshells.

2.4. Darkfield Hyperspectral Imaging of Human Breast Tissue Slices. To confirm the presence of nanoshells on the surface of the tissues, HER2-positive cancerous, HER2-negative cancerous and normal tissue samples were incubated with nanoshells as previously described. A thin layer of pathological ink was placed on the tissue surface for orientation. The tissues were embedded in OCT media (BBC chemical) and frozen rapidly over dry ice. The specimens were cut at a section thickness of 8 μm using a Leica CM1850 UV cryostat. Cancerous specimens were sectioned at -20°C and normal specimens at -30°C. The different temperatures were used to maintain optimal tissue morphology as recommended by Leica. Additionally, Magalhães et al. reported on the use of different temperatures to slice normal and cancerous tissue [25]. The sections were immediately placed on superfrost slides (Fisher Scientific) and allowed to dry overnight. The next day the tissue slices were imaged with a 10x objective on an Olympus darkfield microscope equipped with a Cytoviva high-resolution illuminator. Hyperspectral images of the tissue slices were taken using a hyperspectral camera that provides both spatial and spectral data for each image.

Spectral data of each field of view (FOV) was used to determine if nanoshells were present on each slice of tissue. Comparisons were made between tissue surfaces and tissue beyond the surfaces to determine the presence of nanoshells; spectral data from tissue that was not incubated with nanoshells was also used as a negative control.

2.5. Macroscopic Imaging of Human Breast Tissue Specimens. Normal and HER2-positive cancerous breast tissue specimens (from patients who had and had not received neoadjuvant chemotherapy) were imaged using a Zeiss Discovery. V8 stereomicroscope equipped with a VisiLED MC1000 light source. For macroscopic imaging of breast tissue specimens, a thin plastic black stage was placed beneath a glass coverslip to enable ease of tissue placement and to provide a consistent black background among all samples. The specimens (controls and respective nanoshell-labeled counterparts) were placed alongside each other on top of the coverslip. Images were taken at both 1x and 2x magnification under the same lighting conditions.

2.6. Reflectance Confocal Microscopy Imaging of Human Breast Tissue Specimens. Following widefield imaging, the aforementioned samples were prepared for microscopic analysis under reflectance confocal microscopy. For this component of the study, a Lucid VivaScope 2500 inverted confocal microscope was used. Samples were placed directly on glass slides that were modified by the addition of an adhesive 1 mm deep, 20 mm diameter silicon isolator (Invitrogen). To compress the tissue slightly and consistently among samples, an adhesive tissue cassette (Lucid, Inc.) was placed directly on top of the silicone isolators above the tissue specimens. Multiple images were taken at a power of 0.4 mW and at the same distance from the glass surface for both samples and controls. After reflectance imaging, the samples were prepared for histological processing. Additionally, reflectance intensity measurements were recorded using ImageJ processing software as formerly described [11].

2.7. Immunohistochemistry and Histology. Once images were collected under both stereomicroscopy and RCM imaging systems, normal and HER2-positive cancerous samples (with and without previous neoadjuvant chemotherapy) were embedded in OCT media and sectioned to a thickness of 5 μm. Multiple sections from each specimen were prepared for either immunohistochemistry (IHC) or hematoxylin and eosin (H&E) staining. IHC for the HER2 antigen was executed using the Histostain Plus AEC Broad Spectrum Kit (Invitrogen) per manufacturer's instructions. H&E staining was also performed per manufacturer's instructions (Sigma Aldrich) for the alcoholic Eosin Y solution. For image acquisition, a standard brightfield microscope (Zeiss Axioskop 2 equipped with a Zeiss Axiocam MRc5 color camera) was used at a magnification of 20x.

3. Results

3.1. Distribution and Penetration of Gold Nanoshells in Intact Human Breast Tissue. The goal of this study was to evaluate the distribution of anti-HER2-conjugated gold nanoshells on resected intact tissue specimens. For comparison, the nanoshell labeling between HER2-positive and HER2-negative tissue samples was evaluated using a two-photon imaging system. As previously reported, this imaging system is capable of enhancing and capturing the luminescence signature of the gold nanoshells [23] while also collecting a stack of images taken through the depth of the tissue of interest. Figure 2 represents such images of HER2-positive and HER2-negative cancerous tissue samples incubated with HER2-targeted nanoshells. Each sequential increment in the z-direction represents 5 μm into the tissue. Qualitatively, the first image (taken at the surface or at 0 μm) in Figure 2 demonstrates that the nanoshells preferentially label HER2 receptors on the surface of the tissue. Additionally, Figure 2 displays decreased signal as the focal spot from the confocal microscope penetrates further into the tissue. This is believed to be due to a minimal number of nanoshells being able to penetrate the tissue in the limited amount of incubation time, thus decreasing signal collected beyond the surface. A quantitative difference of the nanoshell signal at the surface of the HER2-positive and HER2-negative tissue was calculated. Using ImageJ imaging software, it was determined that approximately 66% of the FOV for HER2-positive tissue was covered in nanoshells versus just 2% for the FOV of the HER2-negative tissue. This confirms the preferential labeling and visualization of HER2-positive tissue using anti-HER2 nanoshells.

To further validate the surface binding of the nanoshells, hyperspectral images of different tissue sections were also acquired. Figure 3(a) shows a representative surface of a HER2-positive tissue section after incubation with anti-HER2 nanoshells. Figure 3(b) illustrates tissue 24 μm beyond the surface of the same tissue. Spectra from multiple ($n = 3$) specimens that were incubated with anti-HER2 nanoshells were acquired, and analysis showed that tissues without nanoshells had very similar spectra across different patients. Figure 3(c) displays the respective spectral information of each FOV shown in Figures 3(a) and 3(b). Additionally, the spectra of HER2-positive tissue without nanoshells have been included as a control. As can be seen in this graph, the spectra of the surface of the HER2-positive tissue incubated with anti-HER2 nanoshells are distinctive from that of the same tissue 24 μm beyond the surface. In fact, the spectra of the tissue beyond the surface of the nanoshell-labeled specimen are very similar to the spectra of the surface of the control. These results support our findings that the targeted nanoshells primarily localized to the surface of the tissue.

3.2. Enhanced Optical Imaging of Intact Ex Vivo Human Breast Cancer Tissue Using Gold Nanoshells. Based on previous results demonstrating the preferential labeling of HER2-targeted nanoshells on the surface of intact *ex vivo* HER2-positive tissue specimens, we assessed the potential of using a standard stereomicroscope to visualize this enhanced contrast. For this component of the study, human breast tissue specimens that overexpressed HER2 receptors at the time of patient diagnosis were evaluated and compared to normal breast tissue. Due to the ultimate goal of utilizing gold nanoshells to rapidly label tumor margins intraoperatively in diverse patient populations, we examined tissue from patients who had and had not undergone neoadjuvant chemotherapy. All tissue samples were incubated with either antibody diluent buffer or the anti-HER2-targeted nanoshells for 5 minutes at 37°C. As shown in Figure 4, which represents raw images taken with a stereomicroscope, intact tissue specimens incubated with antibody diluent alone showed no markings or features characteristic of nanoshells. However, tissue specimens incubated with the anti-HER2-targeted nanoshells demonstrate numerous particles on the surfaces of the tissues. Qualitatively, the HER2-positive tissue from the patient who did not undergo previous chemotherapy shows the greatest labeling with the targeted nanoshells. The HER2-positive tissue from the patient who did undergo neoadjuvant chemotherapy does demonstrate enriched nanoshell labeling when compared to normal tissue, though not to the same extent as the patient without previous chemotherapy. In contrast, the normal tissue shows the least amount of nanoshell labeling, and only a few areas of nanoshells can be visually perceived.

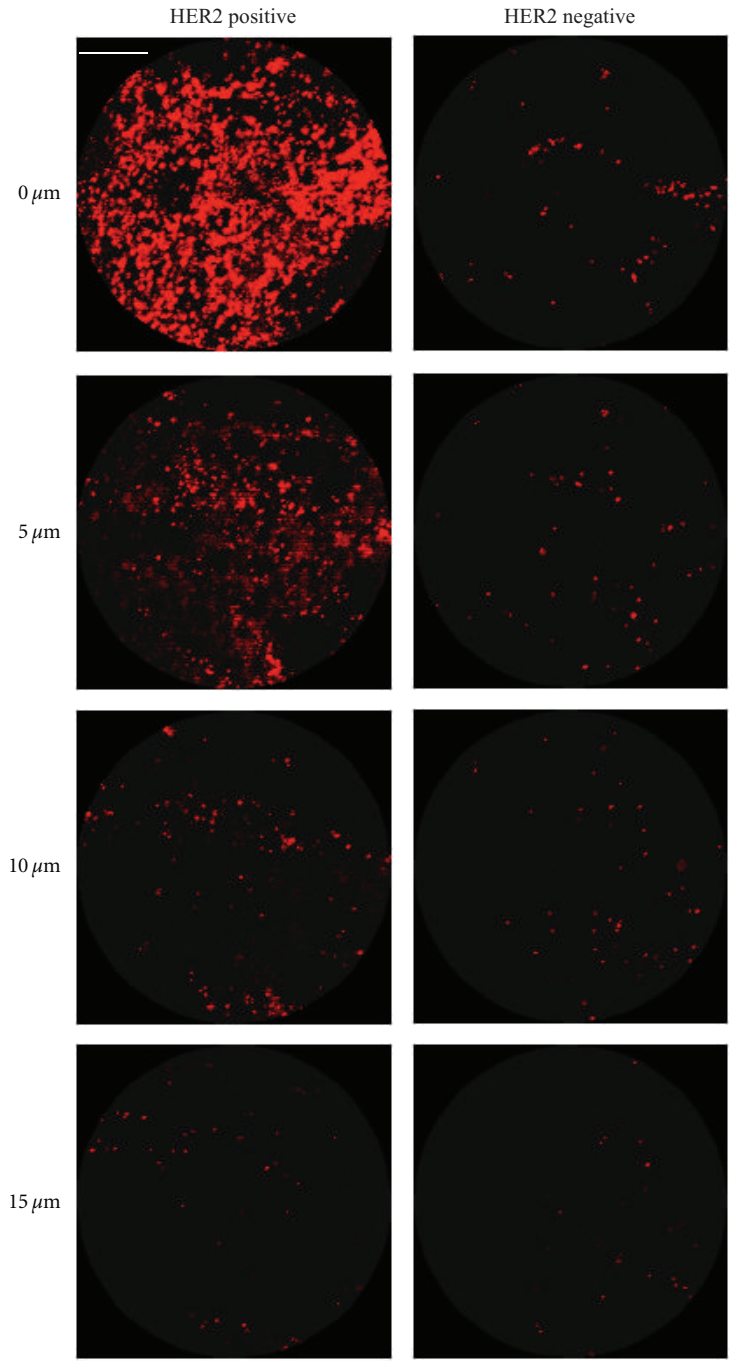

Figure 2: *Z*-stack two-photon luminescence images of HER2-positive and HER2-negative tissue incubated with HER2-targeted nanoshells for 5 minutes at 37°C. Each progressive image represents an increase in depth penetration of 5 μm. Magnification = 20x. Scale bar = 50 μm.

While the degree of nanoshell labeling can be visualized without image adjustments under a standard stereomicroscope, the superior extent of this labeling can be seen more clearly after a simple contrast enhancement using imaging software (ImageJ). As seen in Figure 5(a), the nanoshells are even more discernable against the tissue background regardless of inherent tissue constituents.

To validate the enhanced nanoshell labeling seen by macroscopic imaging, the surfaces of the same tissue samples were also imaged using reflectance confocal microscopy (Figure 5(b)). Concurring with the stereomicroscopic images, we see dramatic nanoshell surface labeling when using targeted nanoshells with previously untreated HER2-positive tissue. For the HER2-positive sample that had formerly undergone chemotherapy, we also see enhanced nanoshell labeling, though to a lesser degree than the untreated sample as suggested by the stereomicroscopy results. The normal breast tissue displays the least amount of

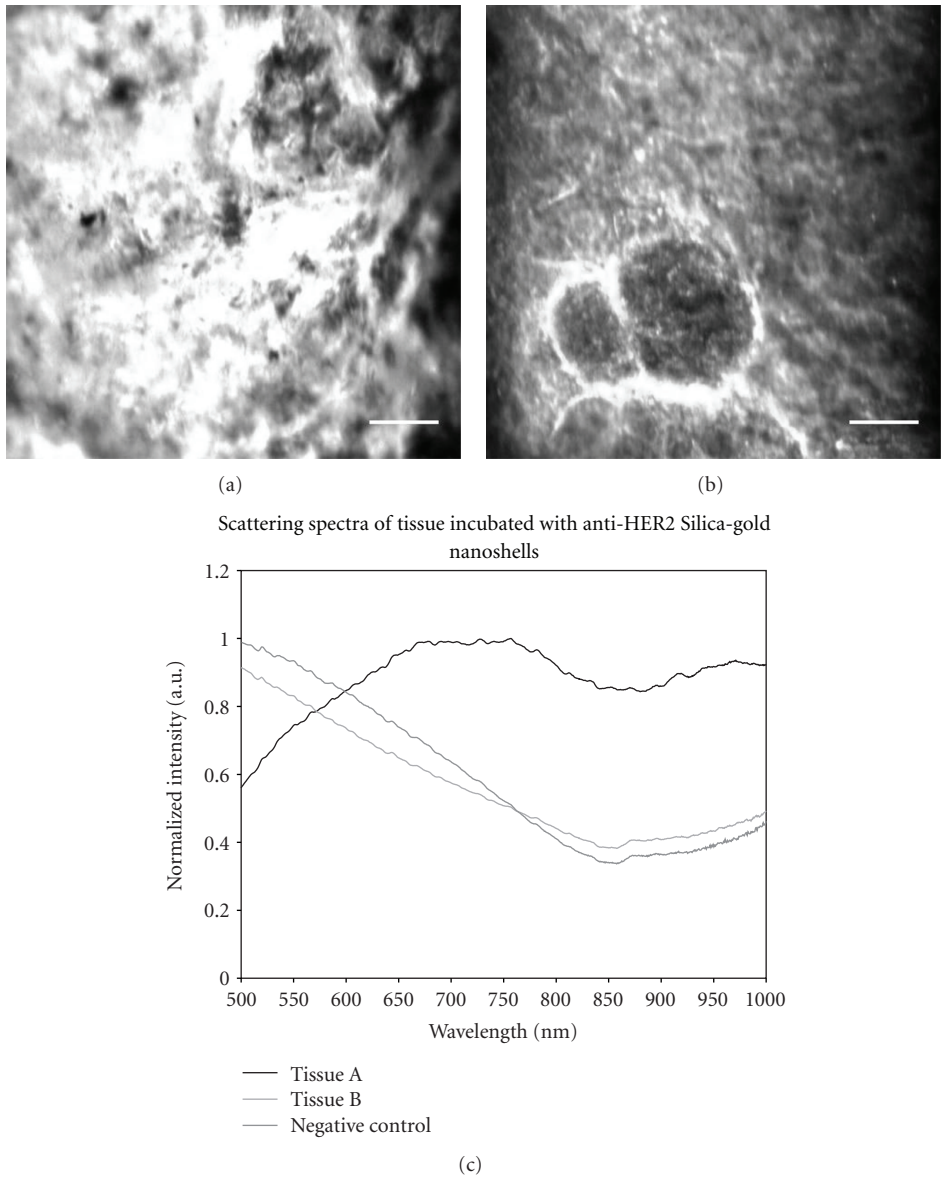

Figure 3: Darkfield images of HER2-positive tissue sectioned after incubation with anti-HER2-targeted silica-gold nanoshells. (a) Surface of HER2-positive tissue, (b) 24 μm beyond the surface of the same tissue. (c) Scattering spectra of the fields of view depicted in (a) and (b). Additionally, spectra from the surface of HER2-positive tissue not incubated with silica-gold nanoshells are shown as a negative control. Scale bar = 50 μm.

surface labeling with only minimal nanoshells evident with either imaging system. Reflectance intensity measurements (data not shown) were ~2.5 to 3 times greater for both the HER2-positive tissue sample receiving chemotherapy and for the HER2-positive tissue not receiving chemotherapy when compared to the normal tissue sample.

Subsequent histological analysis shown in Figure 5(c) reveals that the distribution of HER2 receptors seen with nanoshell-enabled contrast corresponds to that seen with IHC against HER2. The HER2 expression seen by IHC is greater for the previously untreated HER2-positive tissue sample than for the sample that had undergone neoadjuvant chemotherapy. This is believed to be due to the effects of chemotherapy. Rasbridge et al. previously demonstrated that patient response to chemotherapy is highly variable, with patients previously negative for HER2 overexpression occasionally becoming positive after treatment and patients previously positive for HER2 overexpression subsequently becoming negative [26]. Although patient response to chemotherapy varies, tissues previously identified as overexpressing HER2 receptors during initial diagnosis, regardless of chemotherapy exposure, demonstrate enhanced nanoshell labeling over normal tissue. Additionally, H&E-stained sections of all tissue samples have been included (Figure 5(d)) to illustrate the microscopic characteristics and differences associated with cancerous versus noncancerous conditions.

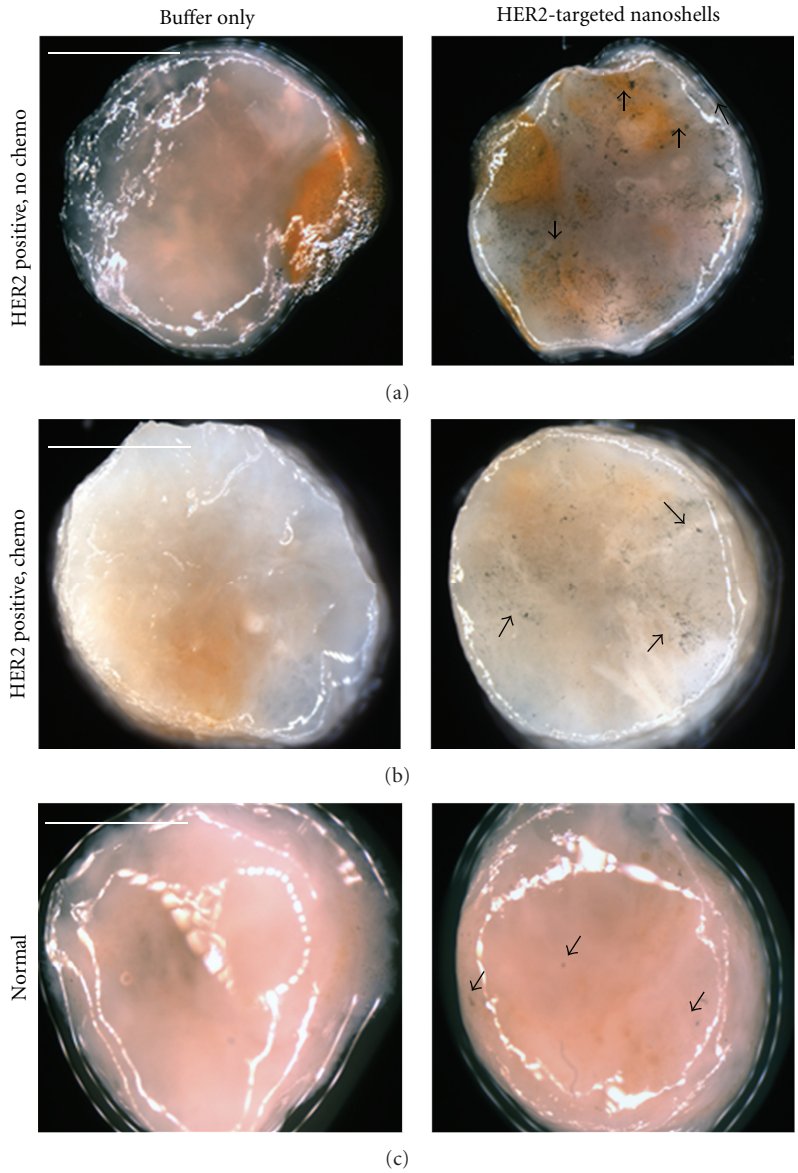

Figure 4: Raw stereomicroscope images of (a) and (b) HER2-overexpressing cancerous and (c) normal tissue incubated with either buffer or HER2-targeted nanoshells for 5 minutes at 37°C. Cancerous tissue taken from a patient (a) without chemotherapy and (b) following neoadjuvant chemotherapy. Arrows represent nanoshells. Images taken at 2x. Scale bars = 2.5 mm.

4. Discussion

In this study we demonstrated the ability to use targeted gold nanoshells to rapidly improve visualization of a specific biomarker associated with disease aggression and progression (HER2) in intact *ex vivo* human breast tissue and confirmed binding location via confocal and darkfield hyperspectral microscopy. By utilizing silica-gold nanoshells designed as rapid diagnostic imaging agents, surgeons and pathologists may be able to realize tumor margin status directly in the operating room after both macroscopic and microscopic assessment. While multiple methods of intraoperative tumor margin detection are currently under investigation [27–31], we are developing an inexpensive and portable system for rapidly analyzing *ex vivo* specimens based on the desire to enhance current methodologies without delay in clinical translation due to regulatory concerns associated with *in vivo* systems.

The ability to enhance contrast of malignancy using topically applied agents has previously been demonstrated for oral and breast tissue using fluorescently labeled deoxyglucose and epidermal growth factor (EGF) conjugates [32–34] as well as cervical tissue using fluorescently labeled gold nanoparticles targeted to EGF receptors [35]. However, these studies employed incubation times ranging from 20–45 minutes, which exceeds the length of time currently needed to obtain tumor margin status using frozen section histology. Additionally, the aforementioned studies utilized

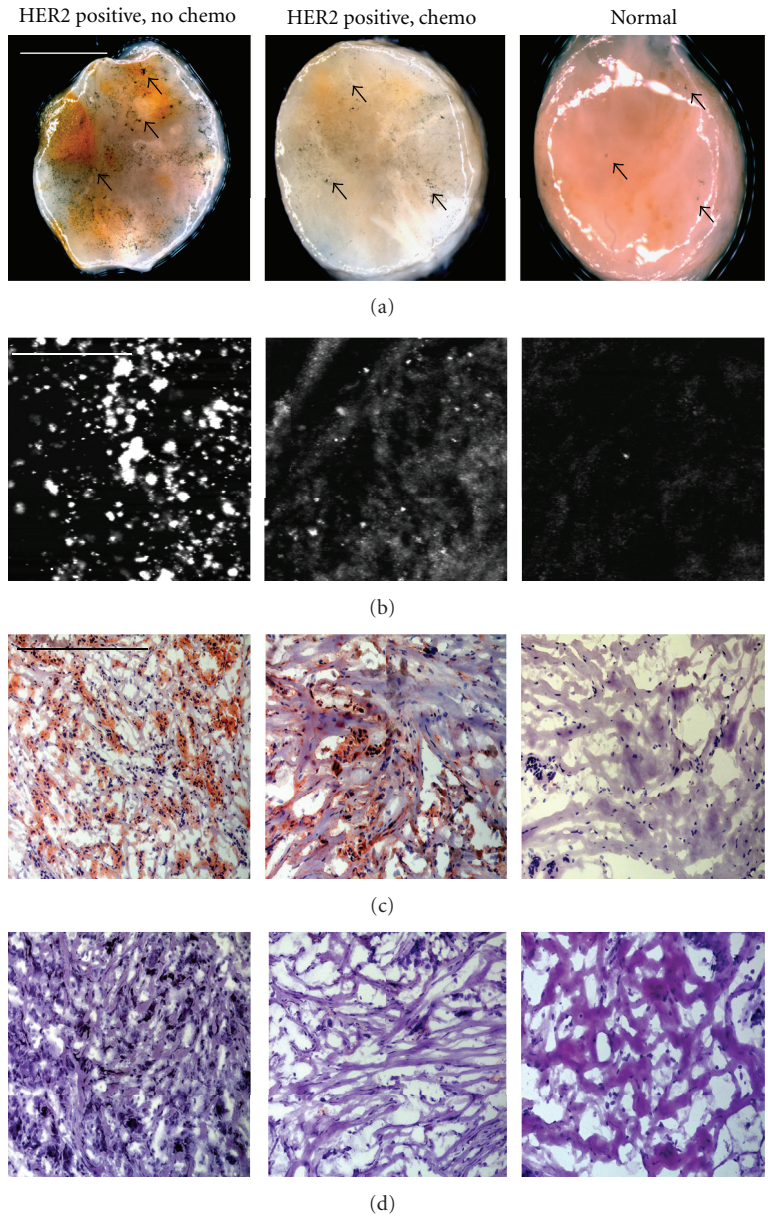

Figure 5: (a) Stereomicroscopic images of HER2-overexpressing breast tissue (with and without neoadjuvant chemotherapy) and normal breast tissue incubated with HER2-targeted nanoshells for 5 minutes at 37°C after contrast enhancement. Magnification at 2x; scale bar = 2.5 mm. Arrows represent nanoshells. (b) Respective reflectance confocal microscopy images of tissue samples from (a). Power = 0.4 mW and scale bar = 75 μm. Respective (c) HER2 immunohistochemistry and (d) H&E results taken under brightfield microscopy under 20x magnification. Scale bar = 0.35 mm.

optical clearing agents, which may be necessary for particles that target intracellular biomarkers [36, 37]. Nevertheless, gold nanoshells targeted to extracellular biomarkers may offer more favorable opportunities for *ex vivo* intraoperative tumor margin detection without the need for lengthy incubation times or the use of optical clearing agents.

Recently, we verified that silica-based gold nanoshells could be used to enhance contrast of both HER2-overexpressing cells and tissue sections within 5 minutes of incubation time [10, 11]. However, translating this technology towards clinical relevancy requires the ability to assess whole, unsectioned specimens. Here, we confirm that gold nanoshells, when targeted to HER2 receptors, can be used to distinguish intact HER2-overexpressing *ex vivo* tissue from normal tissue within the same incubation time, and we demonstrate that this difference can be observed macroscopically. These results are supported by microscopic imaging and immunohistochemistry against HER2.

By employing macroscopic imaging intraoperatively, clinicians may be better able to distinguish cancerous and normal breast tissue prior to further microscopic analysis and subsequent histological processing. Ultimately, this system could also be used for other diagnostic applications, for other anatomical locations, and for other biomarkers

associated with disease. By facilitating fast and accurate tumor margin results intraoperatively as a supplement to current diagnostic methods, we expect to reduce the amount of time spent in surgery due to inadequate tissue removal.

To translate these findings more readily to the clinic, we are presently developing a low-cost widefield imaging system that can be used to detect the overexpression of HER2 (and other extracellular biomarkers) through contrast enhancement provided by gold nanoshells. In addition, we plan to collect data from diverse patient populations and assess results with fresh tissue samples. In this way, the use of gold nanoshells may demonstrate widespread efficacy or be limited only to specific patient subsets.

Authors' Contributions

Bickford and Langsner contributed equally to this work.

Acknowledgments

The authors thank the Cooperative Human Tissue Network for providing fresh frozen tissue samples. The authors thank Glenn P. Goodrich and Nanospectra Biosciences, Inc. for providing nanoshells used in the studies. The authors also thank Nadhi Thekkek for assistance with ImageJ data acquisition. This work was supported by a Department of Defense Congressionally Directed Breast Cancer Research Program Era of Hope Scholar Award to Rebekah Drezek, the Center for Biological and Environmental Nanotechnology (EEC-0118007 and EEC-0647452). L. Bickford thanks the Department of Defense (DoD) for training support through the National Defense Science & Engineering Graduate Fellowship (NDSEG) Program.

References

[1] A. C. Society, "Breast Cancer Facts and Figures 2005-2006," American Cancer Society, Inc., 2010, http://www.cancer.org/Research/CancerFactsFigures/BreastCancerFactsFigures/breast-cancer-facts–figures-2005-2006.

[2] R. G. Steen, *A Conspiracy of Cells*, Plenum Press, New York, NY, USA, 1993.

[3] C. M. Mojica, R. Bastani, W. J. Boscardin, and N. A. Ponce, "Low-income women with breast abnormalities: system predictors of timely diagnostic resolution," *Cancer Control*, vol. 14, no. 2, pp. 176–182, 2007.

[4] B. Fisher, S. Anderson, J. Bryant et al., "Twenty-year follow-up of a randomized trial comparing total mastectomy, lumpectomy, and lumpectomy plus irradiation for the treatment of invasive breast cancer," *The New England Journal of Medicine*, vol. 347, no. 16, pp. 1233–1241, 2002.

[5] R. G. Pleijhuis, M. Graafland, J. de Vries, J. Bart, J. S. de Jong, and G. M. van Dam, "Obtaining adequate surgical margins in breast-conserving therapy for patients with early-stage breast cancer: current modalities and future directions," *Annals of Surgical Oncology*, vol. 16, no. 10, pp. 2717–2730, 2009.

[6] A. Oouchi, K. I. Sakata, H. Masuoka et al., "The treatment outcome of patients undergoing breast-conserving therapy: the clinical role of postoperative radiotherapy," *Breast Cancer*, vol. 16, no. 1, pp. 49–57, 2009.

[7] C. S. Melanie, W. N. Kent, J. Z. Mark et al., "The importance of the lumpectomy surgical margin status in long term results of breast conservation," *Cancer*, vol. 76, pp. 259–267, 1995.

[8] N. Cabioglu, K. K. Hunt, A. A. Sahin et al., "Role for intraoperative margin assessment in patients undergoing breast-conserving surgery," *Annals of Surgical Oncology*, vol. 14, no. 4, pp. 1458–1471, 2007.

[9] R. A. Graham, M. J. Homer, C. J. Sigler et al., "The efficacy of specimen radiography in evaluating the surgical margins of impalpable breast carcinoma," *American Journal of Roentgenology*, vol. 162, no. 1, pp. 33–36, 1994.

[10] L. R. Bickford, J. Chang, K. Fu et al., "Evaluation of immunotargeted gold nanoshells as rapid diagnostic imaging agents for HER2-overexpressing breast cancer cells: a time-based analysis," *Nanobiotechnology*, vol. 4, no. 1–4, pp. 1–8, 2008.

[11] L. R. Bickford, G. Agollah, R. Drezek, and T.-K. K. Yu, "Silica-gold nanoshells as potential intraoperative molecular probes for HER2-overexpression in ex vivo breast tissue using near-infrared reflectance confocal microscopy," *Breast Cancer Research and Treatment*, vol. 120, no. 3, pp. 547–555, 2010.

[12] K. Sokolov, M. Follen, J. Aaron et al., "Real-time vital optical imaging of precancer using anti-epidermal growth factor receptor antibodies conjugated to gold nanoparticles," *Cancer Research*, vol. 63, no. 9, pp. 1999–2004, 2003.

[13] X. Liu, Q. Dai, L. Austin et al., "A one-step homogeneous immunoassay for cancer biomarker detection using gold nanoparticle probes coupled with dynamic light scattering," *Journal of the American Chemical Society*, vol. 130, no. 9, pp. 2780–2782, 2008.

[14] R. Nahta, D. Yu, M. C. Hung, G. N. Hortobagyi, and F. J. Esteva, "Mechanisms of disease: understanding resistance to HER2-targeted therapy in human breast cancer," *Nature Clinical Practice. Oncology*, vol. 3, no. 5, pp. 269–280, 2006.

[15] D. J. Slamon, G. M. Clark, S. G. Wong, W. J. Levin, A. Ullrich, and W. L. McGuire, "Human breast cancer: correlation of relapse and survival with amplification of the HER-2/neu oncogene," *Science*, vol. 235, no. 4785, pp. 177–182, 1987.

[16] D. G. Hicks and S. Kulkarni, "HER2+ breast cancer," *American Journal of Clinical Pathology*, vol. 129, pp. 263–273, 2008.

[17] S. Vosoughhosseini, M. Lotfi, A. Fakhrjou et al., "Analysis of epidermal growth factor receptor in histopathologically tumor-free surgical margins in patients with oral squamous cell carcinoma," *African Journal of Biotechnology*, vol. 11, pp. 516–520, 2012.

[18] C. Loo, A. Lin, L. Hirsch et al., "Nanoshell-enabled photonics-based imaging and therapy of cancer," *Technology in Cancer Research and Treatment*, vol. 3, no. 1, pp. 33–40, 2004.

[19] C. Loo, L. Hirsch, M. H. Lee et al., "Gold nanoshell bioconjugates for molecular imaging in living cells," *Optics Letters*, vol. 30, no. 9, pp. 1012–1014, 2005.

[20] C. Loo, A. Lowery, N. Halas, J. West, and R. Drezek, "Immunotargeted nanoshells for integrated cancer imaging and therapy," *Nano Letters*, vol. 5, no. 4, pp. 709–711, 2005.

[21] W. Stöber, A. Fink, and E. Bohn, "Controlled growth of monodisperse silica spheres in the micron size range," *Journal of Colloid and Interface Science*, vol. 26, no. 1, pp. 62–69, 1968.

[22] D. G. Duff, A. Baiker, and P. P. Edwards, "A new hydrosol of gold clusters. 1. Formation and particle size variation," *Langmuir*, vol. 9, no. 9, pp. 2301–2309, 1993.

[23] L. Bickford, J. Sun, K. Fu et al., "Enhanced multi-spectral imaging of live breast cancer cells using immunotargeted gold nanoshells and two-photon excitation microscopy," *Nanotechnology*, vol. 19, no. 31, Article ID 315102, 2008.

[24] E. S. Day, L. R. Bickford, J. H. Slater, N. S. Riggall, R. A. Drezek, and J. L. West, "Antibody-conjugated gold-gold sulfide nanoparticles as multifunctional agents for imaging and therapy of breast cancer," *International Journal of Nanomedicine*, vol. 5, no. 1, pp. 445–454, 2010.

[25] T. Magalhães, A. von Bohlen, M. L. Carvalho, and M. Becker, "Trace elements in human cancerous and healthy tissues from the same individual: a comparative study by TXRF and EDXRF," *Spectrochimica Acta B*, vol. 61, no. 10-11, pp. 1185–1193, 2006.

[26] S. A. Rasbridge, C. E. Gillett, A. M. Seymour et al., "The effects of chemotherapy on morphology, cellular proliferation, apoptosis and oncoprotein expression in primary breast carcinoma," *British Journal of Cancer*, vol. 70, no. 2, pp. 335–341, 1994.

[27] A. Haid, M. Knauer, S. Dunzinger et al., "Intra-operative sonography: a valuable aid during breast-conserving surgery for occult breast cancer," *Annals of Surgical Oncology*, vol. 14, no. 11, pp. 3090–3101, 2007.

[28] T. Karni, I. Pappo, J. Sandbank et al., "A device for real-time, intraoperative margin assessment in breast-conservation surgery," *American Journal of Surgery*, vol. 194, no. 4, pp. 467–473, 2007.

[29] L. Tafra, R. Fine, P. Whitworth et al., "Prospective randomized study comparing cryo-assisted and needle-wire localization of ultrasound-visible breast tumors," *American Journal of Surgery*, vol. 192, no. 4, pp. 462–470, 2006.

[30] M. Bakhshandeh, S. O. Tutuncuoglu, G. Fischer, and S. Masood, "Use of imprint cytology for assessment of surgical margins in lumpectomy specimens of breast cancer patients," *Diagnostic Cytopathology*, vol. 35, no. 10, pp. 656–659, 2007.

[31] N. Nitin, L. C. Alicia, M. Tim et al., "Molecular imaging of glucose uptake in oral neoplasia following topical application of fluorescently labeled deoxy-glucose," *International Journal of Cancer*, vol. 124, no. 11, pp. 2634–2642, 2009.

[32] V. E. Strong, J. Humm, P. Russo et al., "A novel method to localize antibody-targeted cancer deposits intraoperatively using handheld PET beta and gamma probes," *Surgical Endoscopy and Other Interventional Techniques*, vol. 22, no. 2, pp. 386–391, 2008.

[33] R. J. Langsner, L. P. Middleton, J. Sun et al., "Wide-field imaging of fluorescent deoxy-glucose in ex vivo malignant and normal breast tissue," *Biomedical Optics Express*, vol. 2, no. 6, pp. 1514–1523, 2011.

[34] N. Nitin, K. J. Rosbach, A. El-Naggar, M. Williams, A. Gillenwaterand, and R. R. Richards-Kortum, "Optical molecular imaging of epidermal growth factor receptor expression to improve detection of oral neoplasia," *Neoplasia*, vol. 11, no. 6, pp. 542–551, 2009.

[35] J. Aaron, N. Nitin, K. Travis et al., "Plasmon resonance coupling of metal nanoparticles for molecular imaging of carcinogenesis in vivo," *Journal of Biomedical Optics*, vol. 12, no. 3, Article ID 034007, 2007.

[36] A. L. van de Ven, K. Adler-Storthz, and R. Richards-Kortum, "Delivery of optical contrast agents using Triton-X100, part 1: reversible permeabilization of live cells for intracellular labeling," *Journal of Biomedical Pptics*, vol. 14, no. 2, Article ID 021012, 2009.

[37] A. L. van de Ven, K. Adler-Storthz, and R. Richards-Kortum, "Delivery of optical contrast agents using Triton-X100, part 2: enhanced mucosal permeation for the detection of cancer biomarkers," *Journal of biomedical optics*, vol. 14, no. 2, Article ID 021013, 2009.

Hindawi Publishing Corporation
Journal of Oncology
Volume 2012, Article ID 605076, 7 pages
doi:10.1155/2012/605076

Research Article

Analytical Study of the Effect of the System Geometry on Photon Sensitivity and Depth of Interaction of Positron Emission Mammography

Pablo Aguiar[1,2] and Cristina Lois[2]

[1] *Nuclear Medicine Department (IDICHUS), 15706 Santiago de Compostela, Spain*
[2] *Molecular Imaging Group (IDIS), 15706 Santiago de Compostela, Spain*

Correspondence should be addressed to Pablo Aguiar, pablo.aguiar.fernandez@sergas.es

Received 14 June 2012; Revised 6 July 2012; Accepted 9 July 2012

Academic Editor: Alvaro Ruibal

Copyright © 2012 P. Aguiar and C. Lois. This is an open access article distributed under the Creative Commons Attribution License, which permits unrestricted use, distribution, and reproduction in any medium, provided the original work is properly cited.

Positron emission mammography (PEM) cameras are novel-dedicated PET systems optimized to image the breast. For these cameras it is essential to achieve an optimum trade-off between sensitivity and spatial resolution and therefore the main challenge for the novel cameras is to improve the sensitivity without degrading the spatial resolution. We carry out an analytical study of the effect of the different detector geometries on the photon sensitivity and the angle of incidence of the detected photons which is related to the DOI effect and therefore to the intrinsic spatial resolution. To this end, dual head detectors were compared to box and different polygon-detector configurations. Our results showed that higher sensitivity and uniformity were found for box and polygon-detector configurations compared to dual-head cameras. Thus, the optimal configuration in terms of sensitivity is a PEM scanner based on a polygon of twelve (dodecagon) or more detectors. We have shown that this configuration is clearly superior to dual-head detectors and slightly higher than box, octagon, and hexagon detectors. Nevertheless, DOI effects are increased for this configuration compared to dual head and box scanners and therefore an accurate compensation for this effect is required.

1. Introduction

Breast cancer is one of the most commonly diagnosed cancers and one of the leading causes of cancer related deaths in women [1]. Early detection of the disease can improve the treatment effectiveness and often also the patient's quality of life. A number of imaging techniques can be used to aid in the diagnosis and staging of breast cancer, being anatomical imaging techniques such as X-ray mammography, ultrasonography, and magnetic resonance imaging (MRI) the most employed [2–4]. However, these techniques are affected by two factors that limit their effectiveness: breast density and the woman's hormonal status [5, 6]. Because of these limitations, many women with suspicious breast masses have to undergo invasive breast biopsies for accurate diagnosis.

Metabolical imaging techniques such as positron emission tomography (PET) are increasingly being used in oncology [7]. PET is not affected by the limiting factors mentioned above and it has been shown to be more accurate in differentiating cancerous and benign breast lesions than the anatomical techniques alone [8]. Thus, PET potentially translates into reduction in unnecessary breast biopsies, which could significantly lower costs associated with breast cancer detection and staging, and reduce patient trauma.

Positron emission mammography (PEM) cameras are novel-dedicated PET systems optimized to image the breast. By reconstructing the radiotracer distribution inside the breast, tomographic images of breast lesions are obtained in a noninvasive procedure. Compared to conventional whole-body PET systems, PEM cameras cover a smaller field of view that is limited to a single breast. The detectors are arranged around the breast so that their performance can be higher at a lower cost. The photon sensitivity of a PET system is related to the ratio between detected and emitted photons (i.e., detected counts and injected activity) and is mainly determined by the system geometry and the type and volume

(thickness) of the detector. Thus, the sensitivity is increased in PEM cameras compared to conventional PET due to the proximity of the detectors to the breast. Due to this, gamma rays penetrate a significant distance into the detector before detection. This distance is called depth of interaction (DOI) and it can produce an uncertainty in the calculation of the photon interaction point. This intrinsic uncertainty is also related to the positron range, photon noncollinearity, [9], and the tomographic reconstruction algorithm [10] which are the limiting factors of the spatial resolution of PET and PEM systems [11]. For conventional PET scanners the DOI effect is limited by using a relatively large detector diameter and a FOV close to the system center.

In breast PET cameras, it is essential to achieve an optimum trade-off between sensitivity and spatial resolution. Therefore the main challenge for the novel cameras is to improve the sensitivity without degrading the spatial resolution. Due to this, to increase the sensitivity by arranging the detectors closer to the breast, the DOI has to be measured and then its effects corrected, avoiding mis-positioning errors that decrease the spatial resolution. Recently, several studies described a number of detector designs with DOI information and different correction methods [12–15]. In general, when the photons reach the detector surface with small angles of incidence or close to the perpendicular direction, the DOI effects can be accurately corrected. By contrast, when the angle of incident is higher and the photons reach the detector surface close to the parallel direction, the DOI correction is often less accurate.

In last years, an increasing number of PEM prototypes and commercial systems were proposed [16–19] using very different detector geometries. Although all proposed PEM scanners offer significantly higher sensitivity than conventional PET, different performance between the proposed PEM scanner geometries can be found. In general, a PEM scanner consists of a bed and a gantry supporting the detectors. Several PEM scanners can be defined based on the arrangements of panel detectors. Firstly, scanners can have four panel detectors (in a box configuration) or only two detectors (dual head). A second class of PET scanners can include polygonal or even ring arrangements of several panel detectors which are fixed cameras, that is, the rotation is not necessary to acquire all angles.

The understanding of the properties of the detection systems used in PEM systems is essential for establishing appropriate operating criteria or designing schemes. In PET and PEM, two gamma photons (511 keV) from a positron-electron annihilation process are detected by means of a scintillator material. This material involves the conversion of the photon pair into visible light. Due to that the scintillator is optically coupled to a photomultiplier tube (PMT) the visible light can be converted to an electrical signal. This information is used to compute the spatial location of the photon interactions (photon interaction point) and the total energy deposited. When two photons from the same annihilation are detected in time coincidence then a line-of-response (LOR) can be defined and an event useful for the tomographic reconstruction is recorded. Nevertheless, some photons may escape after depositing only part of their energy into the crystal or even without interacting so that the event may be lost. The probability that a photon is detected depends on the scintillation material used and the crystal thickness.

Several authors have investigated the relation between the performance of a PEM scanner and its detector geometry configuration. Thus, Moses and Qi [20] carried out a comparison between the most common geometry based on a pair of parallel detector planes (dual head) and a rectangular box detector configuration. The results showed that the box geometry encircling the breast had better performance than the dual head detector as long as the DOI effect is compensated. More recently, Habte et al. [21] studied in detail the performance of different detector configurations using Monte Carlo simulation. Simulation results showed that the best performance was found for a PET scanner built from detectors arranged into a box-shaped geometry. The sensitivity for the box detector geometry was even higher than other geometries based on polygonal detectors encircling the breast. This is because when the detectors are arranged into a cylindrical system a significant number of intermodule gaps is produced by the rectangular-shaped detectors. This gaps provide a path for some photons escape.

In this paper, we carry out an analytical study of the effect of different detector geometries on the photon sensitivity and on the angle of incidence of the detected photons which is related to the DOI effect. To this end, dual-head detectors are compared to box and different polygon detector configurations including rectangular parallelepiped crystals filling the intermodule gaps in order to avoid the drawback of these scanner geometries.

2. Material and Methods

2.1. Detection Systems. The most common PEM scanner geometry based on dual head detectors was compared to other geometries encircling the breast that included box and polygonal arrangements of panel detectors. As reported by Habte et al. [21], the drawback of these scanner geometries based on detectors formed into a cylindrical system configuration is that produce gaps which a decrease of the system sensitivity. In this regard, the gaps effect is increased when the number of detector modules of the scanner configuration is increased and it is lower for box configuration than for other detector configuration based on polygons of more sides. In order to avoid the gaps effect, we use rectangular parallelepiped detector modules filling the inter-module gaps. As it is shown in Figure 1 the use of these crystals can fill in the gaps with additional material that allows the detection of Compton-scattered photons.

Figure 2 shows the different arrangements based on polygons (hexagon, octagon and dodecagon), four detectors (box) and two detectors considered for our purpose. Polygonal and box configurations are built by using parallelepiped detector modules. The distance between opposing detectors is 200 mm.

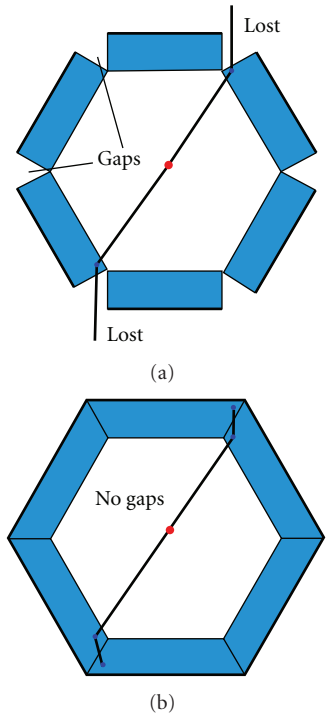

Figure 1: Effect of intermodule wedge-shaped gaps (a) with respect to a camera with filled gaps (b).

The configuration based on two detectors makes possible to decrease this distance and therefore distances of 200 mm, 100 mm, 50 mm, and 25 mm are also considered.

2.2. Physical Performance of PET Scanners. The physical performance of a PET scanner can be studied by using different parameters.

2.2.1. Sensitivity. Sensitivity of a PET scanner is defined as the rate in counts per second between detected true coincidence events and a given source activity. It depends on the material used as scintillator crystal, the geometry of the arrangements of the detectors, the energy threshold, and the time coincidence window.

2.2.2. Uniformity. Uniformity is defined as the maximum relative deviation of counts obtained from an acquisition by using an extended uniform source. It depends on multiple factors such as PMT performance, inhomogeneities of the scintillator crystal, or changes in sensitivity along the FOV.

2.2.3. Spatial Resolution. Spatial resolution of a PET scanner is defined as its ability to distinguish between two points after image reconstruction, that is, it is the distance between adjacent detection points. The spatial resolution can be characterized by the full width half maximum (FWHM) in mm of the image of a point source in air. It depends on the interaction point estimation (intrinsic spatial resolution) and the tomographic reconstruction algorithm.

2.3. Analytical Estimation of Photon Sensitivity. The photon sensitivity of a PET system is determined by the intrinsic efficiency (E_i) that is related to the detector material, the geometric efficiency (E_g) that is related to the detector configuration, and the threshold (E_{th}) related to the energy and coincidence windows:

$$S_{\text{PET}} = E_i \cdot E_g \cdot E_{\text{th}}. \tag{1}$$

2.3.1. Intrinsic Efficiency. E_i is the average intrinsic photon stopping efficiency and it is defined as the probability that two annihilation photons traversing the detector material are absorbed. It is given as the squared of the single efficiency of detecting each photon (E_{i1} and E_{i2}):

$$E_i = E_{i1} \cdot E_{i2} = \left(1 - e^{-\mu(E_1)\cdot x_1}\right) \cdot \left(1 - e^{-\mu(E_2)\cdot x_2}\right), \tag{2}$$

where x_1 (and x_2) is the thickness of the crystal traversed along the incident line of each photon. It depends on the angle of incidence θ of the each incoming photon: for perpendicular photon incidence x_1 is equal to the detector thickness; for all other photon incidences ($\theta > 0$) it is higher than the detector thickness. Finally, $\mu(E_1)$ (and $\mu(E_2)$) is the total linear attenuation coefficient (photoelectric and Compton scatter) of the crystal material at the each incoming photon energy. It depends on the photon energy but also on the density and atomic number of the detector material.

Figure 3 shows the distribution of photon interaction points of a high number of incoming photons of 511 keV for LYSO crystal blocks of $200 \times 200 \times 20\,\text{mm}^3$ which are considered for our evaluation. This material possesses excellent characteristics for detecting 511 keV photons such as the atomic number ($Z = 65$), the density ($d = 7.1\,\text{g/cm}^3$), and the attenuation coefficient is ($\mu = 0.83\,\text{cm}^{-1}$).

2.3.2. Geometric Efficiency. E_g is the total solid angle coverage of the detectors and it is defined as the probability that two annihilation photons intercept the detector area. The total solid angle fractional coverage (Ω) of the system is given as follows:

$$E_g = \frac{\Omega}{4\pi} = \frac{\iint \vec{r} \cdot d\vec{S}}{4\pi\pi^2}, \tag{3}$$

where r is the distance from the image point to the detector bin (higher efficiency is obtained for image points placed close to the detector) and dS is the surface normal vector of an infinitesimal area of the detector (Figure 4).

An estimation of the total solid angle (Ω) can be obtained by dividing the area of each detector into finite detector elements so that E_g is calculated as follows:

$$E_g = \sum_{i=1}^{i=n\,\text{bins}} \frac{\cos(\theta\theta \cdot \Delta S)}{4\pi\pi^2}, \tag{4}$$

where θ is the angle of incidence ($\theta = 0^\circ$ corresponds to an incident photon perpendicular to the detector surface and $\theta = 90^\circ$ to an incident photon parallel to the detector surface) and ΔS is the area of the finite detector element.

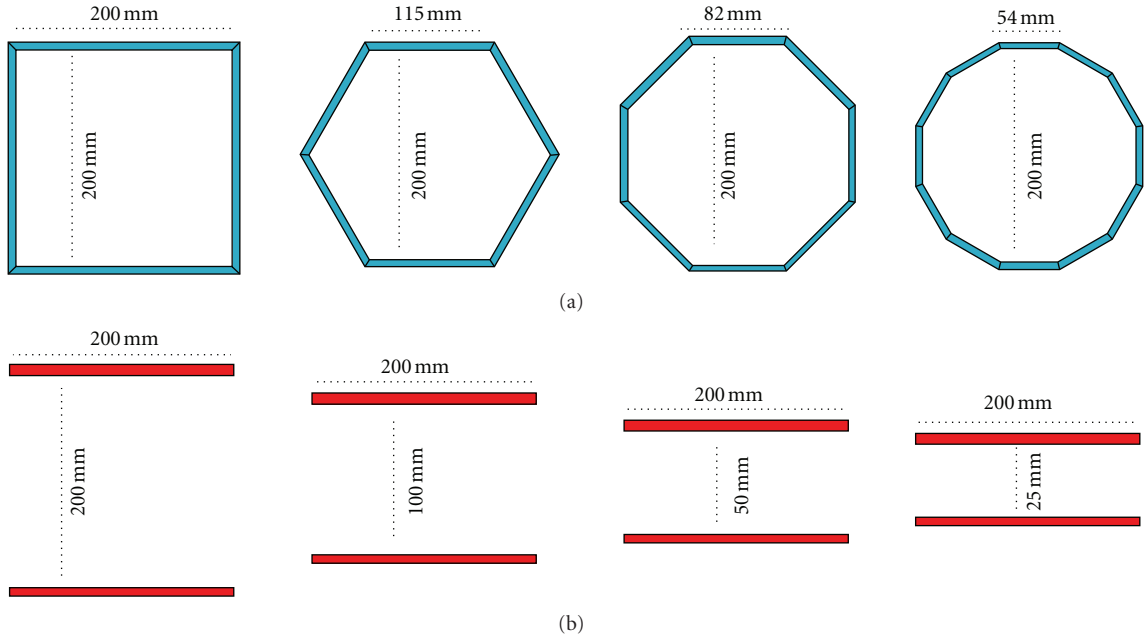

Figure 2: Different arrangements of panel detectors for a PEM scanner. They are based on polygons (a) and different two detectors schemes (b).

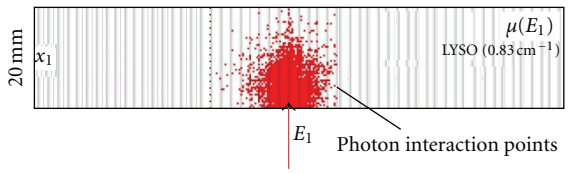

Figure 3: Intrinsic efficiency.

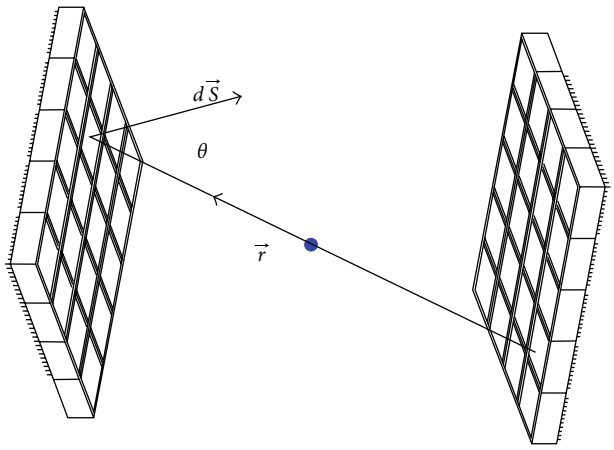

Figure 4: Analytical estimation of the geometric efficiency.

2.4. Angle of Incidence. As can be observed in Figure 5, many photons penetrate a significant distance into the detectors before they are detected. This distance is called depth of interaction (DOI). Due to the proximity of the detectors to the breast the angle of incidence θ can be very high and therefore this effect can cause a deterioration of the intrinsic spatial resolution.

If the incoming photon direction or angle of incidence is θ and the DOI is d_{DOI} then the mis-positioning of the photon interaction point with respect to the real position is estimated as follows:

$$\Delta = d_{\text{DOI}} \cdot \sin(\theta). \tag{5}$$

The mis-positioning originated from the DOI effect is obtained for the different detector configurations in order to evaluate the need of accurate methods to compensate this effect.

Table 1: Sensitivity at a centered point for a distance of 200 mm between opposing detectors.

Configuration	Sensitivity at center
Dual detector	8.4%
Box detector	33.3%
Hexagon detector	34.0%
Octagon detector	34.2%
Dodecagon detector	34.5%

3. Results and Discussion

3.1. Photon Sensitivity. The photon sensitivity at a centered point was obtained for the different detector arrangements and it is shown in Table 1. The different PEM scanner geometries considered were dual, box, hexagon, octagon, and dodecagon configurations with a distance of 200 mm between opposing detectors such as shown in Figure 2. The photon sensitivities were obtained without considering

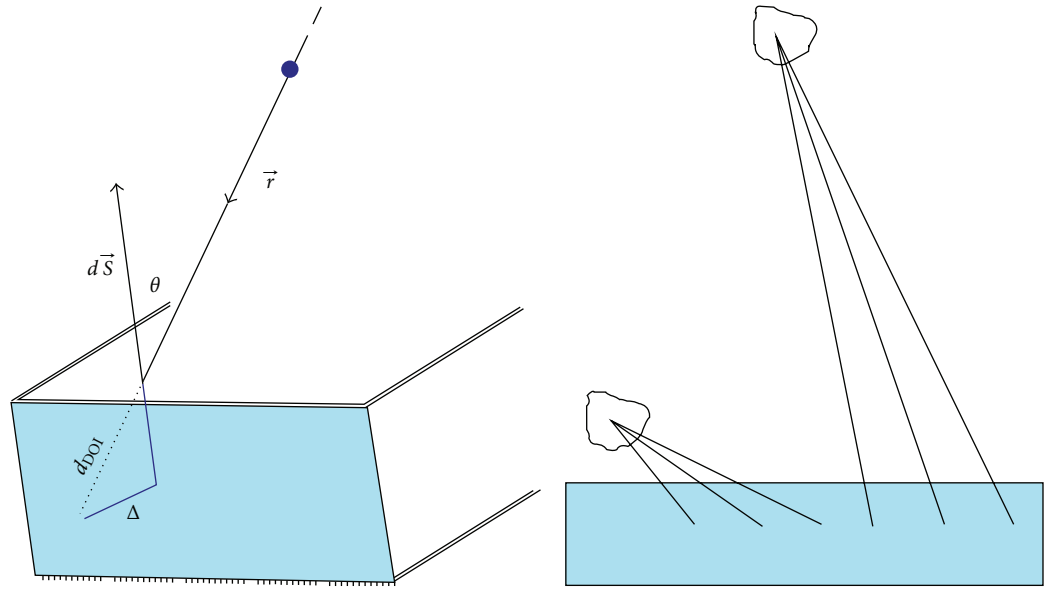

Figure 5: DOI and mis-positioning (Δ) in photon interaction point (a). This effect increases with the proximity of the detectors to the breast, due to that the angle of incidence is increased (b).

Table 2: Sensitivity at a centered point for dual head cameras for different distances between opposing detectors.

Distance (FOV)	Sensitivity at center
200 mm	8.4%
100 mm	14.8%
50 mm	19.6%
25 mm	22.2%

the threshold (E_{th}) related to the energy and coincidence windows. As expected, higher sensitivity was obtained for box and the different polygon detectors compared to the sensitivity of dual detector configuration. This is because the dual detector configuration does not completely close the ring around the object. No significant differences were found between the box detector and the different polygon detector configurations. This is because of the fact that there are not intermodule gaps as in the results shown by Habte et al. [21] and therefore the only differences between box and polygon configurations come from the term in E_g formula related to the angle of incidence.

Although the dual head configuration showed a lower sensitivity than the polygon configurations it has the advantage that the distance between opposing detectors can be decreased in order to adapt it to the object size. This is particularly interesting due to the variable size of breast in women. Thus, the distance between opposing detector can be decreased for small breast. This is clearly an advantage of dual head cameras with respect to fixed cameras. Table 2 shows that the sensitivity at a centered point increases when the distance between opposing detectors is decreased.

3.2. Uniformity. Figure 6 shows the uniformity in terms of the sensitivity changes along the FOV for dual head and polygon (dodecagon) cameras. These sensitivity images were obtained for a distance of 200 mm between opposing detectors such as shown in Figure 2. The sensitivity is clearly more uniform for polygon configuration compared to the sensitivity for dual-head cameras. This means that the signal-to-noise ratio in the reconstructed image for polygon scanners will be similar for each point of the FOV. Nevertheless the signal-to-noise ratio will be higher for central points and decreases towards the limits of the FOV for dual-head cameras. This different behaviour can be seen in Figure 7 that shows the transverse sensitivity profile along the FOV for dual-head and polygon cameras.

3.3. DOI and Intrinsic Spatial Resolution. The averaged mis-positioning of the photon interaction point due to the DOI effect at a centered point is shown in Table 3 for the different scanner geometries. For the dual detector configuration the mis-positioning increased when the distance between opposing detector is decreased. For the box detector configuration the mis-positioning was slightly lower than for the different polygon detectors. No significant differences were found between the various polygon detectors. The averaged mis-positioning values at the edge of the FOV were lower than the mis-positioning values at the center of the FOV for all geometries but for the box configuration. Very high maximum mis-positioning values were found for all geometries at center and edge of the FOV.

These results show a significant effect of the DOI on the mis-positioning of the photon interaction point and therefore on the intrinsic spatial resolution for all detector geometries. Furthermore, this becomes an essential issue to

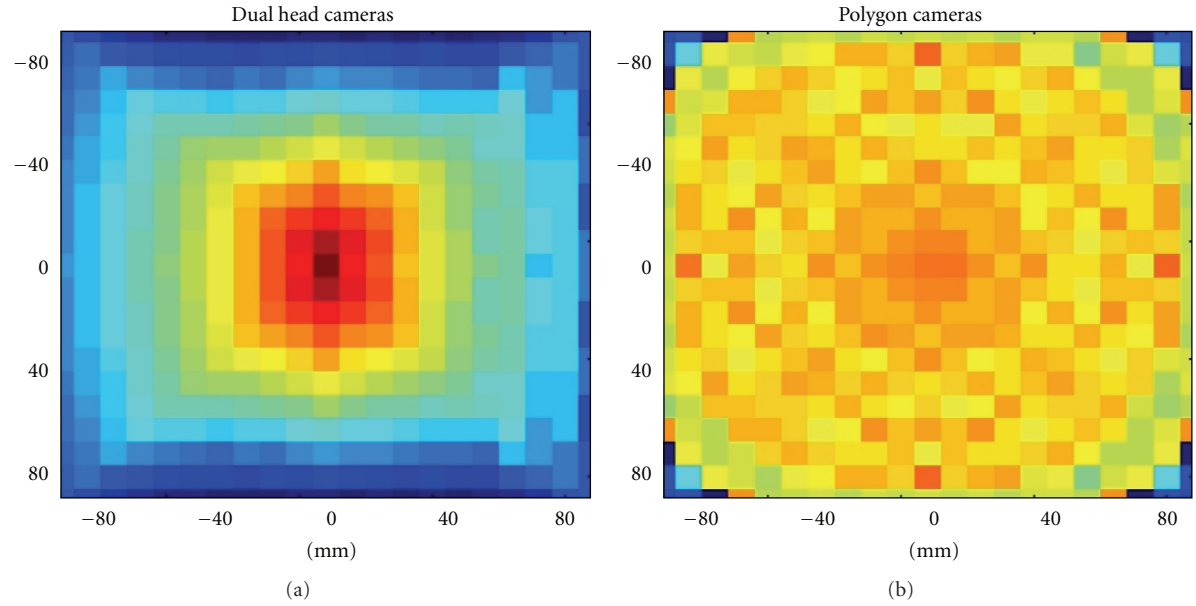

Figure 6: Sensitivity along the FOV for dual-head cameras (a) and polygon cameras (b).

Table 3: Mis-positioning of the photon interaction point due to the DOI effect at center and edge (80 mm) of the FOV.

Configuration	FOV (mm)	Mis-positioning center FOV (mm)		Mis-positioning edge FOV (mm)	
		Averaged	Maximum	Averaged	Maximum
Dual detector	200	2.9	8.1	1.9	5.8
	100	4.0	9.4	2.6	6.7
	50	4.6	9.8	3.0	7.0
	25	4.8	10.0	3.1	7.1
Box detector	200	3.8	8.1	4.1	9.7
Hexagon detector	200	5.0	7.5	2.9	9.2
Octagon detector	200	4.7	7.3	2.5	9.3
Dodecagon detector	200	4.4	7.2	1.7	9.3

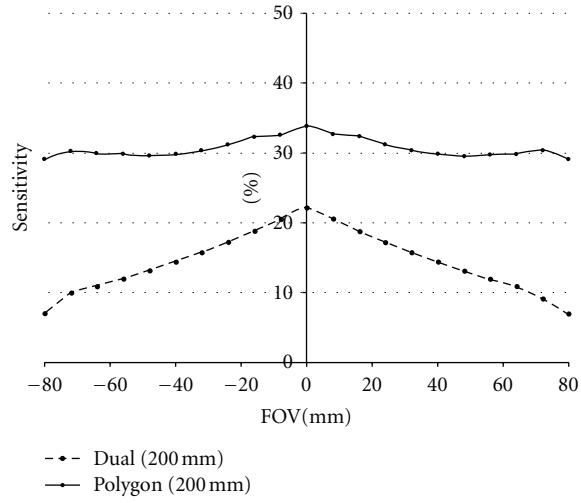

Figure 7: Transverse profiles of sensitivity for dual-head cameras (left) and polygon cameras (right).

achieve a high performance of the scanner since this effect is greater at the center than at the edge of the FOV.

4. Conclusions

An analytical study of the performance of different PEM detector geometries in terms of photon sensitivity and DOI effect was carried out in order to find an optimal arrangement of the detectors. To this end, dual-head detectors were compared to box and different polygon detector configurations.

Our results showed that higher sensitivity and uniformity are obtained for box and polygon detector configurations compared to dual-head cameras. For the polygon configurations the sensitivity is only moderately increased when the number of detectors is raised. The variable size of breast in women is an advantage for dual-head cameras with respect to to fixed cameras. Thus, for dual head cameras the sensitivity can be increased for small breasts by decreasing the distance

between opposing detectors. Nevertheless this translates in an increase of the mis-positioning of the photon interaction point due to the DOI effect.

The optimal configuration in terms of sensitivity is a PEM scanner based on a polygon of twelve (dodecagon) or more detectors. We have shown that this configuration is clearly superior to dual-head detectors and slightly higher than box, octagon, and hexagon detectors. Nevertheless, DOI effects are increased for this configuration compared to dual-head and box scanners and therefore an accurate compensation for this effect is required.

Acknowledgments

This work was supported in part by Fondo de Investigaciones Sanitarias ISCIII PS09/01206 and Xunta de Galicia 10CSA918001PR. P. Aguiar was awarded a Sara Borrell fellowship 2010 by ISCIII.

References

[1] A. Jemal, F. Bray, M. M. Center, J. Ferlay, E. Ward, and D. Forman, "Global cancer statistics," *CA Journal*, vol. 61, no. 2, pp. 69–90, 2011.

[2] I. Khalkhali, I. Mena, and L. Diggles, "Review of imaging techniques for the diagnosis of breast cancer: a new role of prone scintimammography using technetium-99 m sestamibi," *European Journal of Nuclear Medicine*, vol. 21, no. 4, pp. 357–362, 1994.

[3] E. Warner, D. B. Plewes, R. S. Shumak et al., "Comparison of breast magnetic resonance imaging, mammography, and ultrasound for surveillance of women at high risk for hereditary breast cancer," *Journal of Clinical Oncology*, vol. 19, no. 15, pp. 3524–3531, 2001.

[4] L. Esserman, D. Wolverton, and N. Hylton, "Magnetic resonance imaging for primary breast cancer management: current role and new applications," *Endocrine-Related Cancer*, vol. 9, no. 2, pp. 141–153, 2002.

[5] P. A. Carney, D. L. Miglioretti, B. C. Yankaskas et al., "Individual and combined effects of age, breast density, and hormone replacement therapy use on the accuracy of screening mammography," *Annals of Internal Medicine*, vol. 138, no. 3, pp. 168–175, 2003.

[6] C. D. Lehman, C. Gatsonis, C. K. Kuhl et al., "MRI evaluation of the contralateral breast in women with recently diagnosed breast cancer," *The New England Journal of Medicine*, vol. 356, no. 13, pp. 1295–1303, 2007.

[7] L. G. Strauss and P. S. Conti, "The applications of PET in clinical oncology," *Journal of Nuclear Medicine*, vol. 32, no. 4, pp. 623–648, 1991.

[8] W. A. Berg, K. S. Madsen, K. Schilling et al., "Breast cancer: comparative effectiveness of positron emission mammography and MR imaging in presurgical planning for the ipsilateral breast," *Radiology*, vol. 258, no. 1, pp. 59–72, 2011.

[9] C. S. Levin and E. J. Hoffman, "Calculation of positron range and its effect on the fundamental limit of positron emission tomography system spatial resolution," *Physics in Medicine and Biology*, vol. 44, no. 3, pp. 781–799, 1999.

[10] P. Aguiar, M. Rafecas, J. E. Ortuno et al., "Geometrical and Monte Carlo projectors in 3D PET reconstruction," *Medical Physics*, vol. 37, no. 11, pp. 5691–5702, 2010.

[11] J. R. Stickel and S. R. Cherry, "High-resolution PET detector design: modelling components of intrinsic spatial resolution," *Physics in Medicine and Biology*, vol. 50, no. 2, pp. 179–195, 2005.

[12] C. Bircher and Y. Shao, "Use of internal scintillator radioactivity to calibrate DOI function of a PET detector with a dual-ended-scintillator readout," *Medical Physics*, vol. 39, no. 2, pp. 777–787, 2012.

[13] F. Godinez, A. J. Chaudhari, Y. Yang, R. Farrell, and R. D. Badawi, "Characterization of a high-resolution hybrid DOI detector for a dedicated breast PET/CT scanner," *Physics in Medicine and Biology*, vol. 7, no. 57, pp. 3435–3449, 2012.

[14] H. T. van Dam, S. Seifert, R. Vinke et al., "A practical method for depth of interaction determination in monolithic scintillator PET detectors," *Physics in Medicine and Biology*, vol. 56, no. 13, pp. 4135–4145, 2011.

[15] K. M. Champley, L. R. MacDonald, T. K. Lewellen, R. S. Miyaoka, and P. E. Kinahan, "DOI-based reconstruction algorithms for a compact breast PET scanner," *Medical Physics*, vol. 38, no. 3, pp. 1660–1671, 2011.

[16] L. MacDonald, J. Edwards, T. Lewellen, D. Haseley, J. Rogers, and P. Kinahan, "Clinical imaging characteristics of the positron emission mammography camera: PEM Flex Solo II," *Journal of Nuclear Medicine*, vol. 50, no. 10, pp. 1666–1675, 2009.

[17] M. C. Abreu, P. Almeida, F. Balau et al., "Clear-PEM: adedicated pet camera for improved breast cancer detection," *Radiation Protection Dosimetry*, vol. 116, no. 1–4, pp. 208–210, 2005.

[18] R. R. Raylman, S. Majewski, M. F. Smith et al., "The positron emission mammography/tomography breast imaging and biopsy system (PEM/PET): design, construction and phantom-based measurements," *Physics in Medicine and Biology*, vol. 53, no. 3, pp. 637–653, 2008.

[19] A. Soriano, A. González, A. Orero et al., "Attenuation correction without transmission scan for the MAMMI breast PET," *Nuclear Instruments and Methods in Physics Research A*, vol. 648, supplement 1, pp. S75–S78, 2011.

[20] W. W. Moses and J. Qi, "Instrumentation optimization for positron emission mammography," *Nuclear Instruments and Methods in Physics Research A*, vol. 527, no. 1-2, pp. 76–82, 2004.

[21] F. Habte, A. M. K. Foudray, P. D. Olcott, and C. S. Levin, "Effects of system geometry and other physical factors on photon sensitivity of high-resolution positron emission tomography," *Physics in Medicine and Biology*, vol. 52, no. 13, pp. 3753–3772, 2007.

Hindawi Publishing Corporation
Journal of Oncology
Volume 2012, Article ID 710561, 9 pages
doi:10.1155/2012/710561

Review Article

PET Tracers for Clinical Imaging of Breast Cancer

Iván Peñuelas, Inés Domínguez-Prado, María J. García-Velloso, Josep M. Martí-Climent, Macarena Rodríguez-Fraile, Carlos Caicedo, María Sánchez-Martínez, and José A. Richter

Department of Nuclear Medicine, University Clinic of Navarra, Avenida Pío XII 36, 31008 Pamplona, Spain

Correspondence should be addressed to Iván Peñuelas, ipenuelas@unav.es

Received 12 June 2012; Accepted 13 July 2012

Academic Editor: Alvaro Ruibal

Copyright © 2012 Iván Peñuelas et al. This is an open access article distributed under the Creative Commons Attribution License, which permits unrestricted use, distribution, and reproduction in any medium, provided the original work is properly cited.

Molecular imaging of breast cancer has undoubtedly permitted a substantial development of the overall diagnostic accuracy of this malignancy in the last years. Accurate tumour staging, design of individually suited therapies, response evaluation, early detection of recurrence and distant lesions have also evolved in parallel with the development of novel molecular imaging approaches. In this context, positron emission tomography (PET) can be probably seen as the most interesting molecular imaging technology with straightforward clinical application for such purposes. Dozens of radiotracers for PET imaging of breast cancer have been tested in laboratory animals. However, in this review we shall focus mainly in the smaller group of PET radiopharmaceuticals that have lead through into the clinical setting. PET imaging can be used to target general metabolic phenomena related to tumoural transformation, including glucose metabolism and cell proliferation, but can also be directed to specific hormone receptors that are characteristic of the breast cancer cell. Many other receptors and transport molecules present in the tumour cells could also be of interest for imaging. Furthermore, molecules related with the tumour microenvironment, tumour induced angiogenesis or even hypoxia could also be used as molecular biomarkers for breast cancer imaging.

1. Introduction

PET is a molecular imaging modality in which compounds labelled with positron emitting radioisotopes are used to measure biological processes with only trace amounts of the radiolabelled probes. Molecules labelled with positron-emitting radionuclides are retained in tissues as a result of binding to a receptor, or cell entrapment owing to enzyme-catalyzed conversion after uptake by a cell membrane transporter. Tomographic images of the distribution of the radioactivity within the body can be generated and quantitatively evaluated by coincidence detection of the gamma rays resulting from the mutual annihilation of a positron emitted by the radionuclide and an electron of a nearby atom.

PET radiotracers are molecular probes that can be designed and synthesized to target very many different molecular and cellular events. In the specific case of breast cancer, there is a wide panoply of specific and general targets one could think about. However, being there a great number of molecules labelled with different positron emitting radionuclides (see Table 1) that have been synthesised and tested in vivo in laboratory animals, only a few of them have lead through into the clinical setting. In this review, we shall focus mainly in this smaller group of radiotracers. Papers focused in PET biomarkers for pre-clinical studies can be found elsewhere.

2. Glucose Metabolism

Although the number of PET tracers synthesised and tested *in vivo* largely exceeds 300, only a fraction has been used in humans. In addition, probably more than 90% of the clinical PET studies are performed with the analogue of glucose 2-[^{18}F]-fluoro-2-deoxy-D-glucose (FDG). Uptake and metabolism of FDG within tumour cells is higher than in normal tissue because of increased glycolysis. The incorporation of FDG to the neoplastic cells is favoured by the increase of glucose membrane transporters (GLUTs) which are overexpressed in breast cancer due to the activation of their genes. FDG is phosphorylated to FDG-6-phosphate by hexokinase-1, which also has increased activity in tumour

Table 1: Nuclear characteristics of different selected positron emitters of interest in PET imaging. The maximum positron energy is related to the maximum theoretical resolution using this radionuclide, in such a way that the smaller the positron emission energy, the better the resolution than can be achieved. The branching ratio refers to the approximate number of decay events in which a positron is emitted (this value is 100% for pure positron emitters).

Isotope	Half life	Maximum positron energy (MeV)	Branching ratio (%)
Carbon-11	20 min	0.96	~100
Fluorine-18	110 min	0.63	~100
Copper-64	12.7 h	0.58	~19
Gallium-68	68 min	1.89	~88
Bromine-76	16.2 h	3.94	~100
Zirconium-89	3.26 days	0.89	~23
Iodine-124	4.2 days	2.135	~23

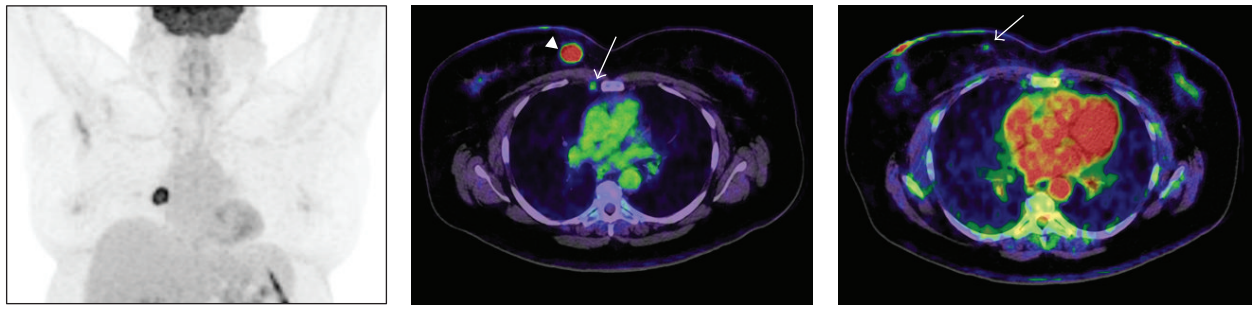

(a) (b) (c)

Figure 1: A 60-year-old female (BMI = 37) with a right-sided infiltrating ductal carcinoma was referred for staging. Images were obtained in a Biograph mCT (Siemens) 60 min after i.v. injection of 478 MBq of FDG. (a) FDG-PET maximum intensity projection of the thorax. (b) Axial fused FDG-PET/CT images of the primary tumour in the upper-inner quadrant (arrowhead) (SUV = 5,3), a metastasic lymph node in the right internal mammary chain (arrow) (SUVmax = 1,38) was found in the PET and histopathologically confirmed. (c) Axial fused FDG-PET/CT image of a second tumour in the same breast identified in FDG-PET (arrow) (SUVmax = 0,5), not detected by conventional imaging techniques and biopsy-proven.

cells due both to genetic and allosteric modifications. Therefore, the detected concentration of labelled FDG is proportional to the uptake and metabolism of glucose.

In patients with breast cancer, FDG PET/CT results in improved sensitivity for the detection of both lymph node infiltration and distant metastases compared to conventional imaging techniques [1]. Therefore, FDG PET/CT offers clinically relevant information on the staging of patients with breast cancer, has prognostic value, and enables the assessment of therapeutic response and relapse. The development of PET scanners dedicated to breast (positron emission mammography) has improved spatial resolution and sensitivity, allowing its clinical application in the study of the primary tumour [2].

Tumour uptake of FDG is variable and depends not only on tumour size, but also on the histological type and histological grade. The hormone receptor status and other immunohistochemical factors with prognostic value are also relevant, such as p53 and Ki-67 expression. FDG uptake is higher in ductal carcinoma than in lobular carcinoma and in patients with poor prognostic features as high grade and hormone receptor negativity [3].

Regarding nodal staging, when FDG PET/CT shows axillary uptake, the positive predictive value of metastatic infiltration is greater than 95%. Despite these findings, lymph node uptake should always be confirmed due to the low specificity of FDG. In addition, FDG PET/CT can show disease not detected by conventional imaging techniques in internal mammary chain and mediastinum [4] (Figure 1). However, when there is no FDG uptake in the axilla, given the low sensitivity due to limitations in detecting lymph node micrometastasis and very small tumours, axillary sentinel lymph node biopsy should be performed for a correct staging [5].

FDG PET/CT contributes significantly both in defining the extent of disease and the choice of appropriate therapy in patients with advanced tumours (Figure 2). FDG PET/CT allows early assessment of therapeutic response in patients receiving neoadjuvant therapy, for evaluation of response to new biotherapies and for prediction of outcome [6].

FDG PET/CT is superior to CT in the diagnosis of tumour recurrence in patients with elevated tumour markers, both in sensitivity, specificity, and overall accuracy, with changes in clinical management in 50% of patients [7].

3. Proliferation

One of the main hallmarks of tumour cells is their ability to sustain chronic proliferation, which represents a key target in

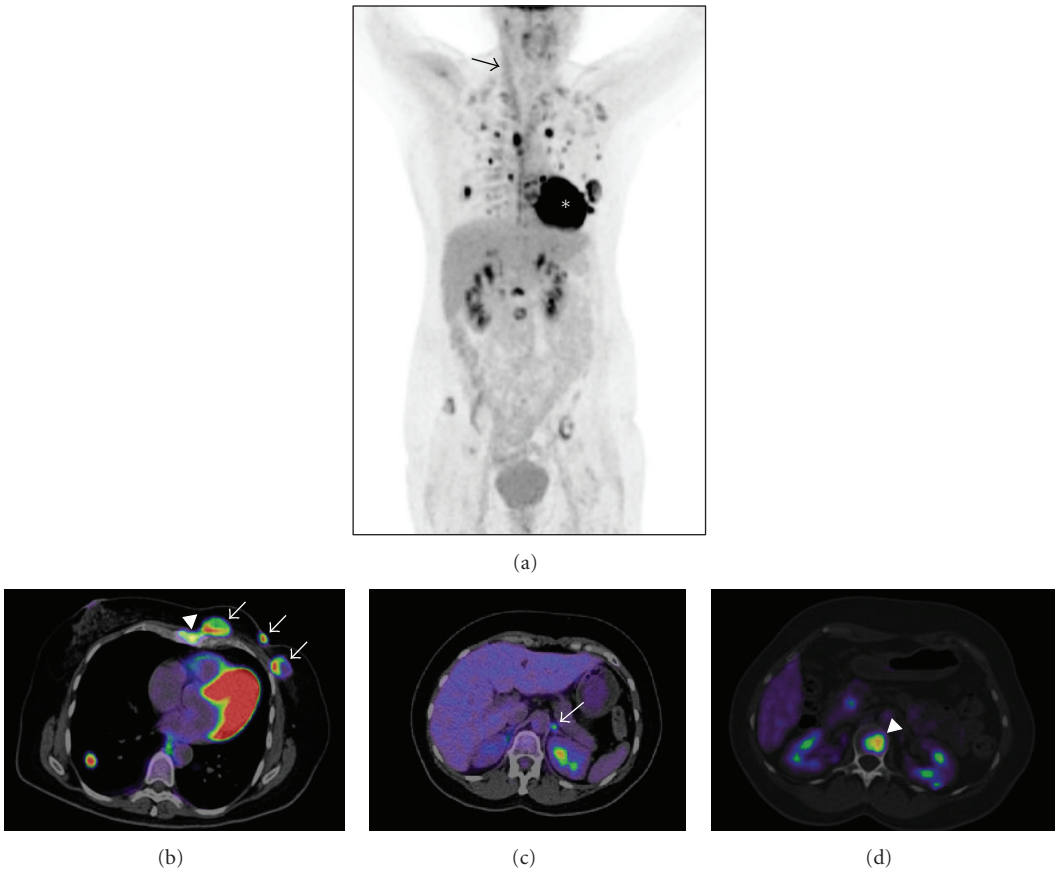

Figure 2: A 47-year-old woman with a left-sided multifocal infiltrating ductal carcinoma, Luminal B, referred for staging. Images were obtained in a Biograph mCT (Siemens) 60 min after i.v. injection of 363 MBq of FDG. (a) FDG-PET whole-body maximum intensity projection: multifocal left-sided breast tumour, lymph node metastasis in the left axilla, left internal mammary chain and mediastinum, left adrenal gland metastasis, multiple bilateral lung metastases, sternal, spine, and pelvic bone metastases. Physiological uptake was identified in paraspinal and supraclavicular fossa brown fat, right sternocleidomastoid muscle (arrow), myocardium (∗), kidneys and bladder. (b) Axial fused FDG-PET/CT image of the multifocal tumour in the left breast (arrows), sternum (arrowhead), and right lung metastasis. (c) Axial fused FDG-PET/CT image of the left adrenal gland metastasis (arrow). (d) Axial fused FDG-PET/CT image of a vertebral metastasis (arrowhead).

the scene of the new anticancer therapeutic agents [8]. The study of the proliferation rate is important not only in the initial staging and characterization of the tumour, but also in the assessment of response, both at an early stage (Figure 3) during the initial treatment schedule—as a way to predict the clinical outcome—or at the end of the treatment.

Back to 1998, Shields et al. [9] developed and tested 3′-deoxy-3′-[^{18}F]fluorothymidine (^{18}FLT) as a biomarker for *in vivo* imaging of cell proliferation, demonstrating that it was resistant to degradation *in vivo*, retained in proliferating tissues by the action of thymidine kinase 1 and produced high-contrast images of normal marrow and tumours.

Although ^{18}FLT is not a routine tool in the clinical practice in breast cancer, it may play an important role in the staging, monitoring, and prediction of response to therapy agents [10]. Moreover, ^{18}FLT strongly correlates with the immunohistochemical proliferation index ki-67 [11]. ^{18}FLT-PET can be of value as an early response predictor for different chemotherapeutic agents. In a prospective study in 20 patients with stages II–IV breast cancer under docetaxel treatment, Contractor et al. [12] aimed to establish biomarkers indicating clinical response to taxanes. Patients underwent a baseline dynamic ^{18}FLT-PET scan followed by a scan 2 weeks after initiating the first or second cycle of docetaxel. ^{18}FLT-derived PET variables were compared with anatomic response after 3 cycles and concluded that changes in tumour proliferation assessed by ^{18}FLT early after initiating docetaxel chemotherapy could predict lesion response with good sensitivity. Furthermore, Kenny et al. [13] demonstrated that ^{18}FLT can detect changes in breast cancer proliferation as early as at 1 week after 5-fluorouracil, epirubicin, and cyclophosphamide therapy. Decreases in the irreversible trapping constant and the standardized uptake value (SUV) at 1 week discriminated between clinical response and stable disease. In an effort to find simplified valuable ^{18}FLT-PET uptake measures, Lubberink et al. [14] studied with a dynamic ^{18}FLT-PET scan 15 patients with locally advanced breast cancer both prior to and after the first cycle of chemotherapy with fluorouracil, epirubicin or doxorubicin, and cyclophosphamide. The authors concluded

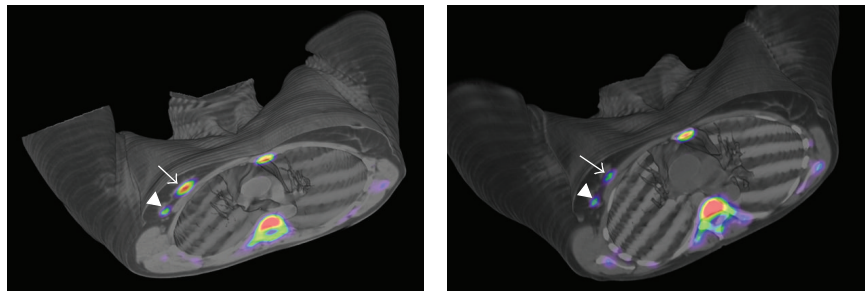

(a) (b)

Figure 3: (a) Baseline PET/CT images obtained in a Biograph Duo LSO (Siemens) 75 min after injection of 405 MBq of ^{18}FLT in a 47-year-old woman with a right-sided infiltrating ductal carcinoma (SUVmax = 5,42) (arrow) and lymph node uptake (SUVmax = 1,85) (arrowhead). Physiological bone marrow uptake was identified. (b) PET/CT images obtained 75 min after injection of 529 MBq of ^{18}FLT after one cycle of neoadjuvant therapy. SUVmax decreased to 3,57 in the primary tumour and to 0,80 in the lymph node, consistent with metabolic response.

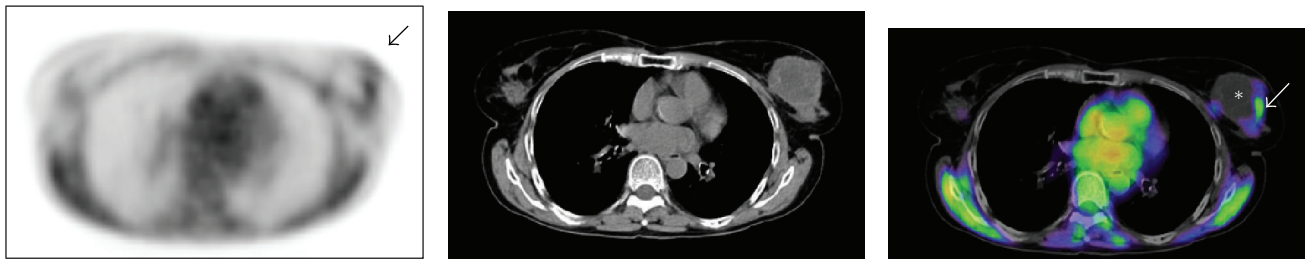

(a) (b) (c)

Figure 4: Axial PET (a), CT (b), and fused PET/CT (c) images obtained in a Biograph Duo LSO (Siemens) two hours after i.v. injection of 368 MBq of FMISO, in a 64-year-old woman with a left-sided triple negative infiltrating ductal carcinoma, T2N1M0. Peripheral tumour uptake of FMISO (SUVmax = 1,44) consistent with hypoxia (arrow), and inside tumour lack of activity due to central necrosis (∗) were observed. Physiological uptake in muscles and mediastinum was identified.

that tumour-to-whole blood ratio may be preferred to SUV as a simplified measure for monitoring response.

4. Hypoxia

Another important hallmark of cancer disease is hypoxia. This microenvironmental factor facilitates the metastasic spread and is related to poor response to radiation, chemotherapy, genetic instability, and selection for resistance to apoptosis due to its effect on various metabolic, molecular-genetic, and pathophysiologic adaptive processes.

Tumour hypoxia is a condition of insufficient O_2 to support metabolism and occurs when tumour outgrows its vascularity supply. It has been identified as one of major independent prognostic factors influencing response to therapy and overall survival in many malignancies, including breast cancer [15, 16].

The occurrence of hypoxia in human tumours has in most cases been inferred from histologic findings and from evidence of hypoxia in animal tumour studies. *In vivo* demonstration of hypoxia required tissue measurements with oxygen electrodes and the invasiveness of this technique has limited its applications. Consequently, there has been a growing impetus to develop noninvasive imaging methods to detect and assess tumour hypoxia.

The first clinical studies to image hypoxia using PET were based on halogenated tracers of 2-nitroimidazoles, such as [^{18}F]fluoromisonidazole (^{18}FMISO) [17]. This compound diffuses through cell membranes and when tissular pO_2 is below 10 mm Hg becomes reduced in viable cells by nitroreductase and once reduced is accumulated intracellularly. Two to four hours after injection, the retention is considered to be specific to cellular hypoxia (Figure 4).

Antiangiogenic therapy has been thought to hold significant potential for the treatment of cancer. However, in the specific case of breast cancer, new research using preclinical models suggests that antiangiogenic agents actually increase invasive and metastatic properties of breast cancer cells by augmenting the population of cancer stem cells by generating intratumoural hypoxia [18]. Albeit no results from human studies have been reported, PET imaging of hypoxia could help shed some light on this cutting-edge story.

Although there are not many published papers on ^{18}FMISO in breast cancer, its utility has been well established in other tumours, such as glioblastoma multiforme, rectal, lung and head and neck carcinomas [19].

Rajendran et al. [20] compared the glucose metabolism (FDG-PET) and hypoxia (^{18}FMISO-PET) in four different types of tumours, including seven patients with breast cancer. They concluded that although hypoxia is a general

factor affecting glucose metabolism, some tumours can have modest glucose metabolism, whereas some highly metabolic tumours are not hypoxic, showing discordance in tracer uptake that can be tumour-type-specific.

5. Radiolabelled Choline Derivatives

Transformation from choline to phosphocholine increases with malignant transformation and progression of mammary epithelial cells *in vitro*. Furthermore, increase in phosphocholine can be attributed to expression of the enzyme choline kinase-α. It is also important to consider that both choline kinase activity and cellular phosphocholine levels are regulated by the growth factor receptor-MAPK pathway, the same one that modulates estrogen-independent growth [21].

Once the fundamentals for the use of N-[^{11}C]methylcholine (^{11}C-choline) were established, Contractor et al. [22] showed that breast tumours were well visualized in 30 of 32 patients with good tumour background ratios, albeit surprisingly a poor association was found with tumour size, estrogen receptor, progesterone receptor, human epidermal growth factor receptor-2, Ki-67, and nodal status.

Albeit the exact biological mechanism of increased ^{11}C-choline uptake in certain tumours is unknown, choline is required for membrane synthesis in actively proliferating cells. Consequently, it could be hypothesized that ^{11}C-choline uptake should be higher in cells undergoing proliferation. More recently, the same group [23] has demonstrated in a set of 21 patients with estrogen receptor positive breast cancer that choline metabolism assessed by ^{11}C-choline PET and proliferation determined by ^{18}FLT-PET were correlated in ER-positive breast cancer, concluding that high ^{11}C-choline uptake is a measure of cellular proliferation in this setting.

Regarding the use of fluorine labelled choline derivatives in diagnosis of breast cancer, no reports can be found in the literature, apart from an incidental finding in a male patient with elevated PSA levels that was studied by ^{18}F-fluorocholine PET for possible diagnosis of prostate cancer [24]. PET/CT images revealed focal uptake in the left breast that was found by biopsy to be an invasive ductal breast carcinoma. Prostate biopsy also revealed prostate cancer corresponding to an area of increased prostatic ^{18}F-fluorocholine uptake.

6. Estrogen Receptors

Endocrine therapy targeting steroid receptors remains the most effective form of systemic therapy in breast cancer. Thus, receptor ligands such as fluorine-labelled estradiol offer the possibility to study the presence of estrogen receptors (ER) in both primary and tumour metastasis, and may be a useful tool in the therapeutic management and prognostic evaluation of breast cancer.

Already back to 1988, Mintun et al. [25] pioneered *in vivo* molecular imaging of breast cancer with PET using the estrogen receptor ligand 16α-[^{18}F]-fluoro-17β-estradiol (^{18}F-FES) in a set of 13 patients with primary breast tumours. They found an excellent correlation between uptake of ^{18}F-FES and estrogen-receptor concentration measured in vitro after excision of the lesions.

Nowadays, whole-body PET with ^{18}F-FES can be seen as a unique method to noninvasively obtain molecular information of ER expression. No other procedure can provide information on a whole body basis of the ER status in metastasic breast cancer. It is well known that ER expression at metastasic sites might not be the same as the ER expression at the primary disease due to relatively common phenotypic changes. In any case, loss of ER expression is more common than gain of ER expression.

Many different studies have shown that ^{18}F-FES PET can reliably detect ER-positive tumour lesions and that ^{18}F-FES uptake correlates with ER expression as measured by immunohistochemical methods. Furthermore, low ^{18}F-FES uptake has been reported to be a strong predictor for failure of antihormonal therapy. For a comprehensive review of ^{18}F-FES PET, see [26] and references therein.

Imaging ER expression by PET can be used to identify, characterize, and follow treatment response to multiple lesions in the same patient. ^{18}F-FES PET also has great potential for evaluating ER activity in metastasic breast cancer, in which patients have many bone lesions that are difficult to biopsy and prone to false-negative ER by immunohistochemistry [27].

Kurland et al. [28] have recently analysed between-patient and within-patient variability in ER binding by ^{18}F-FES-PET and have shown that both ^{18}F-FES uptake and the ^{18}F-FES/FDG ratio varied greatly between patients but were usually consistent across lesions in the same scan. These results seem to provide a reasonable summary of some kind of "synchronous ER expression" for most patients. However, imaging the entire disease burden remains important to identify the subset of patients with mixed uptake, who may be at a critical point in their disease evolution. These results are also supported by van Kruchten et al. [29] that have shown whole-body imaging of ER expression with ^{18}F-FES-PET as a very valuable additional diagnostic tool when standard workup is inconclusive. With the exception of liver metastases, ^{18}F-FES PET can be used to support therapy decisions by improving diagnostic understanding and providing information on ER status of tumour lesions.

In a very thorough study with 312 ^{18}F-FES-PET scans in 239 patients with documented ER positive primary breast cancer, Peterson et al. [30] demonstrated that ^{18}F-FES imaging protocols may be simplified without sacrificing the validity of the results, as calculation of ^{18}F-FES SUV should be sufficient to assess tracer uptake for the purpose of inferring ER expression.

7. Progesterone Receptors

Hormone-sensitive breast cancer is less aggressive than hormone-resistant disease; hormone-sensitive disease occurs more commonly in postmenopausal women and is characterized by longer disease-free and overall survival.

The presence of the progesterone receptor (PR) increases the likelihood of hormone responsiveness, while progesterone receptor-negative tumours are less responsive to therapy, perhaps suggesting that PR may be necessary for adequate therapeutic outcome. Furthermore, the cross-relationship between estrogen and progesterone receptors—being the former a key transcription factor for the activation of the latter—could suggest that the estrogen response pathway may not be functional in these tumours. In this scenario, noninvasive detection and quantification of PR positive or PR negative lesions would be of enormous value, especially considering that discordance of hormone receptor status between the primary tumour and metastatic disease is not uncommon. This difference may influence patient prognosis and response to therapy. Dehdashti et al. [31] have recently used in humans for the first time a fluorine-18-labelled PR-specific ligand and shown that it can be used to assess the PR status of individual breast cancer lesions. However, no significant correlation was demonstrated between the SUVmax and distribution volume ratio for the tracer uptake and receptor status, likely because of small sample size.

8. Radiolabelled Derivatives of P-Glycoprotein Substrates and Inhibitors

Resistance to multiple chemically different drugs is a well-known phenomenon in oncology. Even though the exact cause remains elusive and is multifactorial, membrane proteins that actively remove drugs from the cell are known to play a relevant role.

The best characterized of such drug-resistance proteins is P-glycoprotein (Pgp) (also known as multidrug-resistance protein 1 and ABCB1), a member of the ATP-binding cassette transporters family, which transports substrates across the cell membrane in different conditions. Another relevant member of this family is the breast cancer resistance protein (BCRP, also known as ABCG2). Several PET radiotracers for visualization of Pgp have been described so far [32–36] including carbon-11- and fluorine-18-labelled derivatives of Pgp substrates such as verapamil or loperamide and Pgp inhibitors such as elacridar and tariquidar. The former permit *in vivo* visualization of Pgp function, while the latter can be understood as surrogate markers of Pgp expression levels.

In any case, few Pgp-directed PET tracers have been used in the clinical setting in humans, being probably the paper by Kurdziel et al. [37] describing the human dosimetry and tumour distribution of ^{18}F-fluoropaclitaxel in breast cancer patients one of the more recent reports. These authors show that, albeit in a very small series with only three patients, tumour accumulation of the radiotracer could be detected in all cases and that ^{18}F-fluoropaclitaxel distribution could be used as a surrogate biomarker for paclitaxel and potentially other chemotherapeutic agents.

9. Integrin Ligands

Integrins are obligate heterodimeric proteins involved in cell-cell interaction, interaction of cells with the extracellular matrix, signal transmission, and apoptosis. They are key components of the cell machinery involved in cell signalling, shape, and motility and are part of the complex transduction mechanisms that permit cells to be aware of the changes in their surrounding environment and also participate in the communication of the intracellular changes to the outside.

The $\alpha_v\beta_{3/5}$ subclasses of the integrin family are of particular interest as they are upregulated in tumour neovasculature and on several types of tumour cells (including breast cancer), making them a potentially valuable diagnostic tool. Furthermore, an association between expression of $\alpha_v\beta_{3/5}$ and relapse-free survival in breast cancer has been reported [38], suggesting a prognostic value of imaging such receptors.

Integrin $\alpha_v\beta_3$ has been demonstrated to be involved in tumour transformation, angiogenesis, local invasiveness, and metastatic potential. A number of different positron emitter-labelled ligands have been developed to image integrins, and some have already been used in breast cancer patients. Among them, arginine-glycine-aspartic acid (RGD) peptide ligands have high affinity for these integrins and can be radiolabeled for PET imaging of angiogenesis or tumour development [39].

The ability to noninvasively visualize and quantify $\alpha_v\beta_3$ integrin expression via RGD will provide new opportunities to document tumour integrin levels, more appropriately select patients who are candidates for antiangiogenic treatment and monitor treatment effectiveness in patients with integrin-positive findings.

Back to 2008, Beer et al. [40] reported the use of ^{18}F-Galacto-RGD in a group of 16 breast cancer patients and demonstrated tracer uptake in all primary tumour lesions and metastases (Figure 5) although ^{18}F-Galacto-RGD uptake in the lesions was very heterogeneous in all cases, suggesting elevated but widely varying levels of $\alpha_v\beta_3$ expression in human breast cancer. Immunohistochemical analysis revealed that the detected signal represented a mixture of tracer binding on neovasculature and on tumour cells.

More recently, Kenny et al. [41] have used the cyclic peptide-polymer conjugate ^{18}F-fluciclatide (^{18}F-AH111585), an aminooxy-functionalized double-bridged RGD derivative with optimized stability. ^{18}F-fluciclatide could be used to detect primary and metastatic breast cancer lesions and could be of value for imaging tumours and for pharmacodynamic monitoring of antiangiogenic therapies. In any case, tumour uptake largely varied among individuals and different tumour types, and even between tumours of the same type within one patient. Tomasi et al. [42] have focused on the best quantification approach to analyse the kinetics of ^{18}F-fluciclatide in breast cancer patients.

Other RGD-derived radioligands based on the dimeric RGD moiety such as [^{18}F]FPPRGD2 have also been recently tested in humans [43]. In addition, a quite large number of different derivatives targeted to image the expression of $\alpha_v\beta_3$ integrin have been developed in the last years and tested *in vivo* in small animals, including some very promising gallium-68 labelled RGD peptides [44].

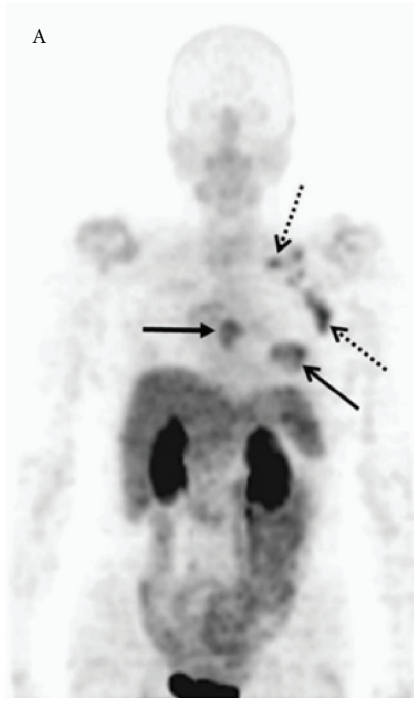

Figure 5: Maximum-intensity projection of ^{18}F-galacto-RGD PET in a 70-year-old patient with invasive ductal breast cancer of left breast (arrow, open tip), axillary lymph-node metastases on left side (arrow, open tip, dotted line), an osseous metastasis to the sternum (arrow, closed tip). Reprinted by permission of the Society of Nuclear Medicine from Beer et al. [40], Figure 2.

10. Monoclonal Antibodies

Immuno-PET has largely been seen as an exciting option for better understanding the *in vivo* behaviour and efficacy of monoclonal antibodies (mAbs) in individual patients. Very many papers have been written to describe the benefits of these visible magic-bullet approach—see [45, 46] and references therein—, and many radiolabelled antibodies and derivatives have been used for small animal imaging.

For labelling intact antibodies with a low-clearance kinetics, longer-lived radioisotopes such as zirconium-89 or iodine-124 are the election of choice, while for radiolabelling mAbs fragments or constructs (minibodies, affibodies, diabodies, etc.) which are more rapidly cleared from the body, shorter-lived positron emitters such as gallium-68 or copper-64 might be ideally suited.

Currently, 12 mAbs have been approved by the FDA for the treatment of cancer, all being intact mAbs [47]. Seven of the mAbs have been approved for the treatment of hematological malignancies, and five for the therapy of solid tumours [48]. However, it has only been very recently that several crucial concurrent achievements have been obtained to allow broad-scale application of (mainly) ^{89}Zr-immuno-PET in clinical mAb development and applications. The aforementioned advances are related with the production and commercial availability of ^{89}Zr for clinical use and the development of chelates for facile and stable coupling of ^{89}Zr to mAbs.

Overexpression of HER2/neu in breast cancer is correlated with a poor prognosis. It may vary between primary tumours and metastatic lesions and change during the treatment. Therefore, there is a need for a new means to assess HER2/neu expression *in vivo*. A ^{68}Ga-labeled HER2 derivative affibody has been used to monitor HER2/neu expression in breast cancer xenografts [49] and preliminary results suggest that it could be sensitive enough to detect different levels of HER2/neu expression *in vivo*. The mAb trastuzumab targets the human epidermal growth factor receptor kinase (ERBB or HER) signaling network and has a history as a therapeutic for metastatic or adjuvant treatment of oncological disease. Upregulation of the ERB2 (HER2/neu) receptor has been associated with metastasis and poor prognosis in many cancers, including breast cancer. Specifically, HER receptors stimulate growth and regulate survival and differentiation. Because of variable HER2/neu receptor expression over time, noninvasive and dynamic measurement methods would be ideal for monitoring potential treatment and disease prognosis.

However, there is only one paper published so far describing the use of immuno-PET in humans and just in fourteen patients [50] and an additional case report [51], but it concludes that PET scanning after administration of ^{89}Zr-trastuzumab allows visualization and quantification of uptake in HER2-positive lesions in patients with metastatic breast cancer. The PET images obtained with ^{89}Zr-trastuzumab revealed high spatial resolution and a good signal-to-noise ratio. Excellent tumour uptake and visualization of HER2-positive metastatic liver, lung, bone, and brain tumour lesions were obtained. ^{89}Zr-trastuzumab PET visualized bony metastatic disease. These early studies show great promise for the potential of ^{89}Zr-trastuzumab in immuno-PET.

11. Exotic Sugar-Like Tracers

A number of different tracers targeting diverse cellular biochemical mechanisms involved in breast cancer have been developed, synthesised, and tested in breast cancer xenograft models. Although an exhaustive list is well beyond the scope of this paper, it is worth citing a couple of very recent articles describing the use of sugar-like derivatives as alternatives to FDG for tumour imaging: a fluorine-18-labelled inositol derivative [52] and a fluorine-18-labelled fructose derivative used to image GLUT5 transporter [53].

References

[1] Z. Garami, Z. Hascsi, J. Varga, T. Dinya, M. Tanyi, I. Garai et al., "The value of 18-FDG PET/CT in early-stage breast cancer compared to traditional diagnostic modalities with an emphasis on changes in disease stage designation and treatment plan," *European Journal of Surgical Oncology*, vol. 38, no. 1, pp. 31–37, 2012.

[2] D. Narayanan, K. S. Madsen, J. E. Kalinyak, and W. A. Berg, "Interpretation of positron emission mammography and MRI by experienced breast imaging radiologists: performance and

observer reproducibility," *American Journal of Roentgenology*, vol. 196, no. 4, pp. 971–981, 2011.

[3] D. Groheux, S. Giacchetti, J. L. Moretti et al., "Correlation of high 18F-FDG uptake to clinical, pathological and biological prognostic factors in breast cancer," *European Journal of Nuclear Medicine and Molecular Imaging*, vol. 38, no. 3, pp. 426–435, 2011.

[4] G. Zornoza, M. J. Gańcia-Velloso, J. Sola, F. M. Regueira, L. Pina, and C. Beorlegui, "18F-FDG PET complemented with sentinel lymph node biopsy in the detection of axillary involvement in breast cancer," *European Journal of Surgical Oncology*, vol. 30, no. 1, pp. 15–19, 2004.

[5] K. L. Cooper, Y. Meng, S. Harnan et al., "Positron emission tomography (PET) and magnetic resonance imaging (MRI) for the assessment of axillary lymph node metastases in early breast cancer: systematic review and economic evaluation," *Health Technology Assessment*, vol. 15, no. 4, pp. 1–134, 2011.

[6] L. K. Dunnwald, R. K. Doot, J. M. Specht et al., "PET tumor metabolism in locally advanced breast cancer patients undergoing neoadjuvant chemotherapy: value of static versus kinetic measures of fluorodeoxyglucose uptake," *Clinical Cancer Research*, vol. 17, no. 8, pp. 2400–2409, 2011.

[7] V. Filippi, J. Malamitsi, F. Vlachou et al., "The impact of FDG-PET/CT on the management of breast cancer patients with elevated tumor markers and negative or equivocal conventional imaging modalities," *Nuclear Medicine Communications*, vol. 32, no. 2, pp. 85–90, 2011.

[8] D. Hanahan and R. A. Weinberg, "Hallmarks of cancer: the next generation," *Cell*, vol. 144, no. 5, pp. 646–674, 2011.

[9] A. F. Shields, J. R. Grierson, B. M. Dohmen et al., "Imaging proliferation in vivo with [F-18]FLT and positron emission tomography," *Nature Medicine*, vol. 4, no. 11, pp. 1334–1336, 1998.

[10] L. B. Been, P. H. Elsinga, J. de Vries et al., "Positron emission tomography in patients with breast cancer using 18F-3′-deoxy-3′-fluoro-L-thymidine (18F-FLT)—a pilot study," *European Journal of Surgical Oncology*, vol. 32, no. 1, pp. 39–43, 2006.

[11] H. Vesselle, J. Grierson, M. Muzi et al., "In vivo validation of 3′deoxy-3′-[18F]fluorothymidine ([18F]FLT) as a proliferation imaging tracer in humans: correlation of [18F]FLT uptake by positron emission tomography with Ki-67 immunohistochemistry and flow cytometry in human lung tumors," *Clinical Cancer Research*, vol. 8, no. 11, pp. 3315–3323, 2002.

[12] K. B. Contractor, L. M. Kenny, J. Stebbing, L. Rosso, R. Ahmad, J. Jacob et al., "18F]-3′deoxy-3′-fluorothymidine positron emission tomography and breast cancer response to docetaxel," *Clinical Cancer Research*, vol. 17, no. 24, pp. 7664–7672, 2011.

[13] L. Kenny, R. C. Coombes, D. M. Vigushin, A. Al-Nahhas, S. Shousha, and E. O. Aboagye, "Imaging early changes in proliferation at 1 week post chemotherapy: a pilot study in breast cancer patients with 3′-deoxy-3′-[18F]fluorothymidine positron emission tomography," *European Journal of Nuclear Medicine and Molecular Imaging*, vol. 34, no. 9, pp. 1339–1347, 2007.

[14] M. Lubberink, W. Direcks, J. Emmering, H. van Tinteren, O. S. Hoekstra, J. J. van der Hoeven et al., "Validity of simplified 3′-deoxy-3′-[(18)F]fluorothymidine uptake measures for monitoring response to chemotherapy in locally advanced breastcancer," *Molecular Imaging and Biology*. In press.

[15] S. A. Hussain, R. Ganesan, G. Reynolds et al., "Hypoxia-regulated carbonic anhydrase IX expression is associated with poor survival in patients with invasive breast cancer," *British Journal of Cancer*, vol. 96, no. 1, pp. 104–109, 2007.

[16] M. Mikhaylova, N. Mori, F. B. Wildes, P. Walczak, B. Gimi, and Z. M. Bhujwalla, "Hypoxia increases breast cancer cell-induced lymphatic endothelial cell migration," *Neoplasia*, vol. 10, no. 4, pp. 380–388, 2008.

[17] P. E. Valk, C. A. Mathis, M. D. Prados, J. C. Gilbert, and T. F. Budinger, "Hypoxia in human gliomas: demonstration by PET with fluorine-18- fluoromisonidazole," *Journal of Nuclear Medicine*, vol. 33, no. 12, pp. 2133–2137, 1992.

[18] S. J. Conley, E. Gheordunescu, P. Kakarala, B. Newman, H. Korkaya, A. N. Heath et al., "Antiangiogenic agents increase breast cancer stem cells via the generation of tumor hypoxia," *Proceedings of the National Academy of Sciences of the United States of America*, vol. 109, no. 8, pp. 2784–2789, 2012.

[19] G. Laking and P. Price, "Radionuclide imaging of perfusion and hypoxia," *European Journal of Nuclear Medicine and Molecular Imaging*, vol. 37, supplement 1, pp. S20–S29, 2010.

[20] J. G. Rajendran, D. A. Mankoff, F. O'Sullivan et al., "Hypoxia and glucose metabolism in malignant tumors: evaluation by [18F]fluoromisonidazole and [18F]]fluorodeoxyglucose positron emission tomography imaging," *Clinical Cancer Research*, vol. 10, no. 7, pp. 2245–2252, 2004.

[21] A. R. de Molina, M. Báñez-Coronel, R. Gutiérrez et al., "Choline kinase activation is a critical requirement for the proliferation of primary human mammary epithelial cells and breast tumor progression," *Cancer Research*, vol. 64, no. 18, pp. 6732–6739, 2004.

[22] K. B. Contractor, L. M. Kenny, J. Stebbing et al., "[11C]choline positron emission tomography in estrogen receptor-positive breast cancer," *Clinical Cancer Research*, vol. 15, no. 17, pp. 5503–5510, 2009.

[23] K. B. Contractor, L. M. Kenny, J. Stebbing, A. Challapalli, A. Al-Nahhas, C. Palmieri et al., "Biological basis of [(1)(1)C]choline-positron emission tomography in patients with breast cancer: comparison with [(1)(8)F]fluorothymidine positron emission tomography," *Nuclear Medicine Communications*, vol. 32, no. 11, pp. 997–1004, 2011.

[24] S. A. Kwee and M. N. Coel, "Detection of synchronous primary breast and prostate cancer by F-18 fluorocholine PET/CT," *Clinical Nuclear Medicine*, vol. 35, no. 2, pp. 128–129, 2010.

[25] M. A. Mintun, M. J. Welch, B. A. Siegel et al., "Breast cancer: PET imaging of estrogen receptors," *Radiology*, vol. 169, no. 1, pp. 45–48, 1988.

[26] L. Sundararajan, H. M. Linden, J. M. Link, K. A. Krohn, and D. A. Mankoff, "18F-Fluoroestradiol," *Seminars in Nuclear Medicine*, vol. 37, no. 6, pp. 470–476, 2007.

[27] L. D. C. Hoefnagel, M. J. van de Vijver, H. J. van Slooten et al., "Receptor conversion in distant breast cancer metastases," *Breast Cancer Research*, vol. 12, no. 5, article R75, 2010.

[28] B. F. Kurland, L. M. Peterson, J. H. Lee, H. M. Linden, E. K. Schubert, L. K. Dunnwald et al., "Between-patient and within-patient (site-to-site) variability in estrogen receptor binding, measured in vivo by 18F-fluoroestradiol PET," *Journal of Nuclear Medicine*, vol. 52, no. 10, pp. 1541–1549, 2011.

[29] M. van Kruchten, A. W. Glaudemans, E. F. de Vries, R. G. Beets-Tan, C. P. Schroder, R. A. Dierckx et al., "PET imaging of estrogen receptors as a diagnostic tool for breast cancer patients presenting with a clinical dilemma," *Journal of Nuclear Medicine*, vol. 53, no. 2, pp. 182–190, 2012.

[30] L. M. Peterson, B. F. Kurland, J. M. Link et al., "Factors influencing the uptake of 18F-fluoroestradiol in patients with

estrogen receptor positive breast cancer," *Nuclear Medicine and Biology*, vol. 38, no. 7, pp. 969–978, 2011.

[31] F. Dehdashti, R. Laforest, F. Gao, R. L. Aft, C. S. Dence, D. Zhou et al., "Assessment of progesterone receptors in breast carcinoma by PET with 21-18F-fluoro-16alpha, 17alpha-[(R)-(1′-alpha-furylmethylidene)dioxy]-19-norpregn- 4-ene-3, 20-dione," *Journal of Nuclear Medicine*, vol. 53, no. 3, pp. 363–370, 2012.

[32] K. Kumata, M. Ogawa, M. Takei, M. Fujinaga, Y. Yoshida, N. Nengaki et al., "Radiosynthesis of [13N]dantrolene, a positron emission tomography probe for breast cancer resistant protein, using no-carrier-added [13N]ammonia," *Bioorganic and Medicinal Chemistry*, vol. 20, no. 1, pp. 305–310, 2012.

[33] N. Tournier, H. Valette, M. A. Peyronneau et al., "Transport of selected PET radiotracers by human P-glycoprotein (ABCB1) and breast cancer resistance protein (ABCG2): an in vitro screening," *Journal of Nuclear Medicine*, vol. 52, no. 3, pp. 415–423, 2011.

[34] K. Kawamura, T. Yamasaki, F. Konno et al., "Synthesis and in vivo evaluation of 18F-fluoroethyl GF120918 and XR9576 as positron emission tomography probes for assessing the function of drug efflux transporters," *Bioorganic and Medicinal Chemistry*, vol. 19, no. 2, pp. 861–870, 2011.

[35] F. Bauer, C. Kuntner, J. P. Bankstahl et al., "Synthesis and in vivo evaluation of [11C]tariquidar, a positron emission tomography radiotracer based on a third-generation P-glycoprotein inhibitor," *Bioorganic and Medicinal Chemistry*, vol. 18, no. 15, pp. 5489–5497, 2010.

[36] B. Dörner, C. Kuntner, J. P. Bankstahl et al., "Radiosynthesis and in vivo evaluation of 1-[18F]fluoroelacridar as a positron emission tomography tracer for P-glycoprotein and breast cancer resistance protein," *Bioorganic and Medicinal Chemistry*, vol. 19, no. 7, pp. 2190–2198, 2011.

[37] K. A. Kurdziel, J. D. Kalen, J. I. Hirsch, J. D. Wilson, H. D. Bear, J. Logan et al., "Human dosimetry and preliminary tumor distribution of 18F-fluoropaclitaxel in healthy volunteers and newly diagnosed breast cancer patients using PET/CT," *Journal of Nuclear Medicine*, vol. 52, no. 9, pp. 1339–1345, 2011.

[38] G. Gasparini, P. C. Brooks, E. Biganzoli et al., "Vascular integrin α(v)β3: a new prognostic indicator in breast cancer," *Clinical Cancer Research*, vol. 4, no. 11, pp. 2625–2634, 1998.

[39] A. J. Beer, H. Kessler, H. J. Wester, and M. Schwaiger, "PET imaging of integrin αVβ3 expression," *Theranostics*, vol. 1, pp. 48–57, 2011.

[40] A. J. Beer, M. Niemeyer, J. Carlsen et al., "Patterns of αvβ3 expression in primary and metastatic human breast cancer as shown by 18F-galacto-RGD PET," *Journal of Nuclear Medicine*, vol. 49, no. 2, pp. 255–259, 2008.

[41] L. M. Kenny, A. Al-Nahhas, and E. O. Aboagye, "Novel PET biomarkers for breast cancer imaging," *Nuclear Medicine Communications*, vol. 32, no. 5, pp. 333–335, 2011.

[42] G. Tomasi, L. Kenny, F. Mauri, F. Turkheimer, and E. O. Aboagye, "Quantification of receptor-ligand binding with [(1)(8)F]fluciclatide in metastatic breast cancer patients," *European Journal of Nuclear Medicine and Molecular Imaging*, vol. 38, no. 12, pp. 2186–2197, 2011.

[43] E. S. Mittra, M. L. Goris, A. H. Iagaru et al., "Pilot pharmacokinetic and dosimetric studies of18F-FPPRGD2: A PET radiopharmaceutical agent for imaging αvβ3 integrin levels," *Radiology*, vol. 260, no. 1, pp. 182–191, 2011.

[44] F. Buchegger, D. Viertl, S. Baechler, V. Dunet, M. Kosinski, C. Poitry-Yamate et al., "68Ga-NODAGA-RGDyK for αvβ3 integrin PET imaging. Preclinical investigation and dosimetry," *Nuklearmedizin*, vol. 50, no. 6, pp. 225–233, 2011.

[45] I. Verel, G. W. M. Visser, and G. A. van Dongen, "The promise of immuno-PET in radioimmunotherapy," *Journal of Nuclear Medicine*, vol. 46, supplement 1, pp. 164S–171S, 2005.

[46] G. A. M. S. van Dongen and M. J. W. D. Vosjan, "Immuno-positron emission tomography: shedding light on clinical antibody therapy," *Cancer Biotherapy and Radiopharmaceuticals*, vol. 25, no. 4, pp. 375–385, 2010.

[47] A. M. Scott, J. D. Wolchok, and L. J. Old, "Antibody therapy of cancer," *Nature Reviews Cancer*, vol. 12, no. 4, pp. 278–287, 2012.

[48] G. Walsh, "Biopharmaceutical benchmarks 2010," *Nature Biotechnology*, vol. 28, no. 9, pp. 917–924, 2010.

[49] G. Kramer-Marek, N. Shenoy, J. Seidel, G. L. Griffiths, P. Choyke, and J. Capala, "68Ga-DOTA-Affibody molecule for in vivo assessment of HER2/neu expression with PET," *European Journal of Nuclear Medicine and Molecular Imaging*, vol. 38, no. 11, pp. 1967–1976, 2011.

[50] E. C. Dijkers, T. H. Oude Munnink, J. G. Kosterink et al., "Biodistribution of 89 Zr-trastuzumab and PET imaging of HER2-positive lesions in patients with metastatic breast cancer," *Clinical Pharmacology and Therapeutics*, vol. 87, no. 5, pp. 586–592, 2010.

[51] S. B. Gaykema, A. H. Brouwers, S. Hovenga, M. N. Lub-de Hooge, E. G. de Vries, and C. P. Schroder, "Zirconium-89-trastuzumab positron emission tomography as a tool to solve a clinical dilemma in a patient with breast cancer," *Journal of Clinical Oncology*, vol. 30, no. 6, pp. 74–75, 2012.

[52] K. McLarty, M. D. Moran, D. A. Scollard et al., "Comparisons of [18F]-1-deoxy-1-fluoro-scyllo-inositol with [18F]-FDG for PET imaging of inflammation, breast and brain cancer xenografts in athymic mice," *Nuclear Medicine and Biology*, vol. 38, no. 7, pp. 953–959, 2011.

[53] M. Wuest, B. J. Trayner, T. N. Grant et al., "Radiopharmacological evaluation of 6-deoxy-6-[18F]fluoro-d-fructose as a radiotracer for PET imaging of GLUT5 in breast cancer," *Nuclear Medicine and Biology*, vol. 38, no. 4, pp. 461–475, 2011.

Hindawi Publishing Corporation
Journal of Oncology
Volume 2012, Article ID 146943, 7 pages
doi:10.1155/2012/146943

Research Article

Initial *In Vivo* Quantification of Tc-99m Sestamibi Uptake as a Function of Tissue Type in Healthy Breasts Using Dedicated Breast SPECT-CT

Steve D. Mann,[1] Kristy L. Perez,[1,2] Emily K. E. McCracken,[3] Jainil P. Shah,[2] Terence Z. Wong,[2] and Martin P. Tornai[1,2,4]

[1] *Medical Physics Graduate Program, Duke University, Durham, NC 27710, USA*
[2] *Department of Radiology, Duke University Medical Center, Durham, NC 27710, USA*
[3] *Duke University Medical School, Durham, NC 27710, USA*
[4] *Department of Biomedical Engineering, Duke University, Durham, NC 27710, USA*

Correspondence should be addressed to Steve D. Mann, steve.mann@duke.edu

Received 20 May 2012; Accepted 14 June 2012

Academic Editor: Alvaro Ruibal

Copyright © 2012 Steve D. Mann et al. This is an open access article distributed under the Creative Commons Attribution License, which permits unrestricted use, distribution, and reproduction in any medium, provided the original work is properly cited.

A pilot study is underway to quantify *in vivo* the uptake and distribution of Tc-99m Sestamibi in subjects without previous history of breast cancer using a dedicated SPECT-CT breast imaging system. Subjects undergoing diagnostic parathyroid imaging studies were consented and imaged as part of this IRB-approved breast imaging study. For each of the seven subjects, one randomly selected breast was imaged prone-pendant using the dedicated, compact breast SPECT-CT system underneath the shielded patient support. Iteratively reconstructed and attenuation and/or scatter corrected images were coregistered; CT images were segmented into glandular and fatty tissue by three different methods; the average concentration of Sestamibi was determined from the SPECT data using the CT-based segmentation and previously established quantification techniques. Very minor differences between the segmentation methods were observed, and the results indicate an average image-based *in vivo* Sestamibi concentration of $0.10 \pm 0.16\,\mu$Ci/mL with no preferential uptake by glandular or fatty tissues.

1. Introduction

Mammography is considered the gold standard for the detection and prebiopsy diagnosis of breast cancer; however, other imaging modalities are beginning to emerge that may allow for alternative techniques for diagnosis or staging of tumors. One such technique developed in our lab is the use of a dedicated breast single photon emission computed tomography and X-ray computed tomography (SPECT-CT) system. Digital mammography suffers from the overlapping of tissues, resulting in difficulty interpreting images in patients with dense breasts. Fully 3-dimensional (3D) imaging modalities, such as CT, are able to overcome the problems associated with limited-view planar systems of mammography or pseudo-3D tomosynthesis. In addition, the diagnostic SPECT system offers unique functional molecular information about the tissue, which may allow for more accurate diagnostics, staging, and treatment response of malignant tissue. Currently, commercially available nuclear medicine breast imaging systems (breast specific gamma imaging or molecular breast imaging systems) utilize planar detectors with compression and limited angular views based on repositioned camera similar to traditional X-ray mammography [1]. Although these systems offer useful information not attainable with conventional mammography and often yield otherwise occult lesions, especially in dense breasted women, the 2-dimensional nature of the systems intrinsically limits their ability to quantify the uptake of radiotracers, such as Tc-99m Sestamibi (MIBI) [2–4]. Additionally, the use of compression adds to the discomfort and apprehension of patients to have such scans. While breast MRI is also compression-free, it is not without discomforts, with common problems including that some women are unable to altogether enter the gantry, the need

for sedatives to help others [5], and universally noted chest (sternal) pain from positioning even though their breasts are not compressed. Additionally, pacemakers and other electromagnetic susceptible devices may complicate MRI procedures. Our system eliminates many of the issues by having a comfortable patient support to rest on and allowing the breast to remain uncompressed while obtaining fully 3D images using a dedicated breast SPECT-CT system located underneath the patient [6].

Tc-99m Sestamibi (MIBI) is a common nuclear medicine imaging agent which has shown to have preferential uptake in breast cancer tissue, with an average reported uptake of 6 : 1 compared to background [7]. However, *in vivo* quantifiable results for MIBI tracer uptake in normal, healthy tissue have yet to be determined. By measuring the average baseline uptake of MIBI in breast tissue, we hypothesize that it may be possible to establish a global threshold for improved diagnosis and staging, especially in women with dense breasts. The objective of this initial study is to measure the average uptake of MIBI in women without any breast cancer history and to determine any differences in MIBI uptake in glandular and fatty breast tissue through the use of various segmentation techniques of the CT images.

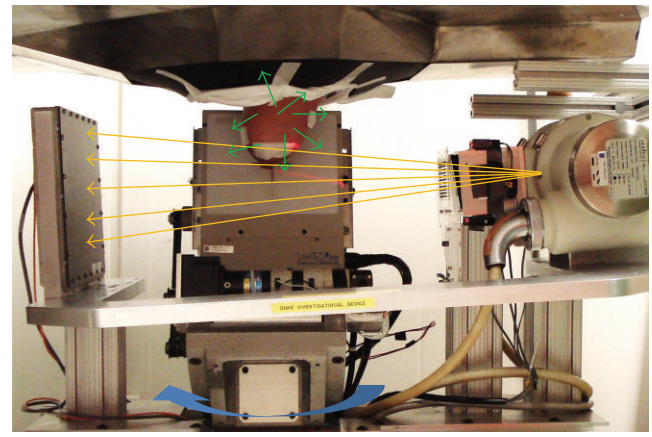

Figure 1: Photograph of the dedicated breast SPECT-CT system. The CT subsystem (left and right) emits a quasimonochromatic X-ray cone beam (orange arrows) with 35 keV mean energy. A rotating plate in front of the CT collimator allows for scatter projection acquisitions. Ribbon lasers mounted on the collimator allow for rapid positioning of the breast into the common FOV. The CZT gamma camera (behind breast) used for SPECT imaging is mounted orthogonally to the CT subsystem and passively detects 140 keV gammas (green arrows) from MIBI.

2. Materials and Methods

Our dedicated breast SPECT-CT system is described extensively in the literature [6, 8–10]. The CT subsystem consists of a digital $25 \times 20\,\text{cm}^2$ flat-panel detector (Paxscan 2520, *Varian Medical Systems, Inc.*) having 127 micron pixelation, and RAD94 (*Varian Medical Systems, Inc.*) tungsten target X-ray source with a cerium-filtered quasimonochromatic X-ray beam with mean energy 35 keV. The SPECT subsystem consists of a $16 \times 20\,\text{cm}^2$ cadmium-zinc-telluride (CZT) LumaGEM 3200S (*Gamma Medica, Inc.*) gamma camera with 2.5 mm pixelation for SPECT imaging mounted orthogonally to the CT subsystem; the SPECT subsystem is capable of fully breast-contoured, sinusoidal trajectories, which allow improved imaging of the chest wall and axilla. The CZT camera has an excellent energy sensitivity and measured resolution of 6.7% at 140 keV, the emission energy of Tc-99m-MIBI. While the CT sub-system is limited to azimuthal rotation, the CZT camera is capable of three degrees of motion: azimuthal rotation, polar angle rotation, and radial position. The numerous motion stages allow for breast-specific contoured trajectories for maximum resolution and imaging volume.

As part of an approved IRB study, seven subjects undergoing presurgical diagnostic parathyroid imaging studies were consented for imaging using our SPECT-CT system. A library database search reveals no link between hyperparathyroidism (one of the most common reasons for parathyroid nuclear imaging at Duke) and breast cancer, save some case reports in the 1970s [11], making this normal-risk population ideal for our studies, where we additionally considered lowering the radiation risk from radiochemical injections to otherwise healthy volunteers. Subjects were scanned in between their routine scintigraphy (10 min post 25 mCi injection) and SPECT (2 hrs post injection) diagnostic parathyroid scans. Subjects' age (34–64), weight, and menstrual cycle were recorded. Volunteers were marked using dual-modality fiducial markers and asked to lie down on a custom radioopaque bed with a flexible center region and opening, allowing one pendant breast to suspend freely in the common field of view (FOV) of the dual-modality system (Figure 1). First, 240 CT cone beam projections using stop-and-shoot were collected in a clockwise fashion about 360°; then, 6 equally distributed scatter projection measurements using a beam stop array (BSA) were acquired in a counterclockwise fashion and subsequently used to scatter correct the CT projections [12]. The total CT scan time was approximately 8 minutes. Finally, 128 SPECT projections (5 s per projection, ~12 min total) using a contoured projected sine wave (PROJSINE) trajectory were acquired [6]. The SPECT data were acquired in list mode and resorted to an 8% primary photopeak energy window about the 140 keV peak of Tc-99m and ~30% scatter window below and abutting the photopeak window. Using quantification procedures previously evaluated on phantoms, the SPECT data were scatter corrected using the dual-energy window method, and attenuation corrected using a SPECT-based uniform attenuation mask with attenuation coefficient of water at 140 keV ($0.1545\,\text{cm}^{-1}$) [6]. Resultant images were decay corrected to the time of injection for analysis. This procedure yields an *in vivo* quantifiable SPECT image volume. To determine the average MIBI concentration in glandular and fatty tissue, specific volumes of interest need to be generated using the segmented CT data, described in the following.

The reconstructed scatter-corrected CT data were analyzed and segmented according to attenuation coefficients. To validate the procedure, varying diameter (6–14 cm) cone

and 12.5 cm diameter cylinder phantoms filled with varying mixtures of water and methanol (100% water to 100% methanol in uniform intervals, to simulate breast tissue) were imaged [13], scatter corrected using our BSA correction technique, and analyzed to determine any postscatter correction effects of object size on the histogram of attenuation values in the image volume (see ahead to Figure 3). The histograms of each slice of the cylinders and cones were fitted to a Gaussian function using nonlinear least squares methods, and the centroids were plotted as a function of cone radius. The results, shown in Figure 2, demonstrate that regardless of the slice position in the cylinder, there is no effect of the intersection of the cone beam X-ray source and fixed diameter of the uniformly filled cylinder; the only effect in attenuation value difference is that due to the nature of the material. The differences between measured and NIST-based narrow beam attenuation coefficients are minor, with the importance being the robustness of the measured value from the cylinder data. A significant dependence of the centroids on object size is noted, however, which may adversely affect simple threshold methods for segmentation.

For the study subjects' data, an edge detection algorithm was used to automatically remove the skin boundary of the breast from the scatter-corrected reconstructed CT images. For comparison, three segmentation techniques of varying computational levels were used for volumetric separation of the glandular and adipose breast tissue. Histograms of reconstructed image slices were first fit with a dual-Gaussian function, defined in (1):

$$A_1 e^{-(x-B_1)^2/C_1^2} + A_2 e^{-(x-B_2)^2/C_2^2}. \quad (1)$$

The simplest method used the entire breast histogram for the curve fitting, with a hard threshold at the minimum between the two Gaussians (Figure 3) used to segment fatty and glandular image-based tissue types. However, this method has potential problems due to the observed radial dependence of the reconstructed attenuation numbers, as described above. This object-size dependence may lead to incorrect binning of pixels when using a global threshold for segmenting a breast. Thus, two additional segmentation techniques were developed to analyze the data on a slice-by-slice basis accounting for the object size.

Both alternative methods utilized the same dual-Gaussian fitting procedure, but for each individual slice (Figure 4). For the first method, the crossing point between the centroids of the two Gaussian functions was calculated and used as a threshold to segment each slice. Depending on the area of the primary image-based breast tissue components, this crossing point was located to either side of the visible minimum of the dual-Gaussian fit. The second method used an iterative approach to find threshold values for each slice that would result in images consisting of at least 95% of the desired tissue type; for slices where the Gaussian overlap was significant, the maximum achievable percentage was chosen.

After segmentation, all nonsegmented CT data sets were coregistered to the SPECT data using the fiducial markers and AMIDE software. Next, MIBI concentrations were measured for the whole breast as well as fatty and glandular tissues from the volumes of interest derived from the three described segmentation procedures. Images were also given to radiologists to read for additional confirmation of our cancer-free assumption.

3. Results

Figure 5 shows the results of the different segmentation methods for one representative data set. Note that the most anterior (nipple) and posterior (chest wall) breast regions were truncated to avoid the reconstruction artifacts in those regions.

The results of the quantitative *in vivo* MIBI measurements are given in Table 1 for each of the three segmentation procedures. Results indicate a lack of tissue-specific preferential MIBI uptake, with an overall average (for the seven subjects) uptake value of $0.10 \pm 0.16\,\mu$Ci/mL for the whole breast. Three of the seven subjects moved significantly during the CT scan or otherwise had truncation artifacts due to the size of the breast; those subjects were excluded from the detailed segmentation analysis.

4. Discussion

Overall *in vivo* quantification results in this initial study indicate an average activity concentration of $0.10 \pm 0.16\,\mu$Ci/mL, but with a fairly large variance across all patients. The large variance is largely due to the low-count statistics obtained by SPECT due to acquisition time restrictions in a clinical setting, with the majority of voxels having a measured uptake of $0\,\mu$Ci/mL. We have previously measured the overall sensitivity of the SPECT system to be accurate for a variety of breast phantom sizes and activity concentrations down to $0.03\,\mu$Ci/mL [6]. The mean results fall within the expected range, as compared with the literature, when accounting for the various corrections applied to our data [14]. Additional subjects may help reduce the variance and allow greater confidence in the expected average MIBI uptake. Results further indicate no preferential uptake of MIBI in glandular or fatty breast tissue. They are also independent of the segmentation method used; this is likely due to the poorer resolution of SPECT (2.5 mm voxels) compared with CT (0.508 mm voxels), which yields minimal gains in accuracy for improved segmentation and registration procedures.

The lack of preferential uptake with MIBI differs from results seen using FDG-PET breast cancer imaging based on clinical scans, likely due to metabolic differences of the tracers [15], but also potentially due to the higher resolution results possible with dedicated imaging modalities. That is, the FDG-PET uptake has not yet been quantified with higher resolution breast PET imaging modalities. Furthermore, our dedicated SPECT system has an intrinsic resolution of 2.5 mm, while clinical SPECT scanners have intrinsic resolutions about 7 mm, before the additional resolution degradation with object distance is considered. Our system has routinely yielded visibility of objects greater than or equal to 4 mm diameters [16] and with accurate quantification.

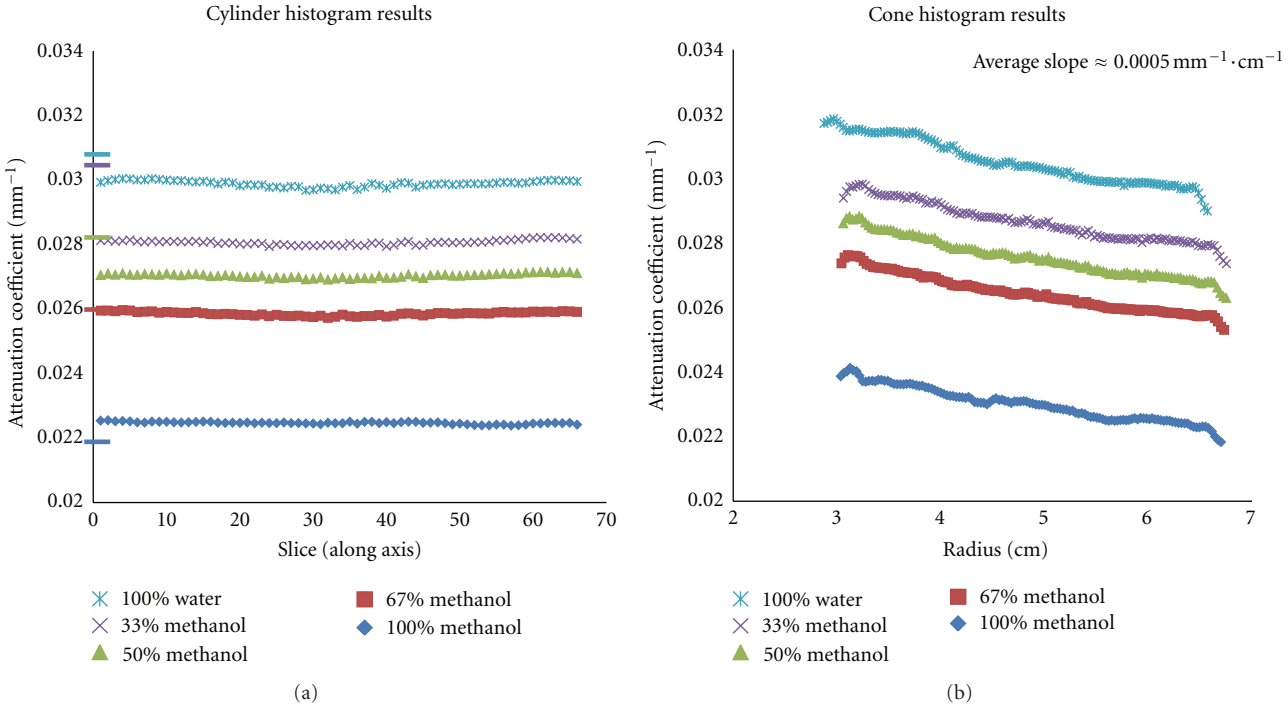

Figure 2: Plots of the centroids of the fitted Gaussian functions for BSA scatter-corrected (a) cylinder and (b) cone phantoms using various mixtures of methanol and water to simulate different uniform tissue densities. NIST-based attenuation values are indicated by matching tick marks on the y-axis of the cylinder graph. The cone phantom results indicate a significant dependence of the measured attenuation value on object size.

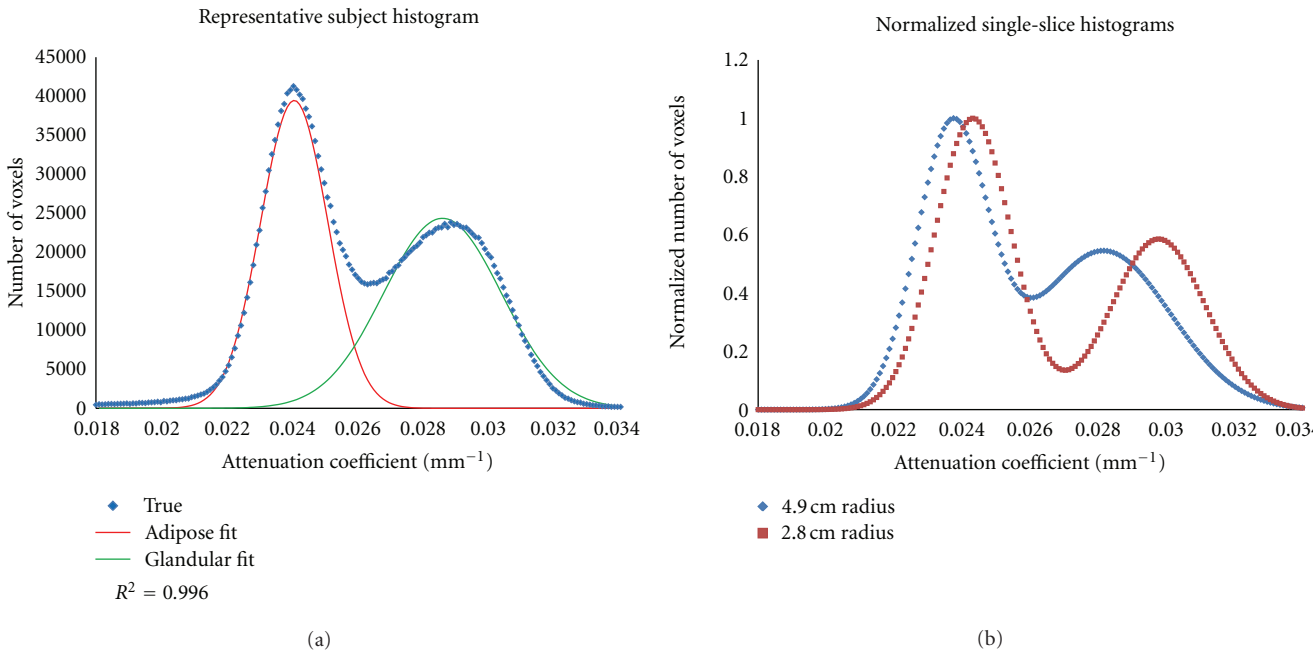

Figure 3: (a) The graph illustrates a representative subject's breast volume histogram and corresponding dual-Gaussian fit. The R^2 value indicates a high quality fit, allowing for various segmentation methods based on the minimum, cross-point, and percentage contribution to be compared. (b) Two normalized representative single-slice histograms from the same subject, along with estimated breast size. The graph clearly demonstrates the shift in attenuation coefficients as a function of object radius.

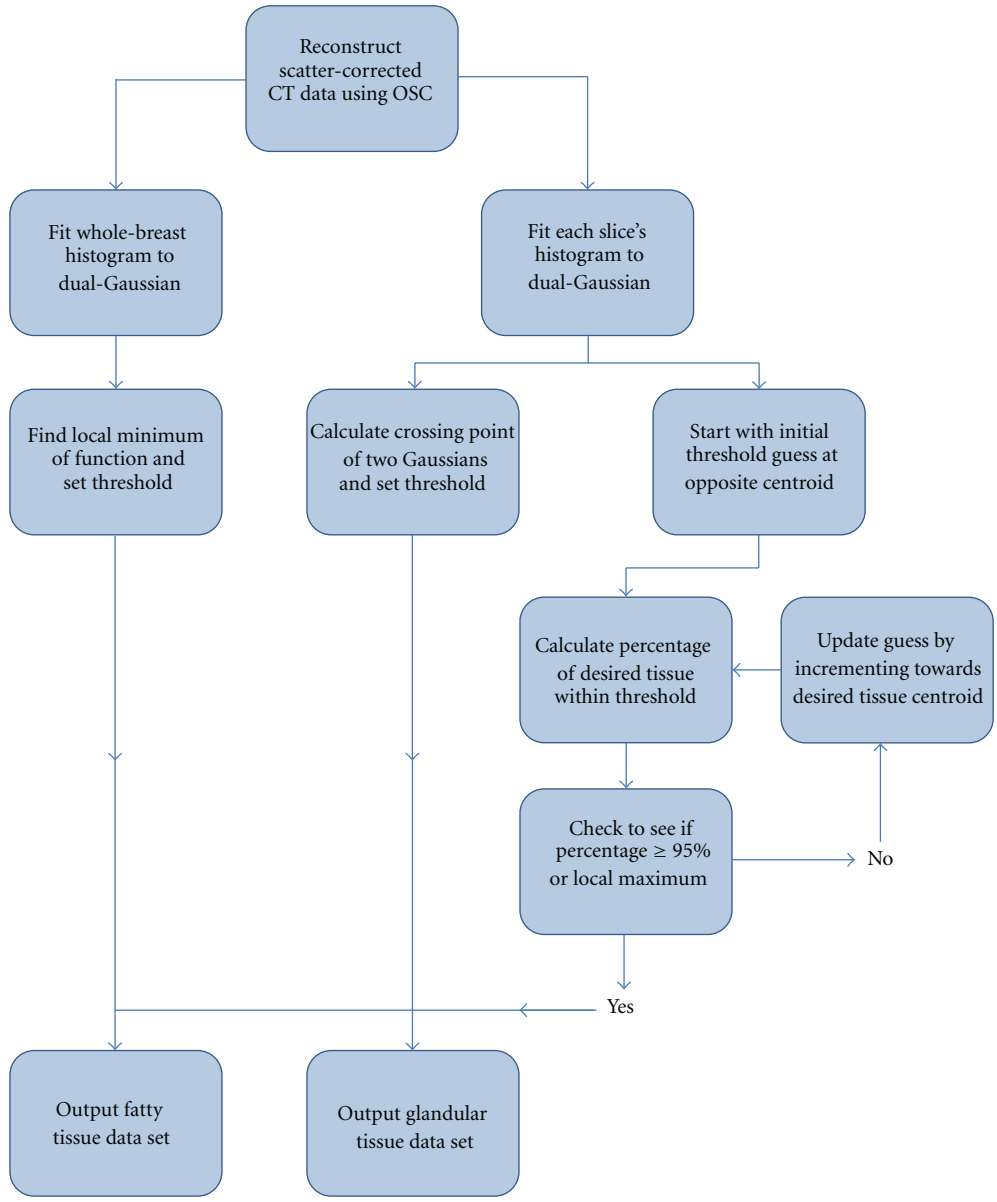

Figure 4: Flowchart diagraming the three segmentation procedures. Each of the three methods uses a dual-Gaussian function to fit the histograms, but the method for choosing an appropriate threshold varies. The simplest method involves choosing the minimum of the total histogram, while more complex methods involve analyzing the percent contribution of each tissue type within the threshold bounds.

Table 1: Results tabulated from the seven patients show no preferential uptake of MIBI in glandular or fatty breast tissue. Average measured uptake values are noisy due to count limitations of *in vivo* SPECT measurements.

Subject	Total breast	Adipose tissue			Glandular tissue		
		Minimum	Cross-point	95% interval	Minimum	Cross-point	95% interval
	Mean (μCi/mL)	Mean (μCi/mL)	Mean (μCi/mL)	Mean (μCi/mL)	Mean (μCi/mL)	Mean (μCi/mL)	Mean (μCi/mL)
1	0.176 ± 0.486	0.154 ± 0.624	0.155 ± 0.623	0.158 ± 0.624	0.20 ± 0.753	0.196 ± 0.747	0.196 ± 0.745
2	0.061 ± 0.388	0.055 ± 0.458	0.054 ± 0.451	0.053 ± 0.471	0.09 ± 0.579	0.082 ± 0.555	0.084 ± 0.552
3	0.168 ± 0.506	0.175 ± 0.601	0.176 ± 0.601	0.179 ± 0.611	0.120 ± 0.492	0.139 ± 0.547	0.129 ± 0.504
4	0.069 ± 0.299	0.066 ± 0.366	0.065 ± 0.360	0.063 ± 0.347	0.077 ± 0.380	0.078 ± 0.394	0.079 ± 0.394
5	0.117 ± 0.520	—	—	—	—	—	—
6	0.038 ± 0.206	—	—	—	—	—	—
7	0.064 ± 0.385	—	—	—	—	—	—
Total	0.10 ± 0.16	0.11 ± 0.26	0.11 ± 0.26	0.11 ± 0.26	0.12 ± 0.27	0.12 ± 0.27	0.12 ± 0.27

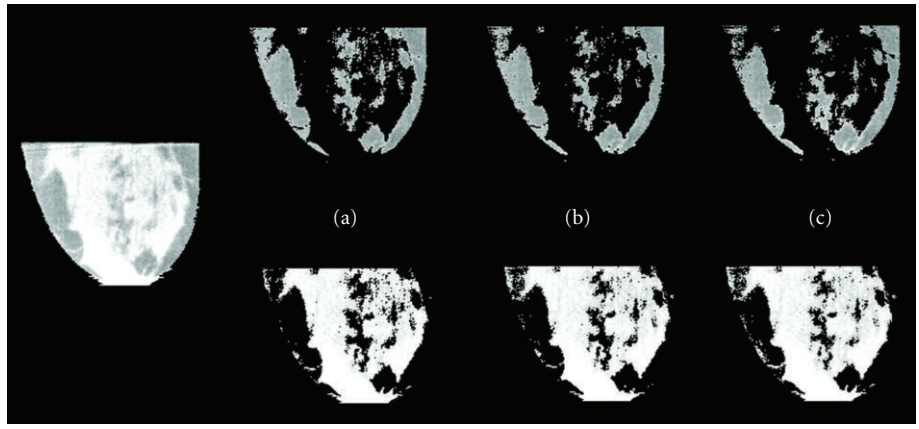

Figure 5: Slice through a representative subject's breast, with the skin removed (left). Segmented images (right) from the same breast using (a) minimum, (b) cross-point, and (c) 95% interval methods described in the text. All images are equivalently windowed and leveled. The minor differences in the resultant images due to the segmentation methods may indicate a lack of need for procedures more sophisticated than a simple threshold.

Approximately 30 subjects are necessary to achieve a 95% confidence in total breast quantification results. Further study on breast cancer confirmed subjects (BIRADS 4 or 5 subjects scheduled for biopsy) may provide complementary information on MIBI uptake concentrations of both the patients' foci as well as the assumed "normal" surrounding tissue. Such results may allow for the development of a universal threshold for diagnosing early-stage breast cancer or be used in staging breast cancer as well as monitoring therapeutic response.

5. Conclusions

No tissue-specific distinction in MIBI uptake was seen in this initial study between glandular and adipose tissues. This implies that menstrual cycle or other biological factors may not affect routine breast imaging with MIBI with respect to baseline background uptake and distribution. One caveat with our results, however, is that more patient data is needed for higher confidence in these initial results. The results are independent of three implemented segmentation procedures, indicating that a simple hard-threshold method may be sufficient for subsequent segmentation of corrected, dedicated breast CT-imaged breast tissue. The potential to use a global lower-level threshold in SPECT to identify regions of interest, especially within dense breasts where we have not observed any detrimental effects, may allow for improved patient care. Further study on normal, otherwise healthy patients is necessary to provide greater confidence in the expected mean MIBI uptake.

Acknowledgments

The authors thank Dr. K. Choudhury for his help in determining the patient number needed for 95% confidence. This work has been funded by the National Cancer Institute of the National Institutes of Health (R01-CA096821 and T32-EB007185). M. P. Tornai is the inventor of this SPECT-CT technology and is named as an inventor on the patent for this technology awarded to Duke (no. 7,609,808). If this technology becomes commercially successful, M. P. Tornai and Duke could benefit financially. The IRB protocol for this study is Pro000026702.

References

[1] M. O'Connor, D. Rhodes, and C. Hruska, "Molecular breast imaging," *Expert Review of Anticancer Therapy*, vol. 9, no. 8, pp. 1073–1080, 2009.

[2] M. S. Rosenthal, J. Cullom, W. Hawkins, S. C. Moore, B. M. W. Tsui, and M. Yester, "Quantitative SPECT imaging: a review and recommendations by the focus committee of the society of nuclear medicine Computer and Instrumentation Council," *Journal of Nuclear Medicine*, vol. 36, no. 8, pp. 1489–1513, 1995.

[3] C. B. Hruska and M. K. O'Connor, "Quantification of lesion size, depth, and uptake using a dual-head molecular breast imaging system," *Medical Physics*, vol. 35, no. 4, pp. 1365–1376, 2008.

[4] R. F. Brem, A. C. Floerke, J. A. Rapelyea, C. Teal, T. Kelly, and V. Mathur, "Breast-specific gamma imaging as an adjunct imaging modality for the diagnosis of breast cancer," *Radiology*, vol. 247, no. 3, pp. 651–657, 2008.

[5] A. K. J. Murphyz and J. A. Brunbergz, "Adult claustrophobia, anxiety and sedation in MRI," *Magnetic Resonance Imaging*, vol. 15, no. 1, pp. 51–54, 1997.

[6] K. L. Perez, S. J. Cutler, P. Madhav, and M. P. Tornai, "Towards quantification of functional breast images using dedicated SPECT with non-traditional acquisition trajectories," *IEEE Transactions on Nuclear Science*, vol. 58, no. 5, pp. 2219–2225, 2011.

[7] J. Maublant, M. De Latour, D. Mestas et al., "Technetium-99m-Sestamibi uptake in breast tumor and associated lymph nodes," *Journal of Nuclear Medicine*, vol. 37, no. 6, pp. 922–925, 1996.

[8] P. Madhav, D. J. Crotty, R. L. McKinley, and M. P. Tornai, "Evaluation of tilted cone-beam CT orbits in the development

of a dedicated hybrid mammotomograph," *Physics in Medicine and Biology*, vol. 54, no. 12, pp. 3659–3676, 2009.

[9] D. J. Crotty, S. L. Brady, D. C. Jackson et al., "Evaluation of the absorbed dose to the breast using radiochromic film in a dedicated CT mammotomography system employing a quasi-monochromatic x-ray beam," *Medical Physics*, vol. 38, no. 6, pp. 3232–3245, 2011.

[10] R. L. McKinley, M. P. Toraai, E. Samei, and M. L. Bradshaw, "Initial study of quasi-monochromatic x-ray beam performance for x-ray computed mammotomography," *IEEE Transactions on Nuclear Science*, vol. 52, no. 5, pp. 1243–1250, 2005.

[11] A. Katz, L. Kaplan, S. G. Massry, R. Heller, D. Plotkin, and I. Knight, "Primary hyperparathyroidism in patients with breast carcinoma," *Archives of Surgery*, vol. 101, no. 5, pp. 582–585, 1970.

[12] P. Madhav, C. M. Li, and M. Tornai, "Development of in vivo characterization of breast tissues through absolute attenuation coefficients using dedicated cone-beam C," in *Medical Imaging: Physics of Medical Imaging*, vol. 7622 of *Proceedings of SPIE*, p. 762209, 2010.

[13] J. Shah, J. H. Pachon, P. Madhav, and M. P. Tornai, "Detailed characterization of 2D and 3D scatter-to-primary ratios of various breast geometries using a dedicated CT mammotomography system," in *Medical Imaging: Physics of Medical Imaging*, vol. 7961 of *Proceedings of SPIE*, p. 796158, February 2011.

[14] M. K. O'Connor, S. W. Phillips, C. B. Hruska, D. J. Rhodes, and D. A. Collins, "Molecular breast imaging: advantages and limitations of a scintimammographic technique in patients with small breast tumors," *Breast Journal*, vol. 13, no. 1, pp. 3–11, 2007.

[15] D. Vranjesevic, C. Schiepers, D. H. Silverman et al., "Relationship between 18F-FDG uptake and breast density in women with normal breast tissue," *Journal of Nuclear Medicine*, vol. 44, no. 8, pp. 1238–1242, 2003.

[16] S. J. Cutler, K. L. Perez, H. X. Barnhart, and M. P. Tornai, "Observer detection limits for a dedicated SPECT breast imaging system," *Physics in Medicine and Biology*, vol. 55, no. 7, pp. 1903–1916, 2010.

Hindawi Publishing Corporation
Journal of Oncology
Volume 2012, Article ID 361341, 7 pages
doi:10.1155/2012/361341

Review Article

Sentinel Node Mapping for Breast Cancer: Current Situation

Sergi Vidal-Sicart[1,2] and Renato Valdés Olmos[3]

[1] *Nuclear Medicine Department, Hospital Clínic Barcelona, 08036 Barcelona, Spain*
[2] *Nuclear Medicine Department, CRC-MAR, 08003 Barcelona, Spain*
[3] *Nuclear Medicine Department, The Netherlands Cancer Institute, Antoni van Leeuwenhoek Hospital, 1066 CX Amsterdam, The Netherlands*

Correspondence should be addressed to Sergi Vidal-Sicart, svidal@clinic.ub.es

Received 19 June 2012; Accepted 3 July 2012

Academic Editor: Alvaro Ruibal

Copyright © 2012 S. Vidal-Sicart and R. Valdés Olmos. This is an open access article distributed under the Creative Commons Attribution License, which permits unrestricted use, distribution, and reproduction in any medium, provided the original work is properly cited.

Axillary node status is a major prognostic factor in early-stage disease. Traditional staging needs levels I and II axillary lymph node dissection. Axillary involvement is found in 10%–30% of patients with T1 (<2 cm) tumours. Sentinel lymph node biopsy is a minimal invasive method of checking the potential nodal involvement. It is based on the assumption of an orderly progression of lymph node invasion by metastatic cells from tumour site. Thus, when sentinel node is free of metastases the remaining nodes are free, too (with a false negative rate lesser than 5%). Moreover, Randomized trials demonstrated a marked reduction of complications associated with the sentinel lymph node biopsy when compared with axillary lymph node dissection. Currently, the sentinel node biopsy procedure is recognized as the standard treatment for stages I and II. In these stages, this approach has a positive node rate similar to those observed after lymphadenectomy, a significant decrease in morbidity and similar nodal relapse rates at 5 years. In this review, the indications and contraindications of the sentinel node biopsy are summarized and the methodological aspects discussed. Finally, the new technologic and histologic developments allow to develop a more accurate and refinate technique that can achieve virtually the identification of 100% of sentinel nodes and reduce the false negative rate.

1. Introduction

Breast cancer is the most common cancer in women worldwide. In 2010, it was estimated that in the USA there were nearly 210,000 new cases of invasive breast cancer and more than 40,000 deaths. Axillary node status is a major prognostic factor in early-stage disease, and this information is important for treatment. Traditional staging needs levels I and II axillary lymph node dissection. Axillary involvement is found in 10%–30% of patients with T1 (<2 cm) tumours. This rate reaches 45% for small T2 tumours (2.1–3 cm) and 55%–70% for larger tumours (>3 cm). Routine axillary lymphadenectomy adds the risk of lymphedema, sensory disturbances, and chronic pain.

Sentinel lymph node biopsy is a minimal invasive method of checking the potential nodal involvement. It is based on the assumption of an orderly progression of lymph node invasion by metastatic cells from tumour site. Thus, the nodal basin is free of malignancy if the sentinel lymph node is not involved. Patients with metastasis to a sentinel node would undergo either immediate or delayed completion lymph node dissection. Randomized trials demonstrated a marked reduction of complications associated with the sentinel lymph node biopsy when compared with axillary lymph node dissection. In the ALMANAC trial, more than 1,000 patients were randomized to undergo either axillary lymphadenectomy or sentinel node biopsy. Lymphedema was present in 13% of the axillary lymphadenectomy group and in 5% of the sentinel node group 12 months after surgery.

In 2005, guidelines from the American Society of Clinical Oncology stressed that a multidisciplinary team should aim at a sentinel node identification rate of 85% with a false-negative rate of 5% or less in order to abandon axillary dissection. False-negative rate is the proportion of axillary node dissection, positive cases with a negative sentinel node at biopsy. False-negative cases may result from massive involvement of the real sentinel node, a circumstance that interferes with the uptake of both radiocolloid and dye and

lymph flow that goes to a node other than the true sentinel node [1].

A meta-analysis of 69 trials with a total of 8,059 patients in whom sentinel node biopsy was followed by axillary dissection showed substantial variability in the performance of the technique throughout different centers. However, recent results from large multi-institutional trials showed that all have achieved excellent identification rates, ranging from 93% to 97%, but that none achieved a false-negative rate lower than 5%. The lowest false-negative rates were obtained in the 2 studies in which preoperative lymphoscintigraphy and dual mapping during surgery were required. In the ALMANAC trial, the false-negative rate was 6.7%. However, if only blue sentinel nodes are considered, the false-negative rate was 9.1% [2–5].

2. Clinical Scenarios and Current Indications

Clinical indications for this approach have been changing through the years and there is still a debate on some of them. Many centers use sentinel node biopsy only in patients with a unifocal tumour smaller than 3 cm, whereas others have extended the application to patients with large T2 or T3 (>5 cm) tumours, multifocal/multicentric carcinomas, or to patients who have received neoadjuvant chemotherapy.

Currently, the sentinel node biopsy procedure is recognized as the standard treatment for stages I and II. In these stages, this approach has a positive node rate similar to those observed after lymphadenectomy, a significant decrease in morbidity and similar nodal relapse rates at 5 years. No significant differences on disease-free survival, overall survival, and local control of disease were seen in case of negative sentinel node [5]. The indications and recommendations of the sentinel node biopsy are summarized in Table 1.

(i) Pregnancy is no contraindication for sentinel node biopsy, but only for blue dye, and it has been demonstrated that the dose to the foetus from this procedure is negligible [6].

(ii) The evidence regarding the safety of sentinel node biopsy is mainly based on studies including T1 and small T2 tumours only. However, in patients with larger tumours (T3-T4), the false negative rate has been similar and no increased axillary recurrence has been reported [6, 7].

(iii) Multifocal breast cancer is defined as separate foci of ductal carcinoma more than 2 cm apart within the same quadrant, while multicentric breast cancer indicates the presence of separate independent foci of carcinoma in different quadrants. The prevalence of axillary metastases and false negative results is higher in multifocal or multicentric tumours. However, the reported axillary recurrence rates are acceptable also in patients with multifocal or multicentric tumours [6–9].

(iv) DCIS does not metastasize to regional lymph nodes. However, invasion is missed in up to 40% of patients in the preoperative diagnosis. Therefore, sentinel node biopsy is recommended in patients undergoing mastectomy. In patients with breast conservation, sentinel lymph node biopsy can be performed as a second operation if invasion is detected in the surgical specimen [6, 10].

(v) Palpable axillary nodes may be tumour negative in up to 40% of the patients. Preoperative axillary ultrasound with fine needle aspiration cytology or core needle biopsy from the suspicious nodes is a widely accepted policy. In many units, sentinel node biopsy is performed also in patients with palpable nodes if negative in the preoperative diagnosis [6].

(vi) Internal mammary sentinel node detection rate is significantly affected by the depth of radiopharmaceutical injection. It is generally recognized that mapping of inner mammary chain requires deep injection (peritumoural or intratumoural) of radiotracer. With this approach, internal mammary chain sentinel nodes have been detected in about 30% of patients with breast cancer, of which about 60%–90% could be harvested during surgery and 11%–27% of them will have metastases. However, the significance of internal mammary sentinel node biopsy is under debate. There is evidence that mapping it leads to stage migration and modification of treatment planning with respect to radiotherapy and systemic therapy, but more evidence is necessary to support that it will improve the outcome of treatment and survival [11, 12].

A second sentinel node biopsy may be performed in patients with a local recurrence after breast conservation and negative axillary sentinel node biopsy. The success rate may be lower when compared with a primary sentinel node biopsy. Furthermore, extra axillary sentinel nodes are visualized more frequently. Sentinel node biopsy can be performed in patients undergoing breast surgery due to a local recurrence after breast conservation in DCIS. Furthermore, plastic surgery with breast augmentation or reduction does not contraindicate the procedure. In prior excisional biopsy the lymph drainage is probably changed in patients who have undergone previous breast surgery (oncologic and nononcologic). Extra-axillary drainage is identified more frequently in reoperative sentinel node biopsy than in former sentinel node biopsy. However, there are evidences that sentinel node biopsy performed in the area of previous breast biopsy do not affect the accuracy of the procedure [6, 13].

(vii) Before neoadjuvant chemotherapy, sentinel node biopsy gives a more precise axillary staging, with more information about the nodal spread. But it may delay the beginning of the therapy, and two surgeries can be necessary. After neoadjuvant chemotherapy, the sentinel node biopsy may lead to an underestimation of the initial stage. On the other hand, axillary nodal status after neoadjuvant therapy is also a highly significant prognostic factor. Pathologic complete response in the axilla can be achieved in up to 40% of the patients. These patients avoid axillary lymph node dissection and associated morbidity. Available data show that there are no significant differences in the success rate of sentinel node biopsy according to clinical tumour size or clinical nodal status, and that the false-negative rate is not affected by tumour response to chemotherapy [14, 15].

Despite this, the current controversy in this scenario lies on the question of axillary lymph node dissection after a positive sentinel node biopsy, mainly stimulated by the recent publication of the ACOSOG-Z0011 data [16].

Table 1: Recommendations for SLN biopsy.

Clinical scenario	Indication of sentinel node biopsy
T1 or T2 tumours	Established
Older age	Established
Obesity	Established
Before preoperative systemic therapy	Established
Male breast cancer	Established
DCIS with mastectomy	Established
Internal mammary chain	Established but controversial
DCIS without mastectomy	Controversial, except for DCIS with suspected or proven microinvasion
Pregnancy	Controversial
Suspicious, palpable axillary nodes	Controversial
T3 or T4 tumours	Controversial
Multicentric or multifocal tumours	Controversial
Prior diagnostic or excisional breast biopsy	Controversial
Prior axillary surgery	Controversial
Prior non-oncologic breast surgery	Controversial
After preoperative systemic therapy	Controversial
Inflammatory breast cancer	Not recommended

DCIS: ductal carcinoma in situ.
Controversial indications suggest that the indication is not universally accepted or the evidence behind the practice is limited.

3. Methodological Aspects

The sentinel node procedure uses a radiotracer, a blue dye, or both to find the node. Radiopharmaceuticals for sentinel lymph node technique are colloids labelled with ^{99m}Tc. These colloids allow sentinel node visualization with a gamma camera before surgery and intraoperative detection with a hand-held gamma probe. Controversies exist with regard to the selection of agents, the size of the particles of the radiotracer, the optimal route for injection, time to scintigraphy and intraoperative detection, and whether or not extra-axillary lymph nodes should be considered as well.

Mariani et al. suggested that ^{99m}Tc-labeled colloids with most of the particles in the 100 to 200 nm size range would be ideal for sentinel node biopsy in breast cancer. The choice of tracer is often guided by local availability. ^{99m}Tc-labeled colloids of human serum albumin are often used in Europe, ^{99m}Tc-sulfur colloid is used in the United States (sometimes after filtration through a 0.1 or 0.2 mm membrane), and ^{99m}Tc-antimony trisulfide in Australia. There is no established difference between a 1-day protocol (same-day imaging and surgery) and a 2-day protocol [6].

Lymphatic drainage of the breast is not completely understood. After an experience of almost 20 years, it is generally assumed that both deep and superficial injection approaches are valid techniques and may be complementary. In most early sentinel node studies, the tracer was injected around the tumour and such peritumoral injection was considered the gold standard against which all other mapping techniques were tested. Many investigators have reported good results using injection into the breast skin over the tumour or using a periareolar, subareolar, or even intratumoural injection. One clearly established advantage of deep injections (peritumoral/intratumoural) is its ability to also reveal extra-axillary drainage. On the other hand, superficial injection techniques (subdermal/areolar) provide a faster lymphatic drainage, yield more radioactive counts at the axillary sentinel nodes, and are independent of the palpable or nonpalpable nature of the tumour. Hence, the tracer is not always transported to the same axillary node, regardless the injection site. However, if the goal is axillary staging only, a superficial tracer injection is preferable due to better visualization of axillary sentinel nodes. If the aim is to stage also the extra-axillary nodal basins, peri- or intratumoural injection should be applied [6, 17, 18].

Lymphoscintigraphy has been an essential component for the preoperative sentinel node identification in breast cancer. Lymphoscintigraphy has the potential to both improve accuracy and reduce morbidity relative to gamma probe alone by providing the surgeon with a roadmap of lymphatic drainage and the location of sentinel nodes [6].

To identify all sentinel nodes and avoid confusion with a stasis in a lymphatic vessel, images are acquired with an adequate delay after injection. Lymphatic drainage can be slower in old or overweight patients. With planar scintigraphy, combining 2 views may help prevent some sentinel nodes from being missed (Figure 1).

The advent of SPECT/CT reinforces the potential of preoperative lymphoscintigraphy. The functional information from SPECT can be combined with the morphological information from CT by applying both techniques in one session. The resulting SPECT/CT fused images depict sentinel nodes in an anatomical landscape providing a helpful roadmap for surgeons. In recent years, SPECT/CT has been used in breast cancer patients with unusual or complex drainage. This is the case in patients with drainage outside the axilla. SPECT/CT can also detect hot nodes missed by planar imaging because

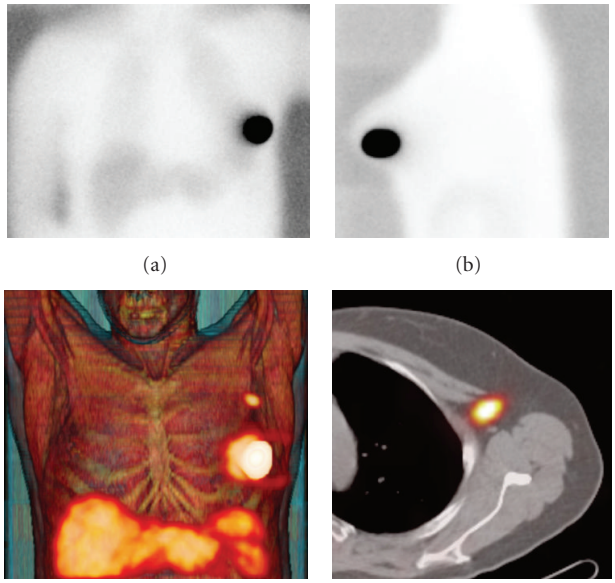

(a) (b) (c) (d)

Figure 1: Planar images (a)-(b) showing no drainage of ^{99m}Tc-nanocolloid from the injection site in left breast. By contrast, fused SPECT/CT with volume rendering (c) shows drainage to the left axilla with one sentinel node in level 1 (d).

of shine-through from the injection site or in overweight patients [19, 20] (Figure 2).

Differentiating a true sentinel node from a secondary echelon node is difficult. Also, lymphatics of a tumor site can drain simultaneously to more than one sentinel node.

Lymphoscintigraphy is able to identify sentinel nodes in a majority of cases by acquiring early and delayed planar images. In current protocols, SPECT/CT is performed following delayed planar images (mostly 2–4 hours after tracer administration). This sequential acquisition is helpful to clarify the role of both modalities. However, it is necessary to specify the criteria for sentinel node identification on preoperative images. Major criteria to identify lymph nodes as sentinel nodes are the visualization of lymphatic ducts, the time of appearance, the lymph node basin, and the intensity of lymph node uptake. Following these criteria visualized radioactive lymph nodes may be classified as follows

(i) Definitively sentinel nodes: this category concerns all lymph nodes draining from the site of the primary tumour through an own lymphatic vessel, or a single radioactive lymph node in a lymph node basin.

(ii) Highly probable sentinel nodes: this category includes lymph nodes appearing between the injection site and a first draining node, or nodes with increasing uptake appearing in other lymph node stations

(iii) Less probable sentinel nodes: all higher echelon nodes may be included in this category.

The use of these categories to characterize radioactive lymph nodes is also helpful for clinical decision making. Lymph nodes of the first two categories (definitively sentinel node or highly probable sentinel node) are the nodes

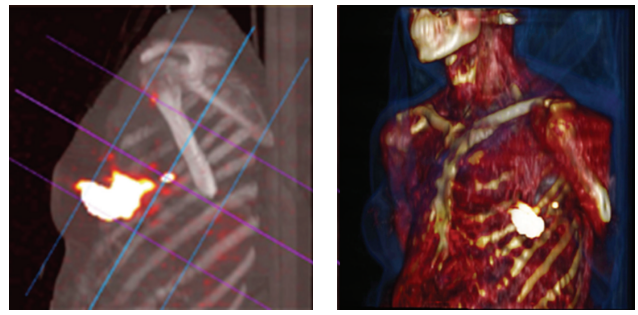

(a) (b)

Figure 2: Fused SPECT/CT (a) displayed with maximum intensity projection (MIP) showing a sentinel node in the left axilla. SPECT/CT with volume rendering for 3D display (b) adds an excellent overview for surgical planning.

recognized by the nuclear physician and that must be removed at the operation room by the surgeon. Less probable sentinel nodes may sometimes be removed depending on the degree of remaining radioactivity measured by the gamma probe during the control of the surgical field [21].

Dyes cause the blue colouring as they pass slowly through the sentinel node. Isosulfan blue is of greater use in the United States, and patent blue V in Europe. Data from NSABP B-32 and ACOSOG-Z0010 with isosulfan, and from ALMANAC with patent blue V, showed that the overall risk of allergic reaction is close to 1% for both dyes, with an approximately 0.1% risk of severe reactions (grade III). Despite a risk of allergic reactions to blue dye, most teams favour the combinative mapping procedure [6].

In one multicentric study, the false-negative rate was 17.7% if only 1 node was resected, 10% if 2, 6.9% if 3, 5.5% if 4, and 1% if 5 or more. These results should not imply removal of multiple nodes for an optimal sentinel node procedure. However, all identified hot or blue nodes should be resected. Careful palpation by the surgeon of the operative field is also required to identify any suggestive large, hard nonblue and nonradioactive nodes [5].

4. New Developments

During the last decade, intraoperative imaging devices have become available for clinical practice and can be used during surgery as they provide information that can be combined with data obtained with conventional gamma probes. However, since nonimaging probes are still the standard equipment for detection of radiolabeled tissue in the operating room, the role of intraoperative imaging is generally limited and constitutes an additional aid to the surgeon. Intraoperative imaging with portable gamma cameras provides real-time imaging with a global overview of all radioactive hot spots in the whole surgical field. Its position can be adjusted to also show sentinel nodes near the injection area, which can easily be missed when using the non-imaging probe.

Some authors have tried to clarify the added value of portable gamma camera in clinical practice. In fact, there is no consensus on the real need for an intraoperative imaging

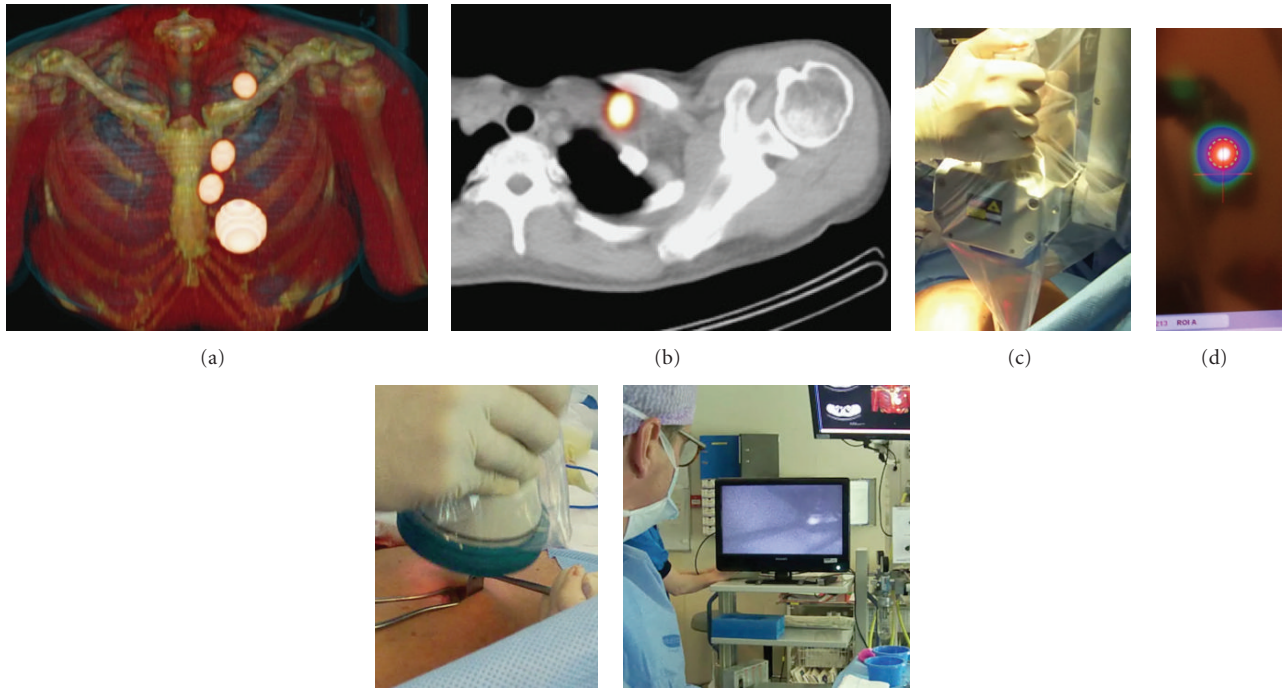

Figure 3: Fused SPECT/CT displayed with volume rendering (a) showing drainage of ICG/^{99m}Tc-nanocolloid to the internal mammary chain and left supraclavicular area. The supraclavicular node is shown on axial SPECT/CT (b). The inferior internal mammary node as well as the supraclavicular one were removed using a portable gamma camera (c) to detect the radioactive signal (d) and a fluorescence camera (e) to localize the fluorescent sentinel node (f).

device to help detection of the sentinel lymph node. The usefulness of the portable gamma cameras in breast cancer patients lies on when no conventional gamma camera is available or in particular cases with extra-axillary drainage (intramammary and internal mammary chain nodes) or when the sentinel lymph node is located very close to the injection site. Although the majority of these cases can be solved with the presurgical information provided by SPECT/CT, real-time images acquired with a portable gamma camera can be an alternative to hybrid imaging. On the other hand, the preoperative anatomical information obtained by SPECT/CT appears to lead to a more optimal use of portable devices for sentinel localization in the operation room. Using an intraoperative imaging device implies the possibility to better planning the procedure and to monitor the lymphatic basin before and after removal of the hot nodes, so to verify completeness of lymph node excision. After excision of each lymph node, a new image is acquired and compared with the situation before excision. If focal radioactivity remains at the same location, it is concluded that another possible sentinel lymph node is still in place [22, 23].

Thanks to novel technological possibilities, combining a spatial localization system and two tracking targets to be fixed on a conventional, hand-held gamma probe results in new 3D visualization of the traditional acoustic signal of the gamma probe. In this regard, the most recent development is the system so-called free-hand SPECT, in which a continuous positioning system installed in the operating room is based on a fix-pointing device, on the patient's body and, respectively, on the hand-held gamma counting probe, thus permitting a virtual reconstruction in a 3D environment. The surgeon can easily check location and depth of the foci of radioactivity accumulation to be resected, and this 3D information may be further used for precise localization and targeting of the radioactive sentinel lymph node(s) and of tumour tissue. The device can ensure permanent assistance and transparent documentation of soft tissue removal during the intervention [24].

On the other hand, the possibility of combining the current radiopharmaceuticals with other agents opens new fields to explore. In this regard, a radiolabeled nanocolloid agent has been combined with ICG, a fluorescent agent, for sentinel node detection. In contrast to the use of a single-fluorescent agent, this bimodal tracer may allow the surgeons to integrate the standard approach based on radioguided detection with a portable gamma camera with a new optical modality based on fluorescent signal detection. This approach is being successfully applied in several malignancies and to localize sentinel nodes outside the axilla in breast cancer (Figure 3) [25].

For all these new intraoperative modalities, the preoperative anatomical SPECT/CT acquisition remains essential and is the starting point for surgical planning.

Before sending for histological examination, any lymph node removed should be rechecked by the probe to demonstrate that they are radioactive. Histopathological assessment of the sentinel lymph node is the golden standard procedure

for the subsequent management of the conservative surgery in breast cancer patients. However, this "golden standard" is highly variable between centres. In many units, the sentinel nodes are assessed intraoperatively using imprint cytology, frozen sectioning, or both, and more thoroughly after the operation. The sensitivity of the intraoperative diagnosis in variable and many units do not adopt it at all. Some molecular methods have been used previously for sentinel node diagnosis but have shown a lack of reproducibility, a longer time for the intraoperative assessment, and an inability to study the whole lymph node. A new molecular method has been developed recently, based on an one-step nucleic acid amplification (OSNA) method. This procedure is in the phase of validation in many centres, although there are others that routinely apply this method [26].

In summary, after two decades of sentinel lymph node biopsy use in breast cancer, this technique is the current standard of care for locoregional staging. However, some concerns remain as there is no only one standardized technique and many controversies are still unsolved. However, with the recent technologic and histologic developments, a more accurate and refinate technique can be achieved by virtually identifying-100% of sentinel nodes and reduce the false negative rate.

References

[1] G. H. Lyman, A. E. Giuliano, M. R. Somerfield et al., "American Society of Clinical Oncology guideline recommendations for sentinel lymph node biopsy in early-stage breast cancer," *Journal of Clinical Oncology*, vol. 23, no. 30, pp. 7703–7720, 2005.

[2] T. Kim, A. E. Giuliano, and G. H. Lyman, "Lymphatic mapping and sentinel lymph node biopsy in early-stage breast carcinoma: a metaanalysis," *Cancer*, vol. 106, no. 1, pp. 4–16, 2006.

[3] G. Gill, "Sentinel-lymph-node-based management or routine axillary clearance? One-year outcomes of sentinel node biopsy versus axillary clearance (SNAC): a randomized controlled surgical trial," *Annals of Surgical Oncology*, vol. 16, no. 2, pp. 266–275, 2009.

[4] A. Goyal, R. G. Newcombe, A. Chhabra, and R. E. Mansel, "Factors affecting failed localisation and false-negative rates of sentinel node biopsy in breast cancer—results of the ALMANAC validation phase," *Breast Cancer Research and Treatment*, vol. 99, no. 2, pp. 203–208, 2006.

[5] D. N. Krag, S. J. Anderson, T. B. Julian et al., "Technical outcomes of sentinel-lymph-node resection and conventional axillary-lymph-node dissection in patients with clinically node-negative breast cancer: results from the NSABP B-32 randomised phase III trial," *The Lancet Oncology*, vol. 8, no. 10, pp. 881–888, 2007.

[6] G. Cheng, S. Kurita, D. A. Torigian, and A. Alavi, "Current status of sentinel lymph-node biopsy in patients with breast cancer," *European Journal of Nuclear Medicine and Molecular Imaging*, vol. 38, no. 3, pp. 562–575, 2011.

[7] T. J. Meretoja, M. H. Leidenius, P. S. Heikkilä, and H. Joensuu, "Sentinel node biopsy in breast cancer patients with large or multifocal tumors," *Annals of Surgical Oncology*, vol. 16, no. 5, pp. 1148–1155, 2009.

[8] A. J. Spillane and M. E. Brennan, "Accuracy of sentinel lymph node biopsy in large and multifocal/multicentric breast carcinoma—a systematic review," *European Journal of Surgical Oncology*, vol. 37, no. 5, pp. 371–385, 2011.

[9] O. R. Brouwer, L. Vermeeren, I. M. van der Ploeg et al., "Lymphoscintigraphy and SPECT/CT in multicentric and multifocal breast cancer: does each tumour have a separate drainage pattern?: results of a Dutch multicentre study (MULTISENT)," *European Journal of Nuclear Medicine and Molecular Imaging*, vol. 39, no. 7, pp. 1137–1143, 2012.

[10] T. J. Meretoja, P. S. Heikkilä, K. Salmenkivi et al., "Outcome of patients with ductal carcinoma in situ and sentinel node biopsy," *Annals of Surgical Oncology*, vol. 19, no. 7, pp. 2345–2351, 2012.

[11] P. Paredes, S. Vidal-Sicart, G. Zanón et al., "Clinical relevance of sentinel lymph nodes in the internal mammary chain in breast cancer patients," *European Journal of Nuclear Medicine and Molecular Imaging*, vol. 32, no. 11, pp. 1283–1287, 2005.

[12] J. C. Bourre, R. Payan, D. Collomb et al., "Can the sentinel lymph node technique affect decisions to offer internal mammary chain irradiation?" *European Journal of Nuclear Medicine and Molecular Imaging*, vol. 36, no. 5, pp. 758–764, 2009.

[13] J. Rodriguez Fernandez, S. Martella, G. Trifirò et al., "Sentinel node biopsy in patients with previous breast aesthetic surgery," *Annals of Surgical Oncology*, vol. 16, no. 4, pp. 989–992, 2009.

[14] A. M. Kelly, B. Dwamena, P. Cronin, and R. C. Carlos, "Breast cancer sentinel node identification and classification after neoadjuvant chemotherapy -systematic review and metaanalysis," *Academic Radiology*, vol. 16, no. 5, pp. 551–563, 2009.

[15] A. Pinero, J. Giménez, S. Vidal-Sicart, and M. Intra, "Selective sentinel lymph node biopsy and primary systemic therapy in breast cancer," *Tumori*, vol. 96, no. 1, pp. 17–23, 2010.

[16] A. E. Giuliano, K. K. Hunt, K. V. Ballman et al., "Axillary dissection vs no axillary dissection in women with invasive breast cancer and sentinel node metastasis: a randomized clinical trial," *Journal of the American Medical Association*, vol. 305, no. 6, pp. 569–575, 2011.

[17] S. H. Estourgie, O. E. Nieweg, R. A. Valdés Olmos, E. J. T. Rutgers, and B. B. R. Kroon, "Lymphatic drainage patterns from the breast," *Annals of Surgery*, vol. 239, no. 2, pp. 232–237, 2004.

[18] M. Noguchi, M. Inokuchi, and Y. Zen, "Complement of peritumoral and subareolar injection in breast cancer sentinel lymph node biopsy," *Journal of Surgical Oncology*, vol. 100, no. 2, pp. 100–105, 2009.

[19] I. M. C. Van Der Ploeg, R. A. Valdés Olmos, O. E. Nieweg, E. J. T. Rutgers, B. B. R. Kroon, and C. A. Hoefnagel, "The additional value of SPECT/CT in lymphatic mapping in breast cancer and melanoma," *Journal of Nuclear Medicine*, vol. 48, no. 11, pp. 1756–1760, 2007.

[20] L. Vermeeren, I. M. C. Van Der Ploeg, R. A. Valdés Olmos et al., "SPECT/CT for preoperative sentinel node localization," *Journal of Surgical Oncology*, vol. 101, no. 2, pp. 184–190, 2010.

[21] S. Vidal-Sicart, O. Roberto Brouwer, and R. A. Valdés-Olmos, "Evaluation of the sentinel lymph node combining SPECT/CT with the planar image and its importance for the surgical act," *Revista Espanola de Medicina Nuclear*, vol. 30, pp. 331–337, 2011.

[22] R. A. Valdés Olmos, S. Vidal-Sicart, and O. E. Nieweg, "SPECT-CT and real-time intraoperative imaging: new tools for sentinel node localization and radioguided surgery?" *European Journal of Nuclear Medicine and Molecular Imaging*, vol. 36, no. 1, pp. 1–5, 2009.

[23] S. Vidal-Sicart, P. Paredes, G. Zanón et al., "Added value of intraoperative real-time imaging in searches for difficult-to-locate sentinel nodes," *Journal of Nuclear Medicine*, vol. 51, no. 8, pp. 1219–1225, 2010.

[24] T. Wendler, K. Herrmann, A. Schnelzer et al., "First demonstration of 3-D lymphatic mapping in breast cancer using freehand SPECT," *European Journal of Nuclear Medicine and Molecular Imaging*, vol. 37, no. 8, pp. 1452–1461, 2010.

[25] O. R. Brouwer, T. Buckle, L. Vermeeren et al., "Comparing the hybrid fluorescent-radioactive tracer Indocyanine green-99mTc-Nanocolloid with 99mTc-Nanocolloid for sentinel node identification: a validation study using lymphoscintigraphy and SPECT/CT," *Journal of Nuclear Medicine*, vol. 53, no. 7, pp. 1034–1040, 2012.

[26] L. Bernet, R. Cano, M. Martinez et al., "Diagnosis of the sentinel lymph node in breast cancer: a reproducible molecular method: a multicentric Spanish study," *Histopathology*, vol. 58, no. 6, pp. 863–869, 2011.

Hindawi Publishing Corporation
Journal of Oncology
Volume 2012, Article ID 814014, 7 pages
doi:10.1155/2012/814014

Review Article

Stem Cells as a Tool for Breast Imaging

Maria Elena Padín-Iruegas and Rafael López López

Hospital Clínico Universitario c/Travesía Choupana s/n. E-15706, Santiago de Compostela, Spain

Correspondence should be addressed to Maria Elena Padín-Iruegas, mariaelena.padin.iruegas@sergas.es

Received 14 June 2012; Accepted 18 June 2012

Academic Editor: Alvaro Ruibal

Copyright © 2012 M. E. Padín-Iruegas and R. López López. This is an open access article distributed under the Creative Commons Attribution License, which permits unrestricted use, distribution, and reproduction in any medium, provided the original work is properly cited.

Stem cells are a scientific field of interest due to their therapeutic potential. There are different groups, depending on the differentiation state. We can find lonely stem cells, but generally they distribute in niches. Stem cells don't survive forever. They are affected for senescence. Cancer stem cells are best defined functionally, as a subpopulation of tumor cells that can enrich for tumorigenic property and can regenerate heterogeneity of the original tumor. Circulating tumor cells are cells that have detached from a primary tumor and circulate in the bloodstream. They may constitute seeds for subsequent growth of additional tumors (metastasis) in different tissues. Advances in molecular imaging have allowed a deeper understanding of the in vivo behavior of stem cells and have proven to be indispensable in preclinical and clinical studies. One of the first imaging modalities for monitoring pluripotent stem cells in vivo, magnetic resonance imaging (MRI) offers high spatial and temporal resolution to obtain detailed morphological and functional information. Advantages of radioscintigraphic techniques include their picomolar sensitivity, good tissue penetration, and translation to clinical applications. Radionuclide imaging is the sole direct labeling technique used thus far in human studies, involving both autologous bone marrow derived and peripheral stem cells.

1. Stem Cells

Stem cells are a scientific field of interest mainly due to their therapeutic potential.

The term of stem cells came up to us via histologists in the nineteenth century, who introduced it as a general, abstract term for cells specifically involved in repair or regeneration. With the discovery in the 1950s that bone marrow cells could reconstitute the hematopoietic systems of irradiated individuals, the modern stem cell concept began to crystallize around the experimental procedures of transplantation and reconstitution [1, 2]. The definition for tissue stem cells proposed by Potten and Loeffler was undifferentiated cells (relative to a functional tissue), capable of proliferation and production of a large number of differentiated functional progeny; they have the ability of self-maintenance of their population and for regeneration of the tissue after injury.

This means that stem cells are defined by virtue of their functional attributes and not by an explicit directly observable characteristic. This *functional definition* is relative to the stem cell role linked to the functional tissue regeneration feature. But this definition doesn't give us any characteristic to identify morphologically the stemness [3].

Another point is the fact that it is assumed that stem cells are undifferenctiated and they come from the earlier stages of the development, This means, in a tissue, we can find various types of stem cells, or a stem cell at different points of maturation. (so, gives a possible way to classify descendent transit and mature cells). Most over could be that there are specific differentiation markers which would enable a distinction of stem cells in relation to each other and in relation to the functional cells they are eventually producing.

Flexibility is a key aspect we should include in the definition of stem cells. It may be possible for a stem cell to cease proliferation, that is, become *quiescent*, in which case it does not act as an actual stem cell, but since it can reenter the cycle it has the potential to act as a stem cell. Likewise a transit cell may not normally self-maintain, but may do so under special circumstances, thereby representing a potential stem cell. The recent discovery that stem cell behaviors can be acquired by ordinary cells following the introduction of a small number of genes has intensified its interest.

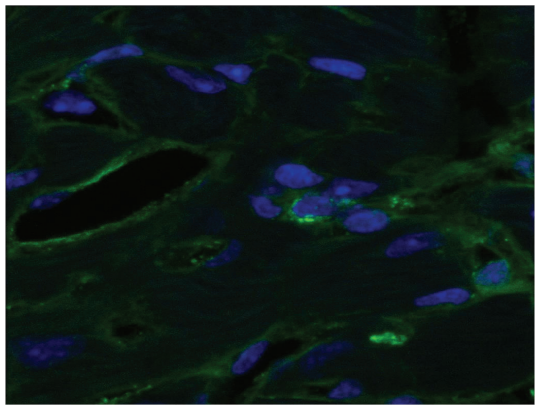

Figure 1: Stem cell niche. C-kit-positive stem cell in the center, surrounded by supporting cells.

With this background, all the stem cells are the same type of cell, but as we refer before there are different groups of them depending on the differentiation state; in this sense the three main groups included: toti or pluripotents, multipotents, and commitment cells. The first group are embryonic cells who have the ability to create any kind of tissue. Second group are cells more differentiated, still stem cells, which can create any kind of tissue derived from one of the embrionary layers, endoderm, mesoderm, or ectoderm, for example, mesenchymal stem cells (MSCs). Finally the third group are those who can generate two or more lineages in a tissue, for example, cardiac stem cells (CSCs) [4].

Focusing on adult stem cells, as we referred before, they distribute in the different adult tissues, but it's very curious they don't have an aleatory distribution. In fact they use to localize in the most protect areas of the tissue, that is, in heart; they are more abundant in the atria and in the apex, the two localizations were the pressure that supports the tissue is minor or in the ventricular area in nervous system. We can find lonely stem cells, but generally they distribute in niches (Figure 1). We define a niche like type of cells and extracellular substrates that can indefinitely house one or more stem cells (SCs) and control their self-reproduction and production of their progeny *in vivo*. So this means they are specific anatomic locations that regulate how they participate in tissue generation, maintenance, and repair. The niche saves stem cells from depletion, while protecting the host from overexuberant stem cell proliferation. It constitutes a basic unit of tissue physiology, integrating signals that mediate the balanced response of stem cells to the needs of organisms. The simple location of stem cells is not sufficient to define a niche. The niche must have both anatomic and functional dimensions. So functions of niches included: spatial organization, filtration of signals (proliferative, apoptotic ...), provided supporting cells, specific unions like cadherins, and determined type division (symmetric or asymmetric) [5].

The niche may also induce pathologies by imposing aberrant function on stem cells or other targets. The interplay between stem cells and their niche creates the dynamic system necessary for sustaining tissues and for the ultimate design of stem cell therapeutics.

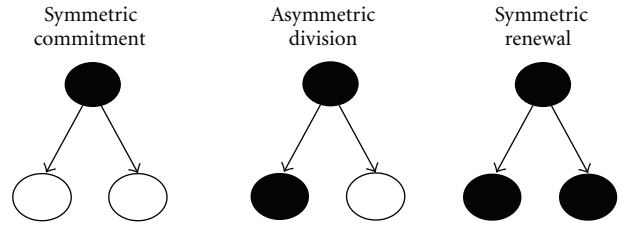

Figure 2: Schema of types division in a stem cell.

An important aspect of the niche is that determining type division of the stem cells. These cells are very special in this aspect too, because usually when a cell enters in cell cycle producing two daughter cells similar to it. In the case of stem cells this can change, so there are two options as follows.

(i) Symmetrical division: the cell gives two daughter cells similar to her, like a regular cell type or two commitment cells.

(ii) Asymmetrical: as the result of a stem cell division we will get two different daughter cells, one similar to the mother and another one that is a commitment cell, so she will be a mature cell (Figure 2).

Once again the regulator of this cellular function is the niche, and this receives the name hypothesis of the free niche. This hypothesis tells us that if there is space for only one stem cell more in the niche, the division will be asymmetrical, but if there is space for two, the division will be symmetrical. Symmetrical division is more frequent in embrionary period and asymmetrical in cellular turnover.

Two proteins are implicated defining the type of division: numb and α-adaptin. When the proteins are homogenously distributed in the cell, the division will be symmetrical; instead if protein concentrates in one cellular extreme, division will be asymmetrical [6].

Contrary to what is thought stem cells don't survive forever. They are affected for senescence too, as demonstrated by the Anversa's work [7, 8]. Telomerase shortening, increase in ROS products, and increase in levels of p53, p16 and p66 were demonstrated in stem cells, all of them shared facts with senescent cells.

Many efforts are being made in the study of the mechanism implicated in stem cells, with therapeutic purposes. Fields like degenerative lesions, tisular necrosis, had all their witness in the application of stem cells. In fact, there are several clinical trials focusing on the substitutive therapy with stem cells, in cardiology, neurology, and orthopedic, but still the results are not as good as researchers and clinicians expect.

2. Cancer Stem Cells

Recently new discovers can be applied to the stem cells knowledge in the oncology field. Nowadays the theory of the origin of the tumors is in the stem cells is more and more

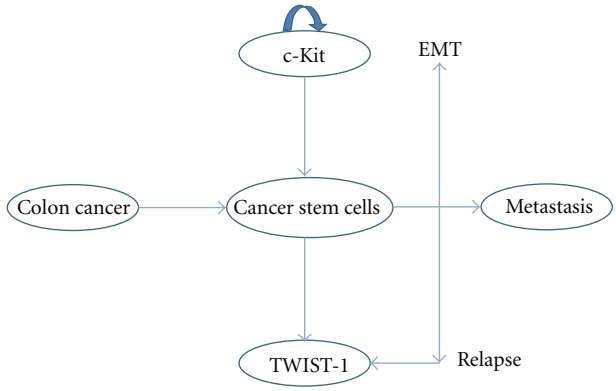

Figure 3: Schema of the theoretical behavior of the stem cells in cancer, its maintenance and transformation to produce distant metastasis.

accepted, and every day there are more researchers focusing their efforts implicated in this aspect.

Cancer stem cells (CaSCs) is best defined functionally, as a subpopulation of tumor cells that can enrich for tumorigenic property and can regenerate the heterogeneity of the original tumor in immunocompromised mice. The existence of CaSCs was hypothesized in the 60′s, and experimentally isolated in the last decades, first in acute myeloid leukemia and later in solid cancers, such as, breast cancer. Importantly, CaSCs were shown to be resistant to conventional therapies, such as, chemotherapy and radiation. Therefore, the prospective isolation, molecular characterization, and therapeutic targeting of CaSCs in cancer will possibly mark major advances in understanding their pathogenesis.

At the same time, the finding that only a small fraction of the cells within malignant tumors can initiate new tumors upon transplantation has led many cancer biologists to embrace the notion that stem cells are the driving force behind malignancies and to advocate redirecting cancer therapy toward controlling or eradicating stem cells. Clearly, we live in an era of biology when ideas and theories about stem cells are a major part of the intellectual landscape [9].

The hypothesis of cancer is a stem cell disease includes that in a tumour we have, at least, two types of cell population: adult tumour cells and stem cell like, as well as in normal tissue. It has been suggested that cancer is due to an alteration in the normal homeostasis of stem cells. The abundance of cancer stem cells is derived for their symmetric division, and this would be the point to eradicate for cancer treatment. The tumor stem cell hypothesis indicates that this type of cell has all the characteristics of the stem cell: capability of self-renewal, unlimited proliferation potential, multiline differentiation, formation of new adult cells, and asymmetric division, and they are originated of the formation of metastasis, meaning that all the adult tumor cells are coming from this kind of cell (Figure 3). For these properties they are called initiating tumor cells too, and probably, are the responsible for tumors refractoriness and recurrence.

3. Circulating Tumor Cells

Another concept is the circulating tumor cells (CTCs) that are cells that have detached from a primary tumor and circulate in the bloodstream. CTCs may constitute seeds for subsequent growth of additional tumors (metastasis) in different tissues [10].

Cells capable of metastasis also acquire the ability to invade another tissue [11]. For epithelial cancers this involves cells undergoing an Epithelial-Mesenchymal Transition (EMT). EMT involves epithelial cells losing their epithelial characteristics and acquiring a more mesenchymal phenotype which occurs as a result of cytoskeletal changes within the cells. These changes allow the cell to acquire a more migratory phenotype [10, 12], increasing the probability of tumour cells entering the blood and lymphatic systems. This process is influenced by chemokines and their receptors which are thought to play an important role in tumour development by influencing tumour transformation, survival, proliferation, invasion, and metastasis and also regulation of angiogenesis and tumour-leukocyte interactions. Despite this, the majority of circulating tumour cells appear to be destroyed [11]. Those that persist may acquire the ability to metastasize and once inside the target organ may undergo Mesenchymal-Epithelial Transition (MET), proliferate and if the environment is conducive the disseminated cells may grow to establish a new tumour thus completing the metastatic process [13].

First evidence indicates that CTCs markers applied in human medicine are conserved in other species. Five of the more common markers including CK19 are also useful to detect CTCs in the blood of dogs with malignant mammary tumors [14].

Standard procedure for isolating circulating stem cells (CTCs) involves cell sorting of a subpopulation on the basis of cell surface markers. Many of these surface markers have been reported as present in the CaSC. These markers change depending on the organ we are considering.

The detection of CTCs may have important prognostic and therapeutic implications but because their numbers can be very small, these cells are not easily detected [15]. Circulating tumor cells are found in different frequencies per mL of whole blood in patients with metastatic disease. To date, a variety of research methods have been developed to isolate and enumerate CTCs [16]. The only USA Food and Drug Administration (FDA) cleared methodology for enumeration of CTCs in whole blood is the CellSearch system. Extensive clinical testing done using this method shows that presence of CTCs is a strong prognostic factor for overall survival in patients with metastatic breast, colorectal, or prostate cancer.

Morphological appearance is judged by human operators and is therefore subjected to large interoperator variation [17]. Several CTCs enumeration methods exist which use morphological appearance to identify CTCs, which may also apply different morphological criteria. A study in prostate cancer showed that many different morphological definitions of circulating tumor cells have similar prognostic value, even though the absolute number of cells found in patients

and normal donors varied by more than a decade between different morphological definitions [18].

The behavior of the cells in cancer and metastasis developing will be better known if we will be able to follow these cells.

4. Stem Cells Imaging: MRI and Radionuclide Imaging (PET and SPECT)

Over the last decade, advances in molecular imaging have allowed a deeper understanding of the *in vivo* behavior of stem cells and have proven to be indispensable in preclinical and clinical studies.

There are two main classes of molecular imaging techniques: direct cell labeling and reporter-gene imaging (Figure 4). The former employs contrast agents, such as, magnetic particles, luminescent nanoparticles, or radionuclides to directly label the cell, whereas the latter genetically alters the cell to transcribe and translate a reporter protein. While direct labeling is both straightforward to implement and is commonly used, the contrast signal is diluted with each cellular division and the technique cannot distinguish viable cells from dead cells [19]. Reporter genes, on the other hand, are only expressed by live cells and the signal is propagated by daughter cells [20]. However, reporter gene imaging requires transfection of genetic material using plasmids, retroviral, or viral vectors, which raises the concern of insertional mutagenesis and may necessitate the use of apoptosis-inducing "suicide genes" before possible future use in the clinic [21, 22].

5. MRI

As one of the first imaging modalities for monitoring pluripotent stem cells *in vivo*, magnetic resonance imaging (MRI) offers high spatial and temporal resolution to obtain detailed morphological and functional information. It requires the uptake of a contrast agent by the stem cell, the most common of which are superparamagnetic iron oxide (SPIO) nanoparticles. SPIOs can induce changes in T2 relaxivity at nanomolar concentrations [23, 24]. There are two main methods by which stem cells can be directly labeled by SPIOs. One method is magneto operation which involves the coating of anionic SPIOs with cationic transfection agents, such as, protamine sulfate or poly-L-lysine [25]. Stem cells subsequently endocytose the resulting complex during incubation for around 24–48 hours [26]. Although many studies have shown that magneto oporation does not affect cell viability or function at low doses [26–28], there is evidence that high doses can inhibit mesenchymal stem cell (MSC) migration and colony formation ability [29].

Several groups have shown the use of SPIOs for non-invasive MRI of neural stem cell migration, engraftment, and morphological differentiation [30, 31]. The contrast signals in these studies were detected for up to six weeks and the stem cells retained the ability to proliferate and differentiate. Other groups have shown that MRI can be used to track mesenchymal stem cells (MSCs) in cardiac repair after myocardial infarction [32]. Here the signals could be detected long term for three to eight weeks. However, one disadvantage inherent to both SPIO-labeling methods is their inability to distinguish viable cells from dead cells or from scavenging macrophages.

6. PET and SPECT

The advantages of radioscintigraphic techniques include their picomolar sensitivity, good tissue penetration, and translation to clinical applications [19]. In fact, radionuclide imaging is the sole direct labeling technique used thus far in human studies, involving both autologous bone marrow-derived stem cells [33] and peripheral hematopoietic stem cells [34–36].

There are two main techniques for radionuclide imaging: positron emission tomography (PET) and single photon emission computed tomography (SPECT). SPECT tracers directly emit a gamma ray in one direction, in contrast to PET tracers, which send two gamma rays in opposite directions and thus possess coincidence detection with a higher spatial resolution. However, SPECT is generally less expensive due to its longer-lived and more readily available radioisotopes.

The most widely used PET isotopes are fluorine-18 (18F), which has a half life of 110 minutes. Copper-64 (^{64}Cu) has a much longer half life of 12.7 hours [37]. ^{64}Cu can offer a longer duration of *in vivo* visualization of stem cell behavior. ^{64}Cu can also be bound to a lipophilic redox-active carrier molecule, pyruvaldehydebis(N4-methylthiosemicarbazone)(PTSM). ^{64}Cu-PTSM has been used to image hESCs differentiated towards renal lineages in fetal rhesus monkeys [38] and has been shown to lack adverse cellular effects [39].

The most widely used SPECT radionuclides are indium-111 (^{111}In), with a half life of 67 hours and the metastable Technetium-99 m (^{99}mTc), with a half-life of 6 hours. While ^{111}In provides a longer time window for cell imaging, ^{99}mTc can be used in higher doses to improve short-term imaging resolution. Several groups have used ^{111}In to image *in vivo* trafficking and biodistribution of MSCs around sites of myocardial injury in the canine [40, 41] and porcine animal models [42]. Human clinical studies have also used ^{111}In-oxine [35, 43, 44] to assess stem cell trafficking in acute and chronic myocardial infarction.

Although both PET and SPECT offer great sensitivity, there are several disadvantages to both techniques, including the leakage of radionuclides into nontarget cells [45], limited time window for imaging due to half-life decay, lower spatial resolution as compared to MRI, and the emission of ionizing radiation that may impair stem cell proliferation and survival.

Pluripotent stem cells share many properties in common with cancer cells, including self-renewal, rapid proliferation, lack of contact inhibition, and high telomerase activity [46, 47]. Furthermore, cellular manipulations, such as, the reprogramming of somatic cells into induced pluripotent stem cells (iPSCs), transfection of reporter genes, and

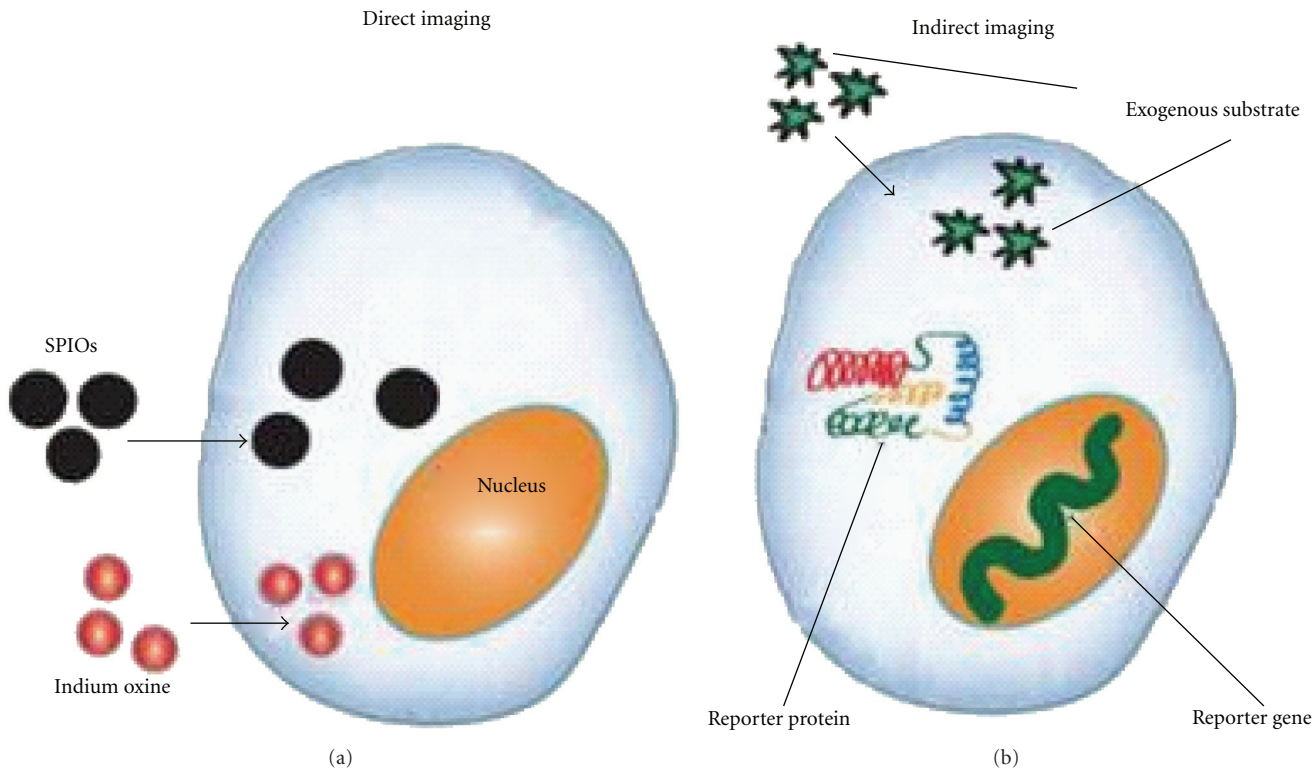

Figure 4: Molecular imaging techniques: direct stem cell labeling and reporter-gene imaging.

overexpression of survival genes, can have unintended tumorigenic side effects. Teratoma formation is another concern, along with its potential to degenerate into malignant teratocarcinomas [46]. Given these risks, understanding stem cell tumorigenicity is of paramount importance for future clinical applications.

One study using a double fusion reporter containing enzyme firefly luciferase (Fluc) and GFP showed that teratoma formation is dependent upon cell number. Assessed over a period of eight weeks, a minimum of 1×105 intramyocardially injected hESCs were required to form teratomas in mice [48]. Furthermore, a lower threshold of 1×104 cells following hind limb injection was required to form teratomas, providing insight into niche dependency [49]. Since angiogenesis is known to play a major role in tumor growth and development, it is important to investigate not only the tumor itself but also its supporting stroma. One study used sodium iodide symporter (NIS) reporter imaging to show that MSCs actively home in on growing tumors, where they differentiate into vasculature and supporting structures [50]. The upregulation of $\alpha v\beta 3$ integrin is also known to play a role in tumor angiogenesis. One study used direct PET imaging with ^{64}Cu-DOTA-RGD4 to target $\alpha v\beta 3$ integrin, which successfully visualized *in vivo* hESC teratoma formation in the mouse model. These findings show that integrins play a major role in teratoma formation and angiogenesis. Moreover, PET imaging may have promising clinical applicability for monitoring tumorigenicity in humans because BLI lacks the ability to penetrate deep tissues.

Due to the risks of teratoma formation, having a reporter gene that serves as both an imaging modality as well as a failsafe suicide switch would be highly desirable. One study used *HSV1-tk* PET reporter imaging to selectively destroy emerging teratomas with the administration of ganciclovir. Future directions for mitigating the risks of tumorigenicity include not only the use of reporter-suicide genes, but also vector-and transgene-free reprogramming of somatic cells into iPSCs and long-term multimodality imaging capable of observing both emerging tumor cells and their supporting stroma.

Although a great deal of information is already known about the survival, biodistribution, tumorigenicity, and immunogenicity of pluripotent stem cells, significant gaps in knowledge remain. Molecular imaging will continue to play a pivotal role in answering crucial questions about clinical applications as well as in helping us understand the underlying mechanisms of stem cell biology.

In fact, a new imaging agent, radio-labelled hedgehog, detects cancer stem cells, potentially allowing for imaging of "stem cell-like" cancer cells by positron emission tomography (PET) in patients with breast cancer, according to results of a pilot study, presented at the American Association for Cancer Research 101st Annual Meeting 2010. Jennifer Sims-Mourtada, Ph.D., Director of molecular research and development at RadioMedix, Inc., Houston, Texas and colleagues tested the ability to detect breast cancer stem-cell-like populations using a protein, sonic hedgehog that was radiolabeled with the positron emitting isotope gallium-68.

Increased activation of the hedgehog pathway is observed in cancer stem cells and aggressive tumours. Binding of the radio-labelled hedgehog to the patched-1 hedgehog receptor on the surface of breast cancer cells occurred, suggesting potential for molecular imaging of breast cancer by PET. A significant increase in binding was observed in cultures enriched for breast cancer stem-like cells.

7. Conclusions

More *in vivo* molecular imaging studies must be conducted to confirm long-term survival of these cells. The safety of stem cell therapy in terms of tumorigenicity and immune rejection must also be thoroughly examined. To that end, molecular imaging studies capable of evaluating the risk of cancer formation long-term or assessing methods of immune suppression for viable engraftment are highly valuable.

References

[1] C. S. Potten and M. Loeffler, "Stem cells: attributes, cycles, spirals, pitfalls and uncertainties. Lessons for and from the crypt," *Development*, vol. 110, no. 4, pp. 1001–1020, 1990.

[2] M. Loeffler and C. S. Potten, "Stem cells and cellular pedigrees a conceptual introduction," in *Stem Cells*, C. S. Potten, Ed., pp. 1–28, Harcourt Brace and Company, San Diego, Calif, USA, 1997.

[3] M. Loeffler and I. Roeder, "Tissue stem cells: definition, plasticity, heterogeneity, self-organization and models—a conceptual approach," *Cells Tissues Organs*, vol. 171, no. 1, pp. 8–26, 2002.

[4] S. Mitalipov and D. Wolf, "Totipotency, pluripotency and nuclear reprogramming," *Advances in Biochemical Engineering/Biotechnology*, vol. 114, pp. 185–199, 2009.

[5] D. T. Scadden, "The stem-cell niche as an entity of action," *Nature*, vol. 441, no. 7097, pp. 1075–1079, 2006.

[6] J. A. Knoblich, "Mechanisms of asymmetric stem cell division," *Cell*, vol. 132, no. 4, pp. 583–597, 2008.

[7] P. Anversa, "Aging and longevity: the IGF-1 enigma," *Circulation Research*, vol. 97, no. 5, pp. 411–414, 2005.

[8] M. Rota, N. LeCapitaine, T. Hosoda et al., "Diabetes promotes cardiac stem cell aging and heart failure, which are prevented by deletion of the p66shc gene," *Circulation Research*, vol. 99, no. 1, pp. 42–52, 2006.

[9] A. D. Lander, "The "stem cell" concept: is it holding us back?" *Journal of Biology*, vol. 8, no. 8, article 70, 2009.

[10] T. Brabletz, A. Jung, S. Spaderna, F. Hlubek, and T. Kirchner, "Migrating cancer stem cells—an integrated concept of malignant tumour progression," *Nature Reviews Cancer*, vol. 5, no. 9, pp. 744–749, 2005.

[11] J. Couzin, "Tracing the steps of metastasis, cancer's menacing ballet," *Science*, vol. 299, no. 5609, pp. 1002–1006, 2003.

[12] B. G. Hollier, K. Evans, and S. A. Mani, "The epithelial-to-mesenchymal transition and cancer stem cells: a coalition against cancer therapies," *Journal of Mammary Gland Biology and Neoplasia*, vol. 14, no. 1, pp. 29–43, 2009.

[13] I. J. Fidler, "The pathogenesis of cancer metastasis: the"seed and soil" hypothesis revisited," *Nature Reviews Cancer*, vol. 3, no. 6, pp. 453–458, 2003.

[14] A. da Costa, J. T. Oliveira, F. Gärtner, B. Kohn, A. D. Gruber, and R. Klopfleisch, "Potential markers for detection of circulating canine mammary tumor cells in the peripheral blood," *Veterinary Journal*, vol. 190, no. 1, pp. 165–168, 2010.

[15] R. A. Ghossein, S. Bhattacharya, and J. Rosai, "Molecular detection of micrometastases and circulating tumor cells in solid tumors," *Clinical Cancer Research*, vol. 5, no. 8, pp. 1950–1960, 1999.

[16] P. Paterlini-Brechot and N. L. Benali, "Circulating tumor cells (CTC) detection: clinical impact and future directions," *Cancer Letters*, vol. 253, no. 2, pp. 180–204, 2007.

[17] A. G. J. Tibbe, M. C. Miller, and L. W. M. M. Terstappen, "Statistical considerations for enumeration of circulating tumor cells," *Cytometry Part A*, vol. 71, no. 3, pp. 154–162, 2007.

[18] F. A. W. Coumans, C. J. M. Doggen, G. Attard, J. S. de Bono, and L. W. M. M. Terstappen, "All circulating EpCAM+CK+CD45-objects predict overall survival in castration-resistant prostate cancer," *Annals of Oncology*, vol. 21, no. 9, pp. 1851–1857, 2010.

[19] M. M. Welling, M. Duijvestein, A. Signore, and L. van der Weerd, "In vivo biodistribution of stem cells using molecular nuclear medicine imaging," *Journal of Cellular Physiology*, vol. 226, no. 6, pp. 1444–1452, 2011.

[20] Z. Li, Y. Suzuki, M. Huang et al., "Comparison of reporter gene and iron particle labeling for tracking fate of human embryonic stem cells and differentiated endothelial cells in living subjects," *Stem Cells*, vol. 26, no. 4, pp. 864–873, 2008.

[21] I. Niculescu-Duvaz and C. J. Springer, "Introduction to the background, principles, and state of the art in suicide gene therapy," *Molecular Biotechnology*, vol. 30, no. 1, pp. 71–88, 2005.

[22] F. Cao, M. Drukker, S. Lin et al., "Molecular imaging of embryonic stem cell misbehavior and suicide gene ablation," *Cloning and Stem Cells*, vol. 9, no. 1, pp. 107–117, 2007.

[23] E. Sykova, P. Jendelova, and V. Herynek, "Magnetic resonance imaging of stem cell migration," *Methods in Molecular Biology*, vol. 750, part 2, pp. 79–90, 2011.

[24] J. A. Frank, B. R. Miller, A. S. Arbab et al., "Clinically applicable labeling of mammalian and stem cells by combining superparamagnetic iron oxides and transfection agents," *Radiology*, vol. 228, no. 2, pp. 480–487, 2003.

[25] D. L. Kraitchman, A. W. Heldman, E. Atalar et al., "In vivo magnetic resonance imaging of mesenchymal stem cells in myocardial infarction," *Circulation*, vol. 107, no. 18, pp. 2290–2293, 2003.

[26] P. W. So, T. Kalber, D. Hunt et al., "Efficient and rapid labeling of transplanted cell populations with superparamagnetic iron oxide nanoparticles using cell surface chemical biotinylation for in vivo monitoring by MRI," *Cell Transplantation*, vol. 19, no. 4, pp. 419–429, 2010.

[27] J. W. M. Bulte, A. S. Arbab, T. Douglas, and J. A. Frank, "Preparation of magnetically labeled cells for cell tracking by magnetic resonance imaging," *Methods in Enzymology*, vol. 386, pp. 275–299, 2004.

[28] J. W. M. Bulte and D. L. Kraitchman, "Iron oxide MR contrast agents for molecular and cellular imaging," *NMR in Biomedicine*, vol. 17, no. 7, pp. 484–499, 2004.

[29] R. Schäfer, R. Kehlbach, M. Müller et al., "Labeling of human mesenchymal stromal cells with superparamagnetic iron oxide leads to a decrease in migration capacity and colony formation ability," *Cytotherapy*, vol. 11, no. 1, pp. 68–78, 2009.

[30] J. W. M. Bulte, T. Douglas, B. Witwer et al., "Magneto-dendrimers allow endosomal magnetic labeling and in vivo

tracking of stem cells," *Nature Biotechnology*, vol. 19, no. 12, pp. 1141–1147, 2001.

[31] M. Hoehn, E. Küstermann, J. Blunk et al., "Monitoring of implanted stem cell migration in vivo: a highly resolved in vivo magnetic resonance imaging investigation of experimental stroke in rat," *Proceedings of the National Academy of Sciences of the United States of America*, vol. 99, no. 25, pp. 16267–16272, 2002.

[32] L. C. Amado, A. P. Saliaris, K. H. Schuleri et al., "Cardiac repair with intramyocardial injection of allogeneic mesenchymal stem cells after myocardial infarction," *Proceedings of the National Academy of Sciences of the United States of America*, vol. 102, no. 32, pp. 11474–11479, 2005.

[33] M. Hofmann, K. C. Wollert, G. P. Meyer et al., "Monitoring of bone marrow cell homing into the infarcted human myocardium," *Circulation*, vol. 111, no. 17, pp. 2198–2202, 2005.

[34] W. J. Kang, H. J. Kang, H. S. Kim, J. K. Chung, M. C. Lee, and D. S. Lee, "Tissue distribution of 18F-FDG-labeled peripheral hematopoietic stem cells after intracoronary administration in patients with myocardial infarction," *Journal of Nuclear Medicine*, vol. 47, no. 8, pp. 1295–1301, 2006.

[35] V. Schächinger, A. Aicher, N. Döbert et al., "Pilot trial on determinants of progenitor cell recruitment to the infarcted human myocardium," *Circulation*, vol. 118, no. 14, pp. 1425–1432, 2008.

[36] C. Dedobbeleer, D. Blocklet, M. Toungouz et al., "Myocardial homing and coronary endothelial function after autologous blood CD34+ progenitor cells intracoronary injection in the chronic phase of myocardial infarction," *Journal of Cardiovascular Pharmacology*, vol. 53, no. 6, pp. 480–485, 2009.

[37] N. Adonai, K. N. Nguyen, J. Walsh et al., "Ex vivo cell labeling with 64Cu-pyruvaldehyde-bis(N4-methylthiosemicarbazone) for imaging cell trafficking in mice with positron-emission tomography," *Proceedings of the National Academy of Sciences of the United States of America*, vol. 99, no. 5, pp. 3030–3035, 2002.

[38] A. F. Tarantal, C. C. I. Lee, C. A. Batchelder, J. E. Christensen, D. Prater, and S. R. Cherry, "Radiolabeling and in vivo imaging of transplanted renal lineages differentiated from human embryonic stem cells in fetal rhesus monkeys," *Molecular Imaging and Biology*, vol. 14, no. 2, pp. 197–204, 2012.

[39] J. Huang, C. C. I. Lee, J. L. Sutcliffe, S. R. Cherry, and A. F. Tarantal, "Radiolabeling Rhesus monkey CD34+ hematopoietic and mesenchymal stem cells with 64Cu-pyruvaldehyde-bis(N4-methylthiosemicarbazone) for MicroPET imaging," *Molecular Imaging*, vol. 7, no. 1, pp. 1–11, 2008.

[40] D. L. Kraitchman, M. Tatsumi, W. D. Gilson et al., "Dynamic imaging of allogeneic mesenchymal stem cells trafficking to myocardial infarction," *Circulation*, vol. 112, no. 10, pp. 1451–1461, 2005.

[41] K. J. Blackwood, B. Lewden, R. G. Wells et al., "In vivo SPECT quantification of transplanted cell survival after engraftment using (111)In-tropolone in infarcted canine myocardium," *Journal of Nuclear Medicine*, vol. 50, no. 6, pp. 927–935, 2009.

[42] S. Lyngbæk, R. S. Ripa, M. Haack-Sørensen et al., "Serial in vivo imaging of the porcine heart after percutaneous, intramyocardially injected 111In-labeled human mesenchymal stromal cells," *International Journal of Cardiovascular Imaging*, vol. 26, no. 3, pp. 273–284, 2010.

[43] M. Kurpisz, R. Czepczyński, B. Grygielska et al., "Bone marrow stem cell imaging after intracoronary administration," *International Journal of Cardiology*, vol. 121, no. 2, pp. 194–195, 2007.

[44] V. Caveliers, G. de Keulenaer, H. Everaert et al., "In vivo visualization of 111In labeled CD133+ peripheral blood stem cells after intracoronary administration in patients with chronic ischemic heart disease," *Quarterly Journal of Nuclear Medicine and Molecular Imaging*, vol. 51, no. 1, pp. 61–66, 2007.

[45] K. Stojanov, E. F. de Vries, D. Hoekstra, A. van Waarde, R. A. Dierckx, and I. S. Zuhorn, "[18F]FDG labeling of neural stem cells for *in vivo* cell tracking with positron emission tomography: inhibition of tracer release by phloretin," *Molecular Imaging*, vol. 11, no. 1, pp. 1–12, 2012.

[46] U. Ben-David and N. Benvenisty, "The tumorigenicity of human embryonic and induced pluripotent stem cells," *Nature Reviews Cancer*, vol. 11, no. 4, pp. 268–277, 2011.

[47] N. G. Kooreman and J. C. Wu, "Tumorigenicity of pluripotent stem cells: biological insights from molecular imaging," *Journal of the Royal Society Interface*, vol. 7, supplement 6, pp. S753–S763, 2010.

[48] A. S. Lee, C. Tang, F. Cao et al., "Effects of cell number on teratoma formation by human embryonic stem cells," *Cell Cycle*, vol. 8, no. 16, pp. 2608–2612, 2009.

[49] K. R. Francis and L. Wei, "Human embryonic stem cell neural differentiation and enhanced cell survival promoted by hypoxic preconditioning," *Cell Death and Disease*, vol. 1, no. 2, article e22, 2010.

[50] R. M. Dwyer, J. Ryan, R. J. Havelin et al., "Mesenchymal stem cell-mediated delivery of the sodium iodide symporter supports radionuclide imaging and treatment of breast cancer," *Stem Cells*, vol. 29, no. 7, pp. 1149–1157, 2011.

Hindawi Publishing Corporation
Journal of Oncology
Volume 2012, Article ID 438647, 8 pages
doi:10.1155/2012/438647

Review Article

Molecular Imaging in Breast Cancer: From Whole-Body PET/CT to Dedicated Breast PET

B. B. Koolen,[1,2] W. V. Vogel,[1] M. J. T. F. D. Vrancken Peeters,[2] C. E. Loo,[3] E. J. Th. Rutgers,[2] and R. A. Valdés Olmos[1]

[1] *Department of Nuclear Medicine, Netherlands Cancer Institute–Antoni van Leeuwenhoek Hospital, Plesmanlaan 121, 1066 CX Amsterdam, The Netherlands*
[2] *Department of Surgical Oncology, Netherlands Cancer Institute–Antoni van Leeuwenhoek Hospital, Plesmanlaan 121, 1066 CX Amsterdam, The Netherlands*
[3] *Department of Radiology, Netherlands Cancer Institute–Antoni van Leeuwenhoek Hospital, Plesmanlaan 121, 1066 CX Amsterdam, The Netherlands*

Correspondence should be addressed to B. B. Koolen, b.koolen@nki.nl

Received 20 April 2012; Accepted 21 May 2012

Academic Editor: Alvaro Ruibal

Copyright © 2012 B. B. Koolen et al. This is an open access article distributed under the Creative Commons Attribution License, which permits unrestricted use, distribution, and reproduction in any medium, provided the original work is properly cited.

Positron emission tomography (PET), with or without integrated computed tomography (CT), using 18F-fluorodeoxyglucose (FDG) is based on the principle of elevated glucose metabolism in malignant tumors, and its use in breast cancer patients is frequently being investigated. It has been shown useful for classification, staging, and response monitoring, both in primary and recurrent disease. However, because of the partial volume effect and limited resolution of most whole-body PET scanners, sensitivity for the visualization of small tumors is generally low. To improve the detection and quantification of primary breast tumors with FDG PET, several dedicated breast PET devices have been developed. In this nonsystematic review, we shortly summarize the value of whole-body PET/CT in breast cancer and provide an overview of currently available dedicated breast PETs.

1. Introduction

Breast cancer is the most frequent type of cancer in women all over the world. In the United States, it is expected to account for 29% (226,870) of all new cancer cases among women in 2012 [1]. After an increase in incidence rates during the 70's and 80's, mainly caused by improvements in early detection, breast cancer incidence in the United States has been relatively stable over the last decade [2]. Overall cancer death rates have been declining consistently since 1991 (23% in men and 15% in women), with breast cancer accounting for 34% of the decrease in women. This decrease largely reflects improvements in early detection and/or treatment [3]; breast cancer screening programs have been launched and improved, various imaging modalities have been developed and modified, and patient-tailored/targeted treatment has been introduced and expanded.

Mammography, ultrasound (US), and magnetic resonance imaging (MRI) are employed as diagnostic tools for several years. Recently, molecular imaging techniques for tumor detection have gained interest. Positron emission tomography (PET), with or without integrated computed tomography (CT), using 18F-fluorodeoxyglucose (FDG) is based on the principle of increased glucose metabolism in malignant tumors and has been investigated frequently in breast cancer. It has been shown to be valuable for locoregional and distant staging in both primary and recurrent breast cancer [4–9]. Based on the association between prognostic characteristics and the degree of primary tumor FDG uptake [10, 11] and promising results regarding response monitoring during neoadjuvant chemotherapy with PET/CT [12], optimal quantification of metabolic activity is desirable. However, uncertainty remains regarding the visualization of primary breast tumors with conventional PET/CT, mainly due to the low sensitivity in small (cT1) breast cancers [13, 14]. These issues have led to the development of high-resolution dedicated breast PET modalities, of which several have been investigated.

In this nonsystematic review, we briefly summarize the value of whole-body PET/CT in breast cancer patients and also report its limitations, which have been the foundation for development of dedicated breast PETs. Hereafter, we

describe the added value of dedicated breast PETs and compare four currently available, in vivo evaluated dedicated breast PETs, subdivided by positioning of breast and patient. Special emphasis will be on the MAMmography with Molecular Imaging (MAMMI) PET, a recently developed high-resolution dedicated breast PET for hanging breast molecular imaging. Finally, we discuss the possible clinical implementation of the dedicated breast PET.

2. Whole-Body 18F-FDG PET and PET/CT

The value of 18F-FDG PET and PET/CT in breast cancer patients has been investigated extensively. It can be used for detection and visualization of the primary tumor. Several studies have demonstrated that tumors with unfavorable prognostic characteristics show a higher degree of FDG uptake [10, 11], but, due to the limited resolution of most whole-body scanners, suboptimal patient positioning, and the partial volume effect, sensitivity for the visualization of small primary tumors (cT1) was found to be low [13–15]. However, optimal patient positioning and reconstruction protocols might improve primary tumor visualization. In our institute, we perform a detailed scan of the thorax for locoregional evaluation with the patient in prone position, the arms above the head, with hanging breasts, and image reconstruction to $2 \times 2 \times 2$ mm voxels. This approach provides high resolution images of the breasts and locoregional lymph nodes without tissue compression and results in improved tumor delineation and less breathing artifacts [16]. Further, it enables image comparison with MRI.

In the diagnostic workup of breast cancer not only visualization of the primary tumor, but also locoregional and distant staging is important. The accuracy of PET/CT for detection of axillary lymph node metastases has predominantly been studied in early stage breast cancer; although sensitivity was suboptimal, specificity and positive predictive value are consistently reported to be high, providing a rationale for omission of the sentinel lymph node procedure and allowing an immediate axillary lymph node dissection in case of an FDG-avid axillary node [8]. Further, PET/CT has been shown to outperform conventional imaging procedures regarding the detection of extra-axillary lymph node metastases and distant metastases in primary stage II and III breast cancer [6, 9]. The yield of PET/CT as a staging device in early stage breast cancer is relatively low, mainly because of the low incidence of distant metastases in this particular group of patients [14, 15]. In patients with breast cancer recurrence, several international guidelines recommend performance of an FDG PET or PET/CT, both for visualization of the recurrence and for the detection of metastases [17, 18]. In Figure 1, examples of the primary tumor, locoregional lymph node metastases, and distant metastases as visualized with conventional whole-body PET/CT are depicted.

3. Dedicated Breast PET Imaging

Although several papers recommend performing a PET/CT for locoregional and distant staging in primary stage II-III or recurrent breast cancer, its use is not advised for the detection or visualization of the primary tumor for several reasons. First, the spatial resolution full width at half maximum (FWHM) of most whole-body scanners is limited to approximately 5 mm. Second, the partial volume effect limits precise imaging and quantification of small tumors. Further, most scans are performed in supine position, which is suboptimal because of tissue compression and blurring of the signal due to the breathing motion [16]. Also, the path of the photons from source to detector is long and involves structures of the entire thorax, resulting in increased likelihood of the photons to be absorbed or scattered and signal loss because of attenuation and decreased contrast.

Despite the limitations in primary tumor visualization with PET and PET/CT, there is an increased demand for accurate tumor visualization with FDG PET and quantification of metabolic activity; PET or PET/CT can be used in patients with dense breast glandular tissue, in which mammography, US, and MRI have been shown to be less accurate [19, 20]. Further, multiple studies have reported a correlation between degree of FDG uptake and histologic subtypes, receptor status, and prognosis, suggesting a potential for tumor characterization [10, 11]. Finally, response monitoring with PET and PET/CT during neoadjuvant chemotherapy has been shown to be promising, with both the degree of FDG uptake at baseline and the relative decrease in FDG uptake between two scans giving information regarding pathological response achievement [12, 21], thereby emphasizing accurate quantification of FDG uptake.

The increased interest in visualizing and quantifying the primary tumor with PET or PET/CT and the currently experienced hindrance and inaccuracy when using whole-body PET/CT scanners have led to the development of dedicated breast PET devices. The high resolution, small voxel size, and short pathway from tumor to detector could improve tumor detection and quantification. Further, PET-guided biopsies could be facilitated, enabling a biopsy from the most proliferative part of the tumor (at the location with highest degree of FDG uptake [22]), especially in tumors with a heterogeneous FDG uptake pattern or in otherwise occult tumors [23, 24]. The dedicated breast PETs can be classified according to the positioning of the breast and patient, using either compression of the breast with upright patient positioning (PEM) or with hanging breast without compression in prone position (PEM/PET, dedicated breast PET/CT, MAMMI PET).

4. Dedicated Breast PET: Compression

4.1. Positron Emission Mammography (PEM). Several solutions for compressed positron emission tomography of the breast are currently available. The positron emission mammography (PEM) system (Naviscan, San Diego, USA) has been investigated most extensively. Thompson et al. have reported its feasibility in 1994, and the first clinical results followed shortly thereafter [25–27]. MacDonald et al. presented the second prototype (PEM Flex Solo II) in 2009 [28]. The system consists of two planar detectors, which

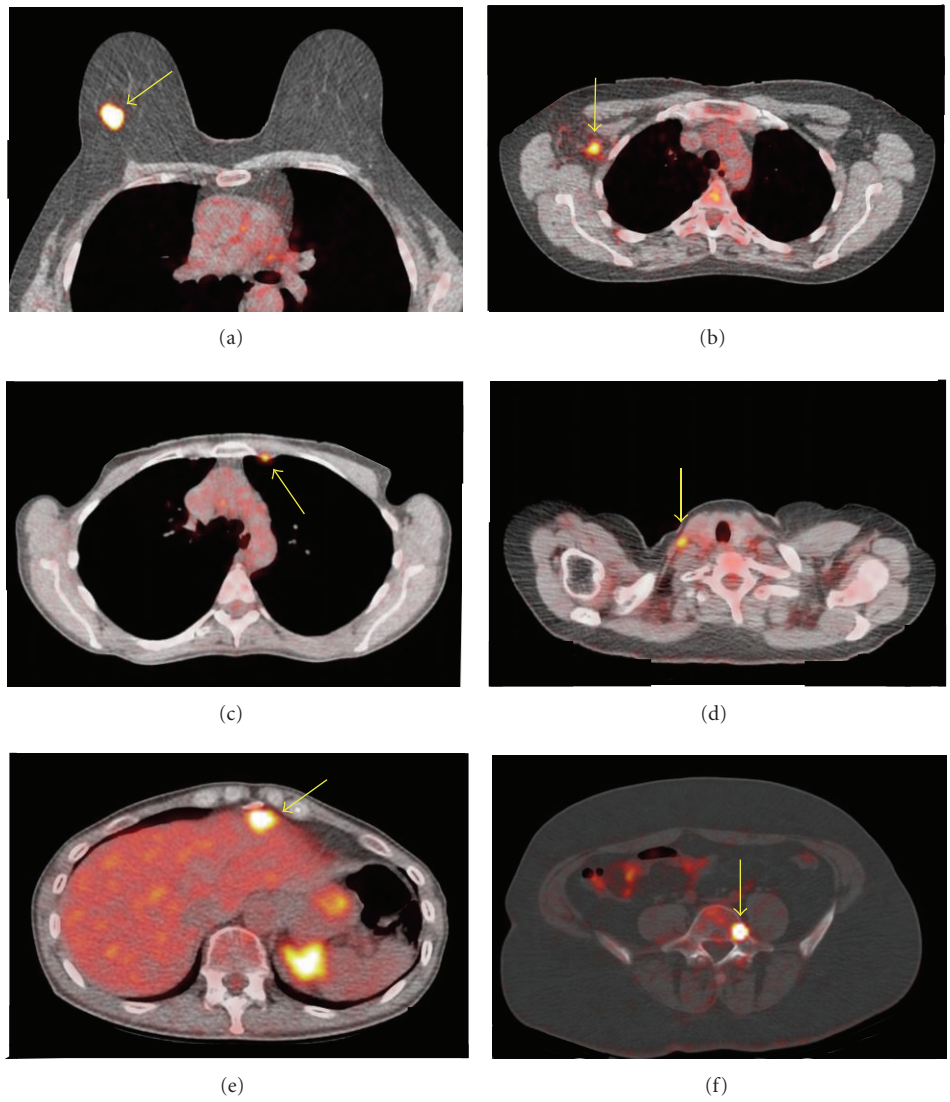

Figure 1: Fused whole-body PET/CT images depicting FDG uptake in the primary tumor (a), an axillary lymph node (b), a lymph node in the internal mammy chain (c), a supraclavicular lymph node (d), the liver (e), and the fifth lumbar vertebra (f).

are integrated in a conventional mammography device, enhancing comparison of PEM and mammography images. In recent studies 301-472 MBq of 18F-FDG is injected intravenously and images are acquired after a resting period of approximately 60 minutes [29–33]. PEM uses breast compression during image acquisition, which takes 10–20 minutes per breast on average. The resolution is 2.4 mm (FWHM), and the maximum field of view (FOV) is 24 × 16.4 cm. Several clinical trials have shown a high sensitivity, specificity, and accuracy for the detection of breast cancer. As compared with conventional whole-body PET/CT scanners, PEM has a higher sensitivity, mainly due to improved detection of small tumors [33]. Further, PEM and magnetic resonance imaging (MRI) yield comparable accuracy for detection of the primary tumor and similar effectiveness regarding presurgical planning [29, 30]. Also, PEM and MRI seemed equally effective in screening the contralateral breast of women with newly diagnosed breast cancer [32]. Finally, a pilot study has shown that PEM-guided biopsy could be safe and effective [34]; the procedure caused no adverse events, but invasive cancer was diagnosed in only 54% of biopsies, while 33% of FDG-avid biopsied lesions were eventually found to be benign. Although no comparisons have been made with stereotactic biopsies or biopsies obtained under US or MRI guidance, in which far more experience has been gained, PET-guided biopsy may be useful in selected cases.

Some disadvantages of the PEM should be acknowledged as well. First, because of compression of the breast, lesions close to the pectoral muscle (posterior localization) are more frequently missed [26, 28, 35, 36]. Also, because of activity at the edge of the FOV or incomplete lesion visualization, quantification of FDG uptake in these tumors is less reliable. Second, a high dose of FDG is generally used, which may come with higher risks on radiation-induced cancer

[37, 38]. Third, compression of the affected breast is unpleasant or painful and, more important, hinders comparison with images obtained with MRI.

5. Dedicated Breast PET: Hanging Breast in Prone Position

5.1. PEM/PET. In 2008 Raylman et al. described the design and construction of the PEM/PET (positron emission mammography/tomography) [39]. It consists of two sets of rotating planar detector heads, generating 3D reconstructed images with a FOV of $15 \times 15 \times 15$ mm^3 and a resolution of 1.84–2.04 mm. A biopsy system is included in the device. First clinical evaluation in five patients with known breast cancer showed promising results, but further evaluation is clearly necessary before implementation in clinical practice [40].

5.2. Dedicated Breast PET/CT. In 2009, Wu et al. and Bowen et al. introduced a dedicated breast PET/CT [41, 42]. Patients are scanned in prone position after insertion of a single breast into an opening in the table. The scanner acquires fully tomographic images of the breast by rotating two PET detectors, a CT detector, and an X-ray tube in the coronal plane around a single breast. First clinical evaluation, using 170-477 MBq of FDG and an imaging time of 12.5 min per breast, showed promising results [42]. However, the addition of a CT seems questionable since CT alone has low accuracy in breast imaging, a relatively simple PET reconstruction model without CT could be used as well (using theoretical attenuation of soft tissue and the anatomical simplicity of the breast as a homogeneous mass), and because it results in increased radiation and corresponding radiation-induced cancer risks.

5.3. MAMMI PET. Recently, the MAMmography with Molecular Imaging (MAMMI) PET, a high-resolution breast PET for hanging breast molecular imaging, has been developed in the context of a European project [43]. Patients are scanned in prone position, without compression of the breast. Through an opening in the table, a single hanging breast is positioned in the detector ring, which consists of 12 detector modules in dodecagon configuration and has a scanner aperture of 186 mm. The axial FOV (breast width) is 170 mm, and the coronal FOV (breast length, from pectoral muscle to nipple) can extend to 170 mm by means of precise motion of the detector arm from which the ring extends. The spatial resolution (FWHM) ranges from 1.6 mm in the center of the FOV to 2.7 mm at the edges of the FOV and voxel size is 1 mm^3. Images are reconstructed in 3D using a maximum likelihood expectation maximization algorithm including an attenuation correction through image segmentation and using 12 iterations. The use of CT for attenuation correction or anatomical localization is unnecessary, thereby preventing additional radiation and the increased risk of radiation-induced cancer.

The first clinical validation study, comparing MAMMI PET with MRI and conventional PET/CT in patients with stage II-III breast cancer, was performed in 32 patients [44]. In this pilot study using the first prototype, a MAMMI PET was performed immediately following the conventional whole-body PET/CT. Approximately 110 minutes after injection of 170-240 MBq of FDG, 97% of tumors were visualized with MAMMI PET, including lesions close to the pectoral muscle. Agreement in FDG uptake between whole-body PET/CT and MAMMI PET was high, but SUVmax as assessed with MAMMI PET was consistently higher in all patients (average ratio 2.7).

Currently the second prototype is available (Figure 2). With the exception of slight adjustments to the scintillation crystals, the technical features remained unchanged. Larger adaptations have been made to the software, integrated positioning table, and handling convenience. In current studies, total acquisition time is 15 minutes per breast, irrespective of the needed number of frames. Development of a biopsy system is in the final stage, and phantom tests for biopsies are scheduled. Examples of MAMMI-generated images are shown in Figures 3 and 4.

6. Comparison of Dedicated PETs

Up till now, most experience has been gained with PEM. However, in contrast with prone positioning dedicated PETs, 2D images are acquired, and limited access to regions close to the pectoral muscle has been described. Compression of the breast facilitates comparison of images and lesion localization with mammography, most frequently used for screening or primary diagnostics; prone positioning generates images that are comparable with whole-body PET/CT and MRI, which are normally used in a more advanced stage of the disease. Acquisition time per breast is comparable for all devices, but the FDG dose is considerably lower for the MAMMI PET. An overview of different characteristics of dedicated PETs is presented in Table 1.

7. Future Directions: Main Purposes and Possible Incorporation in Clinical Practice

When using dedicated breast PET devices, tumor deposits outside the breast cannot be visualized, and therefore staging of breast cancer patients is not possible. The value of dedicated breast PETs should therefore be sought in screening or more accurate imaging of the primary lesion using molecular techniques (Table 2). The addition of molecular imaging to conventional imaging modalities (mammography, US, MRI) could be valuable in patients with very dense breasts, after previous (breast-conserving) surgery, or if the lesion appears to be occult (for instance, if nodal metastases are the presenting symptom). Further, if the required FDG dose could be decreased, dedicated breast PETs could be used as a screening instrument. Also, its use could be of value following inconclusive mammography and/or US for a quick differentiation between benign or malignant disease. The high resolution and small voxel size of these devices could improve the detection of small (cT1) tumors, for which sensitivity of whole-body PET/CT was found to be low,

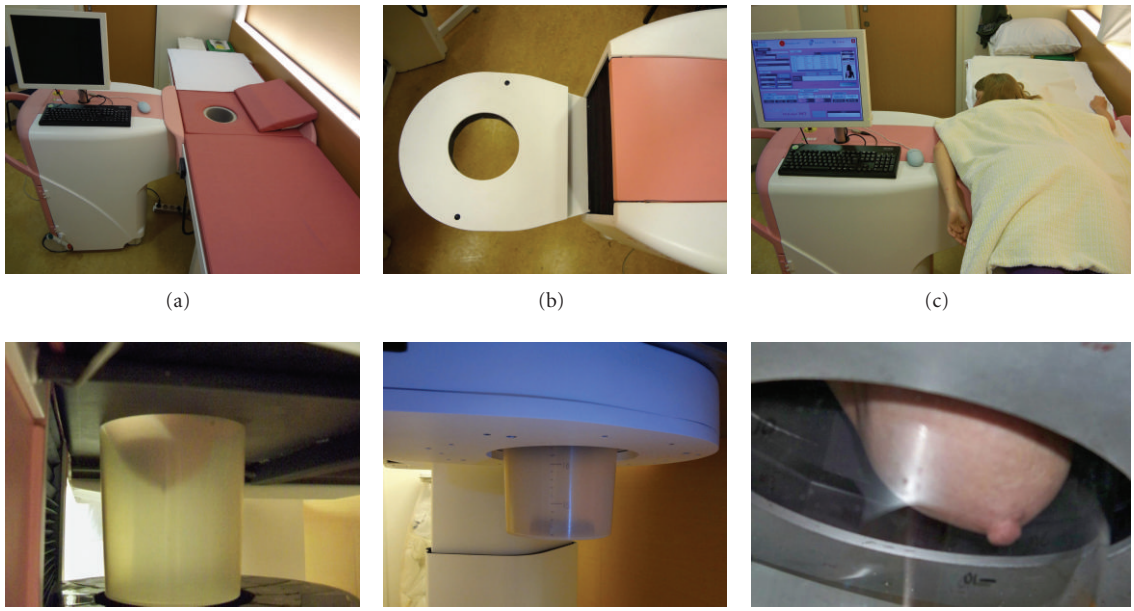

(a) (b) (c)

(d) (e) (f)

Figure 2: MAMMI PET with special bed for hanging breast position (a). Ring device detector (b) enables three-dimensional acquisition and reconstruction after 15–20 minutes of acquisition (c). The hanging breast technique enables a close position of the breast in relation to the detector (d–f).

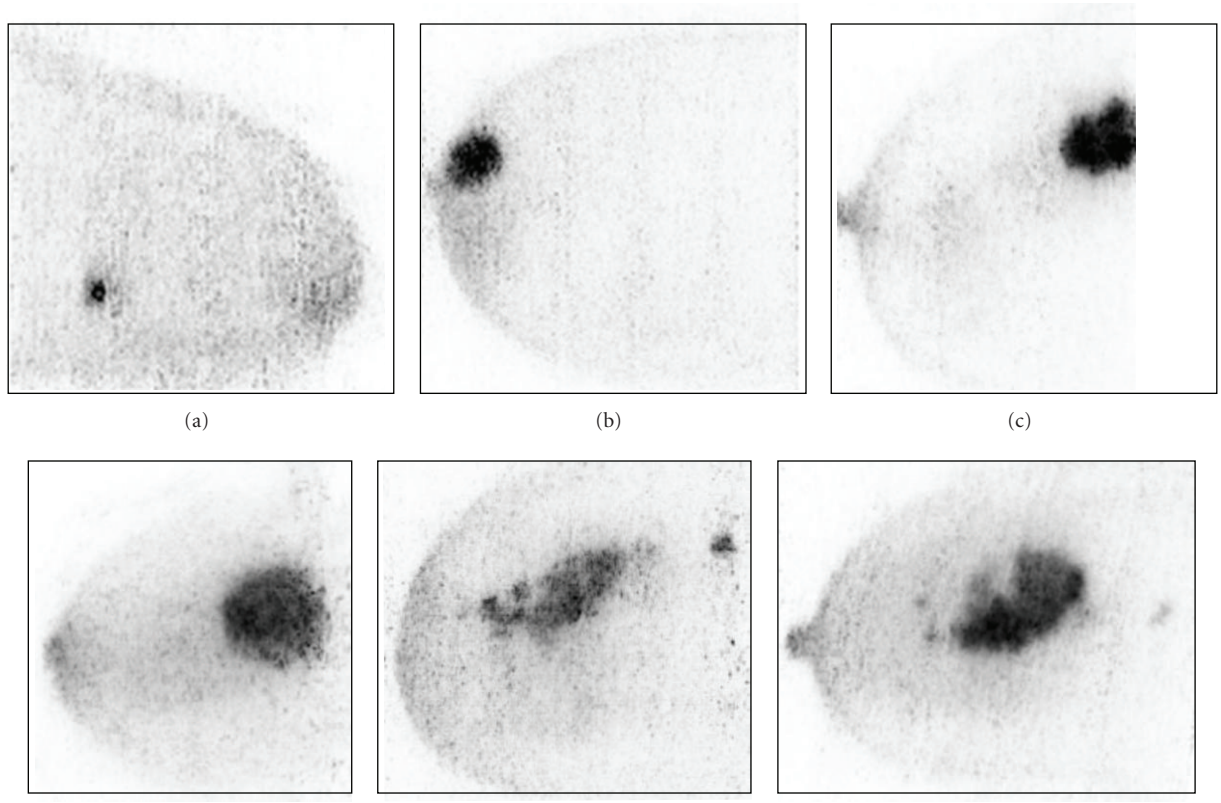

(a) (b) (c)

(d) (e) (f)

Figure 3: MAMMI maximum intensity projections (MIPs) covering the whole volume of the tumor, depicting lesions of 9 mm (a), 2 cm in the area of the nipple (b), and 2.8 cm very close to the thoracic wall (c). Note the heterogeneity of tumor FDG uptake in large tumors (d–f).

Table 1: Comparison of characteristics of four different dedicated breast PETs.

Device	Compression	Resolution FWHM (mm)	FOV	3D	CT	Biopsy	FDG dose (MBq)	Acquisition time per breast (min)	Patients scanned
PEM	Yes	2.4	24 × 16.4 cm	No	No	Yes	301–472	10–20	>750
PEM/PET	No	1.8–2.0	20 × 15 cm	Yes	No	Yes	370–444	3	5
Dedicated breast PET/CT	No	3.27	11.9 × 11.9 cm	Yes	Yes	No	170–477	12.5	4
MAMMI PET	No	1.6–2.7	17 × 17 cm	Yes	No	In progress	180–240	15–20	32

Abbreviations: FWHM: full-width half maximum, FOV: field of view, 3D: three dimensional, CT: computed tomography, FDG: fluorodeoxyglucose, and MBq: megabecquerel.

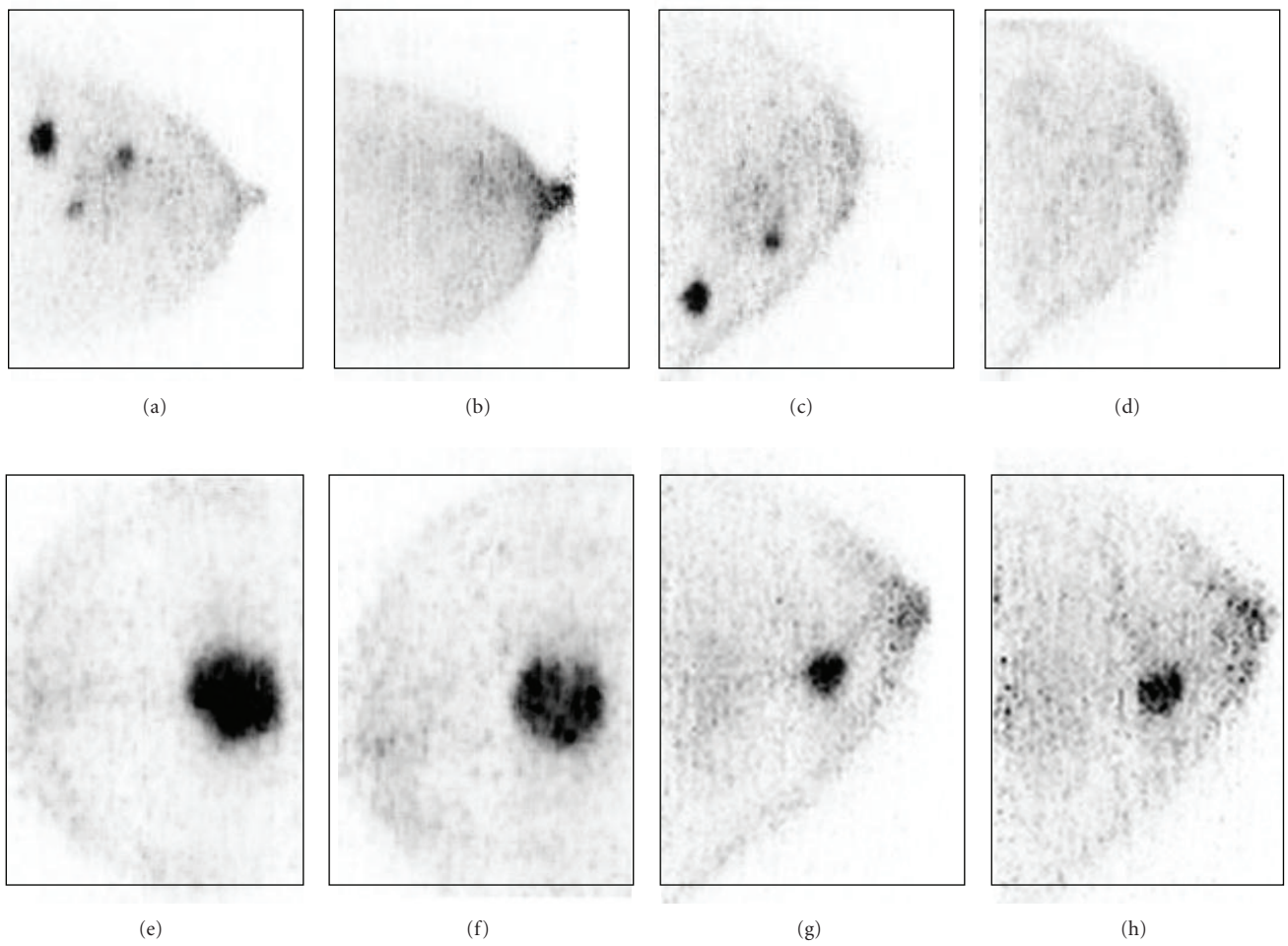

Figure 4: MAMMI maximum intensity projections (MIPs) showing assessment of tumor metabolic response to neoadjuvant chemotherapy in a patient with multifocal breast cancer (a) and disappearance of FDG uptake in the breast lesions (b). The same pattern of complete metabolic response is seen for another patient with two breast tumors (c and d). By contrast, no significant response is seen in a patient with a T2 tumor (e and f) and in another patient with a T1-invasive breast carcinoma (g and h).

and allow for more accurate visualization of heterogeneous tumor FDG uptake. This might be particularly interesting in response monitoring to neoadjuvant chemotherapy, for which promising results have been reported. Finally, further research should be performed regarding FDG-guided biopsy, ensuring tissue sampling from the area with highest degree of FDG uptake, most likely corresponding with the most proliferative part of the tumor.

8. Summary

Whole-body PET/CT has additional value in locoregional and distant staging in both primary and recurrent breast cancer, but sensitivity for detection of (small) lesions in the breast seems suboptimal. Dedicated breast PETs could offer more accurate molecular imaging of breast tumors as compared with conventional PET/CT and might be a

Table 2: Possible indications and applications for dedicated breast PETs in future clinical practice.

Indications and applications for dedicated breast PET
Screening in dense breasts, hindering mammography/ultrasound
Screening in (very) high-risk patients
Occult lesion on conventional imaging
Inconclusive lesion on mammography/ultrasound
Accurate FDG uptake determination in heterogeneous lesions
Primary tumor response monitoring (in node-negative patients)
FDG-guided biopsies

Abbreviations: PET: positron emission tomography, FDG: fluorodeoxyglucose.

valuable addition to conventional imaging modalities. Currently available devices can be categorized according to patient positioning, using either compression of the breast or prone positioning with hanging breast. Although results are promising, further research should be performed before incorporation in daily clinical practice, especially regarding decrease in FDG dose, the additional value following inconclusive mammography and/or US, the use of FDG PET and PET/CT for response monitoring during neoadjuvant chemotherapy, and accuracy of FDG-guided biopsies.

References

[1] R. Siegel, D. Naishadham, and A. Jemal, "Cancer statistics," *A Cancer Journal for Clinicians*, vol. 62, pp. 10–29, 2012.

[2] C. DeSantis, R. Siegel, P. Bandi, and A. Jemal, "Breast cancer statistics," *A Cancer Journal for Clinicians*, vol. 61, pp. 409–418, 2011.

[3] D. A. Berry, K. A. Cronin, S. K. Plevritis et al., "Effect of screening and adjuvant therapy on mortality from breast cancer," *The New England Journal of Medicine*, vol. 353, no. 17, pp. 1784–1792, 2005.

[4] J. J. M. van der Hoeven, N. C. Krak, O. S. Hoekstra et al., "^{18}F positron emission tomography in staging of locally advanced breast cancer," *Journal of Clinical Oncology*, vol. 22, no. 7, pp. 1253–1259, 2004.

[5] D. Fuster, J. Duch, P. Paredes et al., "Preoperative staging of large primary breast cancer with [^{18}F]fluorodeoxyglucose positron emission tomography/computed tomography compared with conventional imaging procedures," *Journal of Clinical Oncology*, vol. 26, no. 29, pp. 4746–4751, 2008.

[6] T. S. Aukema, M. E. Straver, M. J. T. F. D. V. Peeters et al., "Detection of extra-axillary lymph node involvement with FDG PET/CT in patients with stage II-III breast cancer," *European Journal of Cancer*, vol. 46, no. 18, pp. 3205–3210, 2010.

[7] T. S. Aukema, E. J. T. Rutgers, W. V. Vogel et al., "The role of FDG PET/CT in patients with locoregional breast cancer recurrence: a comparison to conventional imaging techniques," *European Journal of Surgical Oncology*, vol. 36, no. 4, pp. 387–392, 2010.

[8] R. Peare, R. T. Staff, and S. D. Heys, "The use of FDG-PET in assessing axillary lymph node status in breast cancer: a systematic review and meta-analysis of the literature," *Breast Cancer Research and Treatment*, vol. 123, no. 1, pp. 281–290, 2010.

[9] B. B. Koolen, M. J. T. F. D. Peeters, T. S. Aukema, W. V. Vogel, H. S. A. Oldenburg, J. A. van der Hage et al., "^{18}F PET/CT as a staging procedure in primary stage II and III breast cancer: comparison with conventional imaging techniques," *Breast Cancer Research and Treatment*, vol. 131, pp. 117–126, 2012.

[10] A. Gil-Rendo, F. Martínez-Regueira, G. Zornoza, M. J. García-Velloso, C. Beorlegui, and N. Rodriguez-Spiteri, "Association between [^{18}F]fluorodeoxyglucose uptake and prognostic parameters in breast cancer," *British Journal of Surgery*, vol. 96, no. 2, pp. 166–170, 2009.

[11] D. Groheux, S. Giacchetti, J. L. Moretti et al., "Correlation of high ^{18}F-FDG uptake to clinical, pathological and biological prognostic factors in breast cancer," *European Journal of Nuclear Medicine and Molecular Imaging*, vol. 38, no. 3, pp. 426–435, 2011.

[12] Y. Wang, C. Zhang, J. Liu, and G. Huang, "Is ^{18}F-FDG PET accurate to predict neoadjuvant therapy response in breast cancer? A meta-analysis," *Breast Cancer Research and Treatment*, vol. 131, no. 2, pp. 357–369, 2012.

[13] N. Avril, C. A. Rose, M. Schelling et al., "Breast imaging with positron emission tomography and fluorine-18 fluorodeoxyglucose: use and limitations," *Journal of Clinical Oncology*, vol. 18, no. 20, pp. 3495–3502, 2000.

[14] T. F. Çermik, A. Mavi, S. Basu, and A. Alavi, "Impact of FDG PET on the preoperative staging of newly diagnosed breast cancer," *European Journal of Nuclear Medicine and Molecular Imaging*, vol. 35, no. 3, pp. 475–483, 2008.

[15] Z. Garami, Z. Hascsi, J. Varga et al., "The value of 18-FDG PET/CT in early-stage breast cancer compared to traditional diagnostic modalities with an emphasis on changes in disease stage designation and treatment plan," *European Journal of Surgical Oncology*, vol. 38, no. 1, pp. 31–37, 2012.

[16] S. Vidal-Sicart, T. S. Aukema, W. V. Vogel, C. A. Hoefnagel, and R. A. Valdés-Olmos, "Added value of prone position technique for PET-TAC in breast cancer patients," *Revista Espanola de Medicina Nuclear*, vol. 29, no. 5, pp. 230–235, 2010.

[17] J. W. Fletcher, B. Djulbegovic, H. P. Soares et al., "Recommendations on the use of ^{18}F-FDG PET in oncology," *Journal of Nuclear Medicine*, vol. 49, no. 3, pp. 480–508, 2008.

[18] N. C. Hodgson and K. Y. Gulenchyn, "Is there a role for positron emission tomography in breast cancer staging?" *Journal of Clinical Oncology*, vol. 26, no. 5, pp. 712–720, 2008.

[19] T. M. Kolb, J. Lichy, and J. H. Newhouse, "Comparison of the performance of screening mammography, physical examination, and breast US and evaluation of factors that influence them: an analysis of 27,825 patient evaluations," *Radiology*, vol. 225, no. 1, pp. 165–175, 2002.

[20] W. A. Berg, L. Gutierrez, M. S. NessAiver et al., "Diagnostic accuracy of mammography, clinical examination, US, and MR imaging in preoperative assessment of breast cancer," *Radiology*, vol. 233, no. 3, pp. 830–849, 2004.

[21] H. M. E. van Ufford, H. van Tinteren, S. G. Stroobants, I. I. Riphagen, and O. S. Hoekstra, "Added value of baseline ^{18}F-FDG uptake in serial ^{18}F-FDG PET for evaluation of response of solid extracerebral tumors to systemic cytotoxic neoadjuvant treatment: a meta-analysis," *Journal of Nuclear Medicine*, vol. 51, no. 10, pp. 1507–1516, 2010.

[22] D. Vriens, J. A. Disselhorst, W. J. G. Oyen, L.-F. de Geus-Oei, and E. P. Visser, "Quantitative assessment of heterogeneity in tumor metabolism using FDG-PET," *International Journal of Radiation Oncology Biology Physics*, vol. 82, no. 5, pp. e725–e731, 2012.

[23] T. A. Yap, M. Gerlinger, P. A. Futreal, L. Pusztai, and C. Swanton, "Intratumor heterogeneity: seeing the wood for the trees," *Science Translational Medicine*, vol. 4, no. 127, Article ID 127ps10, 2012.

[24] M. Gerlinger, A. J. Rowan, S. Horswell et al., "Intratumor heterogeneity and branched evolution revealed by multiregion sequencing," *The New England Journal of Medicine*, vol. 366, no. 10, pp. 883–892, 2012.

[25] C. J. Thompson, K. Murthy, I. N. Weinberg, and F. Mako, "Feasibility study for positron emission mammography," *Medical Physics*, vol. 21, no. 4, pp. 529–538, 1994.

[26] K. Murthy, M. Aznar, C. J. Thompson, A. Loutfi, R. Lisbona, and J. H. Gagnon, "Results of preliminary clinical trials of the positron emission mammography system PEM-I: a dedicated breast imaging system producing glucose metabolic images using FDG," *Journal of Nuclear Medicine*, vol. 41, no. 11, pp. 1851–1858, 2000.

[27] E. A. Levine, R. I. Freimanis, N. D. Perrier et al., "Positron emission mammography: initial clinical results," *Annals of Surgical Oncology*, vol. 10, no. 1, pp. 86–91, 2003.

[28] L. MacDonald, J. Edwards, T. Lewellen, D. Haseley, J. Rogers, and P. Kinahan, "Clinical imaging characteristics of the positron emission mammography camera: PEM Flex Solo II," *Journal of Nuclear Medicine*, vol. 50, no. 10, pp. 1666–1675, 2009.

[29] W. A. Berg, K. S. Madsen, K. Schilling et al., "Breast cancer: comparative effectiveness of positron emission mammography and MR imaging in presurgical planning for the ipsilateral breast," *Radiology*, vol. 258, no. 1, pp. 59–72, 2011.

[30] K. Schilling, D. Narayanan, J. E. Kalinyak et al., "Positron emission mammography in breast cancer presurgical planning: comparisons with magnetic resonance imaging," *European Journal of Nuclear Medicine and Molecular Imaging*, vol. 38, no. 1, pp. 23–36, 2011.

[31] C. L. Wang, L. R. MacDonald, J. V. Rogers, A. Aravkin, D. R. Haseley, and J. D. Beatty, "Positron emission mammography: correlation of estrogen receptor, progesterone receptor and human epidermal growth factor receptor 2 status and ^{18}F-FDG," *American Journal of Roentgenology*, vol. 197, no. 2, pp. W247–W255, 2011.

[32] W. A. Berg, K. S. Madsen, K. Schilling et al., "Comparative effectiveness of positron emission mammography and MRI in the contralateral breast of women with newly diagnosed breast cancer," *American Journal of Roentgenology*, vol. 198, no. 1, pp. 219–232, 2012.

[33] J. S. Eo, I. K. Chun, J. C. Paeng et al., "Imaging sensitivity of dedicated positron emission mammography in relation to tumor size," *Breast*, vol. 21, no. 1, pp. 66–71, 2012.

[34] J. E. Kalinyak, K. Schilling, W. A. Berg et al., "PET-guided breast biopsy," *The Breast Journal*, vol. 17, no. 2, pp. 143–151, 2011.

[35] E. L. Rosen, T. G. Turkington, M. S. Soo, J. A. Baker, and R. E. Coleman, "Detection of primary breast carcinoma with a dedicated, large-field-of-view FDG PET mammography device: initial experience," *Radiology*, vol. 234, no. 2, pp. 527–534, 2005.

[36] W. A. Berg, I. N. Weinberg, D. Narayanan et al., "High-resolution fluorodeoxyglucose positron emission tomography with compression ("positron emission mammography") is highly accurate in depicting primary breast cancer," *The Breast Journal*, vol. 12, no. 4, pp. 309–323, 2006.

[37] R. E. Hendrick, "Radiation doses and cancer risks from breast imaging studies," *Radiology*, vol. 257, no. 1, pp. 246–253, 2010.

[38] M. K. O'Connor, H. Li, D. J. Rhodes, C. B. Hruska, C. B. Clancy, and R. J. Vetter, "Comparison of radiation exposure and associated radiation-induced cancer risks from mammography and molecular imaging of the breast," *Medical Physics*, vol. 37, no. 12, pp. 6187–6198, 2010.

[39] R. R. Raylman, S. Majewski, M. F. Smith et al., "The positron emission mammography/tomography breast imaging and biopsy system (PEM/PET): design, construction and phantom-based measurements," *Physics in Medicine and Biology*, vol. 53, no. 3, pp. 637–653, 2008.

[40] R. R. Raylman, J. Abraham, H. Hazard et al., "Initial clinical test of a breast-PET scanner," *Journal of Medical Imaging and Radiation Oncology*, vol. 55, no. 1, pp. 58–64, 2011.

[41] Y. Wu, S. L. Bowen, K. Yang et al., "PET characteristics of a dedicated breast PET/CT scanner prototype," *Physics in Medicine and Biology*, vol. 54, no. 13, pp. 4273–4287, 2009.

[42] S. L. Bowen, Y. Wu, A. J. Chaudhari et al., "Initial characterization of a dedicated breast PET/CT scanner during human imaging," *Journal of Nuclear Medicine*, vol. 50, no. 9, pp. 1401–1408, 2009.

[43] A. Soriano, A. González, A. Orero et al., "Attenuation correction without transmission scan for the MAMMI breast PET," *Nuclear Instruments and Methods in Physics Research A*, vol. 648, supplement 1, pp. S75–S78, 2011.

[44] B. B. Koolen, T. S. Aukema, A. J. G. Martínez, W. V. Vogel, L. C. Ontanaya, and M. J. T. Peeters, "First clinical experience with a dedicated PET for hanging breast molecular imaging ," *Quarterly Journal of Nuclear Medicine and Molecular Imaging*. In press.

Hindawi Publishing Corporation
Journal of Oncology
Volume 2012, Article ID 213421, 9 pages
doi:10.1155/2012/213421

Review Article

Breast Imaging: How We Manage Diagnostic Technology at a Multidisciplinary Breast Center

Alejandro Tejerina Bernal, Antonio Tejerina Bernal, Francisco Rabadán Doreste, Ana De Lara González, Juan Antonio Roselló Llerena, and Armando Tejerina Gómez

Centro de Patología de la Mama, Fundación Tejerina, José Abascal 40, 28003 Madrid, Spain

Correspondence should be addressed to Alejandro Tejerina Bernal, alejandro.tejerina@cpmama.es and Antonio Tejerina Bernal, antonio.tejerina@cpmama.es

Received 18 April 2012; Accepted 4 June 2012

Academic Editor: Alvaro Ruibal

Copyright © 2012 Alejandro Tejerina Bernal et al. This is an open access article distributed under the Creative Commons Attribution License, which permits unrestricted use, distribution, and reproduction in any medium, provided the original work is properly cited.

This paper discusses the most important aspects and problems related to the management of breast cancer imaging, at a center specialized in breast pathology. We review the established and emerging diagnostic techniques, their indications, and peculiarities: digital mammography, CAD systems, and the recent digital breast tomosynthesis, ultrasound and complementary elastography, molecular imaging techniques, magnetic resonance imaging, advanced sequences (diffusion), and positron emission mammography (PEM). The adequate integration and rational management of these techniques is essential, but this is not always easy, in order to achieve a successful diagnosis.

1. Introduction

Breast cancer remains the most prevalent cancer disease in women of developed countries with great social and economic impact. For all these reasons, the scientific community concentrates on improving imaging methods, developing drugs for new therapeutic targets, and working at well-coordinated multidisciplinary units.

The Breast Pathology Center of Madrid has more than 40 years of experience in this field, with over 60 medical professionals working with and for breast pathology. More than 50,000 patients are examined each year, and over 400 new cancers are diagnosed annually.

Historically, the first treatment which changed the course of the disease was Halsted's radical mastectomy [1], in the late nineteenth century. Many subsequent advances took place, but what really marked a turning point was the idea that a systematic study with mammography, at highest risk ages, could detect and, therefore, change the evolution of breast cancer in population groups.

Imaging techniques have experienced a highly significant development in recent years. The morphological image, of great value, has evolved into a physiological and functional image, capable of providing additional information, very valuable to better understand disease processes. Many technological changes have been established since the development of the first analogue mammography device in the sixties, with which we started working but, undoubtedly, the most important advance has been the introduction of digital mammography.

Ultrasound use increased in relevance over the years as well as its application in the remaining organs and systems, while the image improved with the first static ultrasound devices, nowadays becoming a daily practice routine.

Magnetic resonance imaging (MRI) is at present an almost indispensable technique for local staging and followup of breast cancer, although many technical improvements have been necessary for this imaging test to provide adequate sensitivity and specificity to become widely used.

Thanks to the merging between morphological and molecular techniques, PET-CT has gained importance in cancer staging, including breast cancer, always being open to other specific nuclear medicine studies dealing with the study of the breast, as in the PEM technique, which is beginning to evolve, even though the first clinical studies show very satisfactory results.

This whole technological arsenal must be integrated into breast diagnostic imaging units which, in turn, belong to multidisciplinary breast pathology units. The professionals must be responsible for knowing its extent, indications and limitations, in order to achieve the highest diagnostic performance and, ultimately, an early diagnosis.

2. Digital Mammography and Its Resulting Techniques

2.1. Digital Mammography. Mammography must be an effective universal technique, reproducible, with enough sensitivity and specificity to ensure early detection and influence the course of the disease, decreasing mortality by 20–30% [2].

So, it is the "gold standard" technique for the study of breast pathology and is used in screening studies in women aged between 40–50 years, depending on each country.

In 2000, the Food and Drug Administration (FDA) approved the usage of digital mammography (DM) for diagnostic use, with consequent improvements in image resolution and digital manipulation and storage. These aspects make it a more widespread technology, being practically an essential prerequisite for a breast diagnostic center. In Spain, we became leaders of this technique, which involved time to adapt and change, as the file storage systems (PACS-RIS) as well as the workstations had to be modified.

The DM can be classified into two large groups depending on its usage. Detectors called computed radiography (CR) belong to the first group. These have the advantage of being employed with conventional mammography devices. The second group of detectors (DR) encompasses all those which are integrated within a digital mammography system itself.

At present, there is no scientific doubt with respect to the usefulness of mammography or diagnostic mammography for breast cancer early detection programs, and an improvement in its effectiveness is expected when using new techniques (CAD, tomosynthesis, ultrasound, etc.), which increase the sensitivity and specificity of this imaging test.

2.2. Digital Breast Tomosynthesis (DBT). Mammography continues to have certain limitations inherent to the principle of obtaining a two-dimensional (2D) image of a three-dimensional compressed glandular parenchyma, causing lesions to be masked sometimes due to the superimposition of glandular structures in the X-ray beam.

This structure superimposition can impede visualizing a lesion (false negative) or identifying a lesion as suspicious which finally is a glandular accumulation (false positive) (Figure 1).

Based on this fact, Digital Breast Tomosynthesis arises (DBT). In 2010, we incorporated this new technology at our center, being the first Spanish center and one of the first European centers to work with DBT.

It is a mammography device which uses 3D technology and a rotary head tube, performing different projections of a static breast (Figure 2) with a specified angle (between 15–45°) and employing two types of technology: "continuous" or "step and shoot," depending on the commercial device which is available.

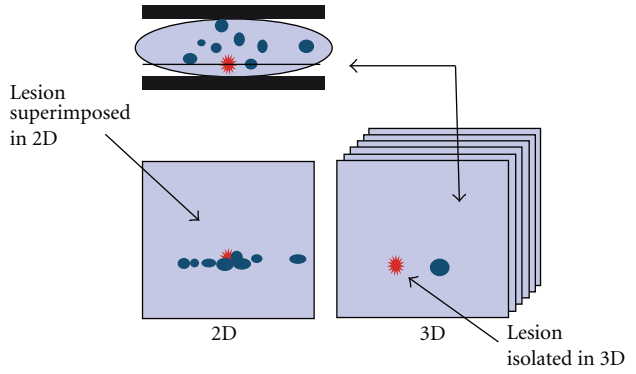

Figure 1: This figure shows, in a 2D mammography, a potentially malignant lesion, in red. This lesion can remain occult between benign lesions, such as cysts represented in blue. However, at the selected tomographic slice, the malignant lesion is visible avoiding the superimposition.

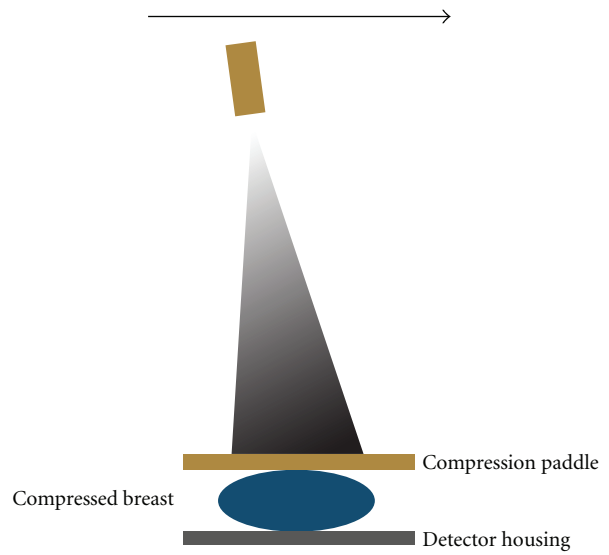

Figure 2: Tomographic projection obtention system using rotatory X-ray tube.

The projections can be obtained craniocaudally (CC) and oblique-medial-laterally (OML), except for some commercial devices which only conduct OML projections.

Then, the images are reconstructed at a cutting thickness between 0.5–1 mm, and they can be visualized at a workstation, with software specialized in tomosynthesis, individually or as a "film," as which is displayed with a conventional scanner. So that a compressed breast, 5 cm thick, will generate 50 tomosynthesis images 1 mm thick.

In this way this is a technique which, conceptually, would be a combination between mammography and scanner and it can be considered a tomographic application of digital mammography.

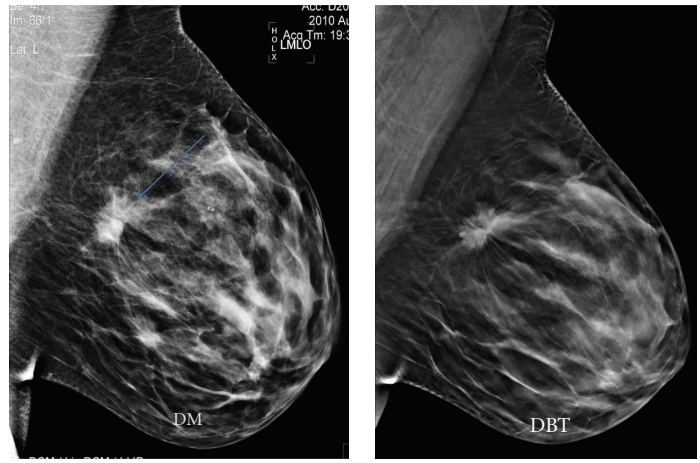

(a) (b)

Figure 3: Lump detected more clearly with the DBT than the DM technique, visualizing better its margins, helping to catalogue it as an image highly suggestive of malignancy, BI-RADS 5.

The radiation dose of a 3D tomosynthesis and 2D mammography study is within the standards accepted by the Mammography Quality Standards Act (MQSA), although the radiation dose is somewhat larger than that generated by the current modern mammography devices with tungsten tubes.

The acquisition time of the study must be low in order to reduce the possibility of motion artifacts and vascular stasis images, due to the elevated compression time, as well as to avoid a prolonged study time which causes discomfort to the patients.

In our case, we always use DBT as a complement to the DM and never as a single study without mammography. After an initial adaptation and training phase in reading these new dynamic images, we conclude that DBT provides an enormous potential as it avoids image overlapping with respect to DM.

For us, the main advantages of carrying out a DBT study, complementary to DM, are therefore based on the following principles:

(i) it improves the display of the lump contour [3], helping their characterization and making a more accurate estimation of the BI-RADS classification (Figure 3);

(ii) it helps detecting distortions, so far hidden in certain mammographies;

(iii) it reduces the number of false positives corresponding to glandular clusters;

(iv) it avoids carrying out a large number of special projections, except for cases where the only findings are microcalcifications [4];

(v) it provides greater security in the study of dense breasts;

(vi) it reduces the number of recalls at screening mammography [5];

(vii) with respect to microcalcification determination, recent studies suggest that it is similar to mammography, even though it provides valuable information as to location and specific provision.

Although its usefulness is undeniable, it is still early, and there are some unresolved issues. There are no accepted protocols for use with respect to whether it must be used in all patients or not, or if both projections must be carried out in each breast always or if it is possible to use tomosynthesis without mammography.

Our group presented protocols for optimal use [6], based on mammographic findings, breast density, clinical symptoms, and background information, which are summarized in the diagrams shown in Figure 4.

For all these reasons, this technique is spreading across European and North American centers, including it in routine diagnostic practice, and there are ongoing studies designed to analyze its role in breast cancer screening.

2.3. Computer-Aided Detection (CAD) Technology for Mammography Reading. The sensitivity and specificity of mammography vary between 70–96% and between 90–95%, respectively [7, 8]. The reasons for this variability lie in the quality of this technique and the individual ability of the radiologist. Several clinical studies have demonstrated that between 30–70% of cancers, diagnosed during a screening program, can be seen on mammograms previously read as normal; in half of the cases, this is due to detection errors and, in the other half, to reading errors [9]. In order to try to overcome these disadvantages, there are different reading techniques. That with best performance appears to be the "double reading," and it is the one used routinely in our center. In recent years, several options have emerged, such as the integration of computer-aided detection systems (CAD) for mammography reading.

These computer systems have been designed as tools to support the radiologist in the detection of suspicious lesions

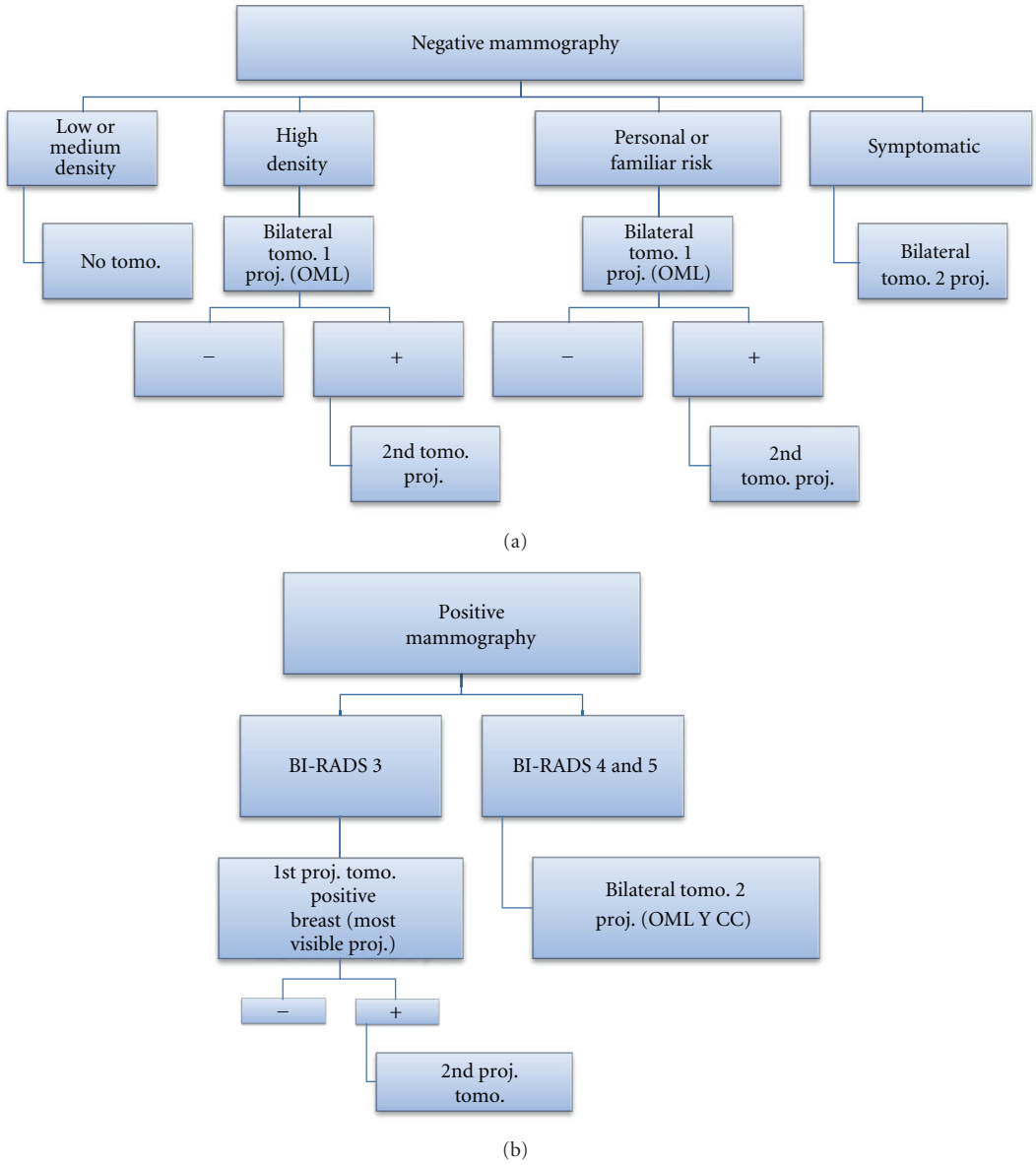

Figure 4: Tomosynthesis usage protocol in case of negative or positive mammography.

for breast cancer. The most developed systems are CAD systems at present, and they are mainly used for screening.

The sensitivity of these systems varies with the type of lesion, and there seems to be higher sensitivity levels in microcalcifications than in detecting lumps or other findings [10].

Some of the disadvantages of CAD systems are their low specificity, the radiologist having to reject false positives detected by the system, creating a lack of confidence, especially in nonexpert radiologists. Furthermore, this may lead to increased reading times, this fact being important when reading screening mammographies.

However, CAD systems, as well as other technologies, are improving significantly, and new CAD systems have emerged even to evaluate tomosynthesis.

For this reason and in our experience, the main advantage of the use of computer-aided systems is its application in screening mammography, mainly for detecting microcalcifications, provided that they are used by mammography expert radiologists.

2.4. Location Systems and Radiological Stereotactic Biopsy. There are at present two groups of stereotactic localization systems which are used for preoperative localization by wire or for biopsy, by means of the core biopsy or vacuum-assisted biopsy (VAB) system, the latter being used more often radiologically guided.

They consist on systems which use a prone table and systems with a vertical or lateral stereotaxic device, aided by a mammography unit, which will be used interchangeably, based on availability of the technique in each center. Except for certain cases, if both systems are available, it seems preferable to use the prone table for biopsies as it is more

comfortable for the patient. For preoperative localization, it will depend more on the availability, at the center, of a mammography device or a prone table, if it were being used at that time for biopsy or for mammography workout.

Additionally, nowadays the assisted biopsy system for tomosynthesis has emerged as several images, though only few, are visible only with this technique, needing guided biopsy by this system. Nevertheless, until we disposed of this type of assisted biopsy system for tomosynthesis, we resolved this problem using a fenestrated compression device, and we were guided by the depth in millimeter slices provided by tomosynthesis, to calculate the exact spot and, in such a way, to be able to place a preoperative wire or to carry out core biopsy although, in order to carry out VAB, we did not dispose of any support, for which it was impossible to conduct.

The type of subsidiary images of radiological biopsies will preferably be microcalcifications, distortions, and focal densities with little if any translation with other imaging techniques.

Sometimes it is necessary to place a metallic marker postbiopsy to serve as a guide for further surgery if necessary.

3. Ultrasound: Elastosonography

Ultrasound is the essential complementary technique for mammography and, in some cases, as in young or pregnant patients, it is the first choice.

Ultrasound systems have improved greatly with the introduction of high-frequency probes, between 12–15 MHz, harmonic images, and 3D images which provide a very high-quality morphological image of the surface. Ultrasound, when used as the first diagnostic technique, has two major disadvantages: the microcalcifications are difficult to detect by ultrasound; it is a technique which depends on the browser, and this can take a very long time. For these reasons, this technique must not be used initially, although it has many indications and utilities.

Elastosonography is a step forward as functional technique.

In a few years time, it has moved from being a technique mainly used to differentiate between cystic and solid images, to be an indispensable complement, establishing the degree of suspicion of a breast lesion not determined by mammography.

As advantages over mammography, we can include its ability to assess the internal structure of lesions in multiple planes, their orientation, morphology and margins, both in predominantly fatty breasts and, above all, in breasts with dense glandular structure, where the mammography is more limited.

3.1. Ultrasound Indications. Breast ultrasound, as initial workup for breast pathology, can be indicated in some cases.

In young women, below 30 years old, with dense breasts and symptomatic, ultrasound constitutes the technique of choice as well as in pregnant or breastfeeding women. In cases of inflammatory disease, ultrasound is better tolerated and superior to mammography when identifying collections. In women with mastectomies, it is used to study the surgical site and to search for recurrences or possible surgery complications.

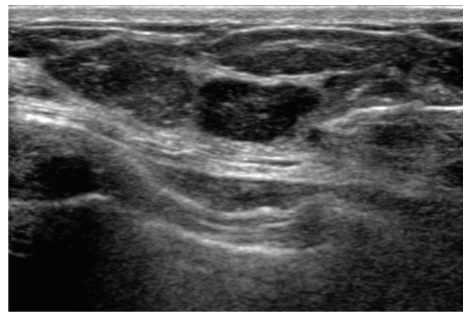

Figure 5: Ultrasound-guided biopsy of a lump from a patient with implant, allowing monitoring at all times the progress of the tip of the needle.

Ultrasound, as a complementary technique to mammography, has a key role in many cases.

To analyze mammographic findings, establishing a BI-RADS ultrasound staging [11]. To examine breast implants although, if there is any doubt, a MR should be carried out. To visualize galactophoric trees in patients with secretions. For negative mammogram and palpable lesion cases, ultrasound plays a crucial role as well as in women with risk factors and dense breasts [12]. For malignancy confirmed cases, ultrasound provides important information about tumor size, pectoral and skin involvement, multifocality and multicentricity, and axillary staging, although its performance is higher when combined with MRI.

Ultrasound, as a guide for interventional procedures and preoperative marking, constitutes another mainstay, being the method to be used due to its comfort, lower cost than with other techniques, and increased safety for the patient, as it monitors at all times the progress of the tip of the needle (Figure 5).

For this reason, whenever a lesion is visible by ultrasound, except for certain cases, it is the method we use for both FNAB or core biopsy. You can also use vacuum-assisted biopsies (VABs), although it is less comfortable due to the greater weight of these devices, its use being limited practically to cases of excision of benign lesions, mainly fibroadenomas or papillomas. And, although it is an accepted technique, it continues to raise controversy at present and, in our experience, its application is limited to very specific cases.

3.2. Elastosonography: A Functional Technique. It is a recent ultrasonic technique based on the same principle as breast palpation, that is, the estimation of the consistency or hardness of the tissues.

It is a comfortable technique, as it does not require more than the same transducer which has been employed for B-mode images, and it is quick as it does not extend the test more than a couple of minutes.

At present, there are two types of sonoelastography: compression elastography and supersonic elastography.

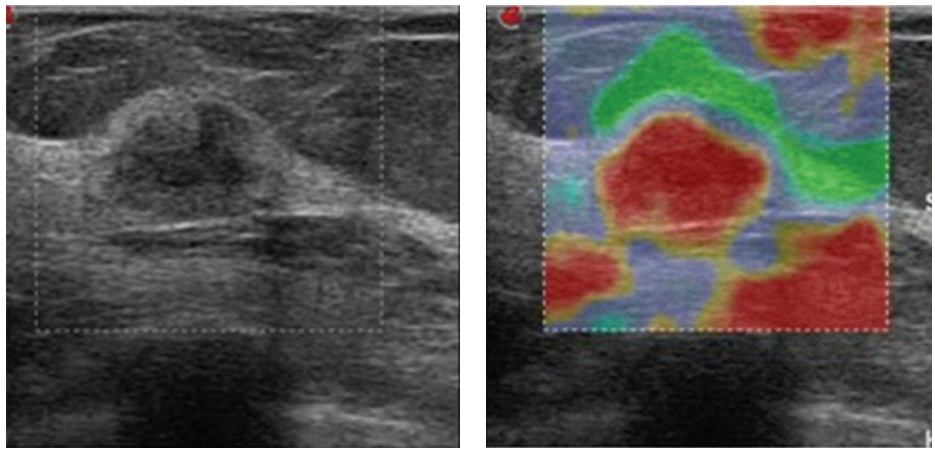

(a) (b)

Figure 6: Comparative B-mode ultrasound image of an unspecified lesion which, on the elastographic map, corresponds to an increased hardness lesion, shown in red. It corresponded to invasive ductal carcinoma.

Compression elastography (*strain imaging*) assesses the deformation of different tissues as a result of the effect of compression waves emitted from the transducer through which we gently compress the skin. This technique is qualitative or semiquantitative, and its results are reflected in two types of elastograms. One of them is based on a gray scale, where the softer tissues appear in white, while the hardest appear in black. Once we differentiate the lesion to examine, which will appear darker than the adjacent tissue structures, we must take a look at the lesion size. Benign lesions tend to have a resulting image smaller than the B-mode image. By contrast, malignant lesions have a greater or equal resulting image than the B-mode image. This phenomenon may be related, according to Insana et al. [13], to the desmoplastic reaction present in most of these lesions. The other elastogram is characterized by presenting in colors both the lesion and the surrounding tissue, depending on their elasticity and according to a color scale that varies depending on the commercial firm (Figure 6). Itoh's group [14] described an elasticity chromatic scale which classified elastographic findings in a manner similar to that used by the BI-RADS classification in B-mode.

Supersonic elastography (*supersonic shear waves imaging*), developed more recently than the previous one, is characterized by the use of transmitted ultrasound pulses at high speed from the same transducer and without compressing the skin. The tissues generate waves in response to these pulses that allow you to know different parameters quantitatively, such as maximum, minimum, or average elasticity of the different structures studied.

Whatever the elostographic system we have available, this technique must be understood as a value added to the B-mode ultrasound. A value that, although being rare in the case of lesions with an ultrasound BI-RADS 2, 4b, 4c, or 5, that is, in those lesions with high probability of benignancy or malignancy, it can be considerable in the case of more uncertain lesions, such as BI-RADS 3 (probably benign) or BI-RADS 4a (low malignancy suspicion). So that this technique, used as complement to B-mode ultrasound in the study of BI-RADS 3 lesions, will be capable of confirming the ultrasound hypothesis of benignancy, thereby reducing the number of unnecessary biopsies and guiding these low-risk patients to a followup with greater safety [15].

4. Magnetic Resonance Imaging: New Advances

Magnetic resonance imaging is a less available than the previously described methodologies, but this does not mean that it has to remain in the background, as it is of great diagnostic value in many cases.

Since the Introduction of contrast agents, improved antenna surface and the development of new imaging protocols, MRI emerged as a promising technique for the detection, diagnosis, and staging of breast cancer.

Its introduction as an imaging test in the field of breast cancer has implied a huge progress due to its high diagnostic performance and ability to detect tumor burden and other pathological conditions, both in morphological and functional terms.

MRI has a number of morphological sequences, highlighting T2 FSE, STIR, and T1, which allow us to evaluate breast tissue density and morphological changes and to assess the condition of the skin, armpits, and the edge of the pectoral muscle.

Having obtained the morphological sequences, the contrast agent is administered in order to assess, by subtraction sequences, MIP and MPR, the uptake of the breast, the possible tumor uptake, and we will evaluate the dynamic sequences, by means of the time/intensity curves.

The perfusion, spectroscopy, and diffusion sequences have not been validated at a large scale and, consequently, they must be conceived as a complement to the sequences described above, while providing a promising future.

Given the high false positive rates produced by this technique, in patients staged by MRI, and based on the fact that additional tumor burden diagnosed by MRI can be treated effectively with adjuvant chemotherapy and radiotherapy,

as was demonstrated by Fisher et al.'s and Veronesi et al.'s clinical trials [16, 17], all this leads to state that this technique has its detractors maintaining that any additional lesion diagnosed by MRI does not have real impact on patient's survival.

A meta-analysis by Houssami and Hayes [18] analyzed the rate of additional disease diagnosed by MRI (16%), and the proportion of patients in which surgical planning was altered (7.8–33%).

The heterogeneity of the literature is due to the fact that, in real clinical practice, not all radiologists work in a multimodality environment, handling all the techniques in harmony and integrating their clinical and radiological breast cancer knowledge. This is reflected by the rate of additional lesions detected by MRI before surgery, making the surgeon and oncologist to distrust this technique.

4.1. Indications for MRI. There are at present some clear indications accepted by the scientific community: to evaluate response in patients treated with chemotherapy, screen high-risk patients, detect primary tumors in patients with nodal metastases of unknown character, and analyze breast implants to rule out rupture. However, there are some clinical applications that are not accepted by all the professionals, the main one being breast cancer staging but, nonetheless, it is already included in routine clinical practice at multiple medical centers and hospitals throughout the world.

Breast cancer staging is essential to establish the type of treatment for the patient and to assess tumor size, the presence of multifocal or bilateral lesions and the expansion to the nipple-areola complex or intraductal component (Figure 7).

In the case of detecting an additional lesion, it will always be necessary to perform a "second-look" ultrasound in the area and to carry out a biopsy of this lesion if it were visible. Our experience is that around 80% of lesions, detected by MRI and not previously identified by conventional methods, are detected by a second-look ultrasound, thereby limiting MRI guided biopsies to very specific cases, ductal enhancements for the most part. Some of the criteria to be analyzed, in order to establish successful staging, will be the percentage change of therapeutic attitude, reexcision rates, and recurrence rates.

Evaluating response to treatment produced by primary chemotherapy is of great importance since it is an *in vivo* chemosensitivity test, allowing varying cancer treatment if not effective. MRI enables establishing the response rate quantifying tumor shrinkage volume (Figure 8) and permitting the oncologist to change the type of neoadjuvant drug in the middle of treatment or to decide at the end of it if it possible to conduct conservative surgical treatment. Nevertheless, there is some tumor under- and over-estimation, a fact largely being solved thanks to diffusion sequences and spectroscopy.

The diagnosis of tumor recurrence is uncommon during the first 18 months after treatment and, in most cases it appears at the surgical bed for the first 5 years. We prefer carrying out MRI after the first 12–18 months of treatment,

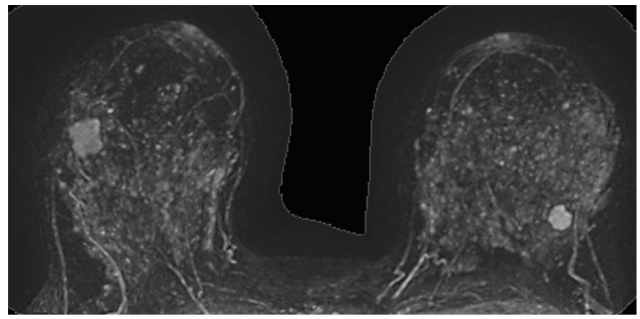

Figure 7: MIP RMI reconstruction. Preoperative staging study due to a right breast lesion, where a second lesion was identified at the left breast, corresponding to synchronic bilateral carcinoma.

in order to avoid the false positives caused by fat necrosis and inflammatory component. Even though, if in our practice we detect a high suspicion of recurrence, we conduct MRI whatever the time elapsed since surgery.

Screening High-Risk Patients. Cancers of patients with BRCA 1 and 2 mutations have particular characteristics. These tumors have well-defined margins, apparently benign, and appearing in very young patients, with a much shorter doubling time than in noncarrier patients, and the most prevalent molecular phenotype has the worst outcome, triple negative. The mammography has less value in these patients as they often have dense breasts due to their youth. It is estimated that the heterofamily factors are among the factors responsible for approximately 10–15% of cases. Several multicenter studies [19] show that the sensitivity of following these patients with MRI is more than twice that with mammography only. For this reason, we prefer following these patients with annual MRI.

Search for Occult Breast Cancer. Occult breast cancer represents less than 1% of all breast cancers. MRI has emerged as the technique of choice before taking any therapeutic approach.

Evaluating Patients with Breast Implants. In this case, MRI plays two key roles: implant rupture detection and cancer detection in patients with implants, which hampers visualizing breast tissue with other types of techniques (Figure 9). It is true that ultrasound has a good sensitivity and specificity also for evaluating implants and can be used as the first technique, leaving MRI for cases of diagnostic uncertainty and for implants and family genetic burden cases.

4.2. Advanced Sequences: Diffusion. Diffusion sequences are based on the principle of mobility of water molecules in a medium. Thus, a high-cellularity structure will have a lower diffusion of its water component due to the high number of cellular elements.

So the diffusion-MRI can be used to calculate the apparent diffusion coefficient (ADC), which is a quantitative measure of water diffusion, providing information about tumor cellularity and membrane integrity, and it is sensitive

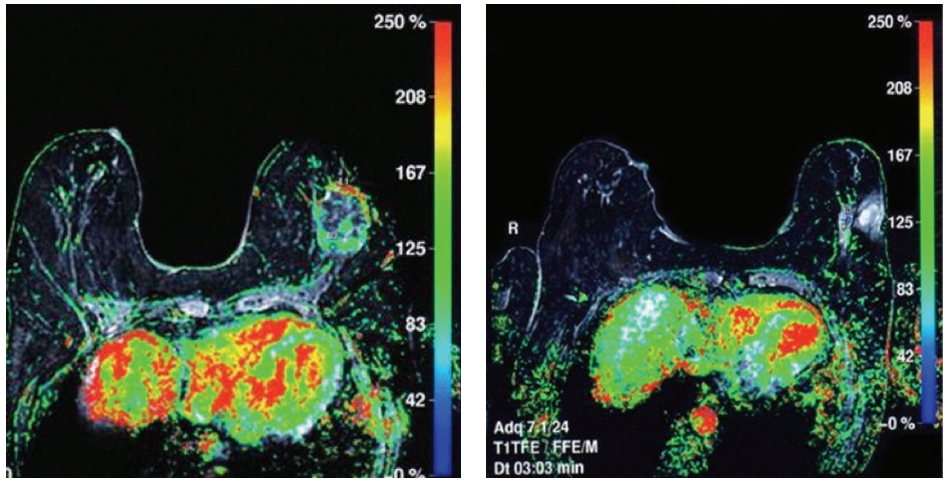

(a) (b)

Figure 8: MRI during neoadjuvant treatment monitoring, where one can visualize macroscopic tumor disappearance corresponding to greater partial response.

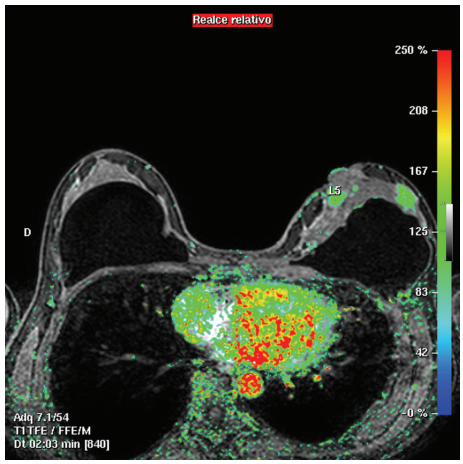

Figure 9: Tumor recurrence at a previously mastectomized patient with bicameral implant.

to the intratumoral changes produced by chemotherapy treatment.

The calculation of ADC can be used as an additional element in the evaluation of a breast lump, joining the established criteria, such as margins, shape, signal characteristics, tumor enhancement, and dynamic study. Apart from its main use, which has been studied many times, and the use of this parameter as a predictor of neoadjuvant treatment response, it can assist in individualized treatment plans and avoid ineffective chemotherapy.

5. PET-CT and PEM

With the merging between morphological and functional techniques, PET-CT studies have become a benchmark for the diagnosis and followup of cancer diseases.

They are used for head and neck tumors, thyroid follicular cancer, single pulmonary nodules, lung cancer, esophageal cancer, colorectal cancer, lymphoma, melanoma, and breast cancer of course.

The metabolic activity of neoplastic tissue, provided by ET, offers additional information about tumor biology and can be used to differentiate between benign and malignant, metastasis identification in early stage for disease staging, treatment response, and tumor aggressiveness.

In breast cancer study, whole-body PET-CT is extremely useful in tumor staging at a distance, especially in advanced stage breast cancer cases and (plays) has a role in locoregional lymph node staging.

However, for breast cancer imaging, it has an important spatial limitation, their sensitivity and specificity figures being 80 and 76%, respectively [20].

5.1. Positron Emission Mammography (PEM). Due to the limited resolution of PET equipment and the space limitations of the current protocols for CT acquisition, small-size breast tumors are not visible using this technique, until they reach a certain size, and they can be visualized with other techniques like MRI. This is what has led to the development of a PET device dedicated to the breast, PEM (positron emission mammography).

The high-resolution PET has been designed to detect small hypermetabolic lesions of external parts, such as the breast.

There are several commercial firms which have developed the PEM and, although they are still in early clinical development, initial results show sensitivity levels of 93% [21], similar to MRI and also high specificity levels 93% [22] higher than MRI.

These results position this technique as promising, with applications in surgical planning, monitoring response to neoadjuvant treatment and recurrence. However, there are some disadvantages related to the cost and technical difficulty of handling radiopharmaceuticals. Another issue to resolve is

which will be the interrelation between MRI and PET and if a coexistence of both techniques is possible or if one of them will prevail over the other. It is still too early, and only time will give us the answer.

6. Conclusion

The constant technological innovation is undeniable both in improving the morphological and the functional techniques. There is a very narrow common future, in which the combined techniques are becoming a present reality for the diagnostic imaging of breast pathology, led by professionals with an increasing degree of specialization.

Nowadays, there are many technological innovations available to us, but it would not be beneficial that, instigated by the novelty, we lost the true meaning of each technique, and if we anticipated issues with no scientific evidence still.

Nonetheless, we must have an open mind to integrate the new emerging techniques with the established ones in order to take advantage of the combination of both.

It is, therefore, important that image specialists, dedicated to breast pathology, work in a multimodal environment, managing the main techniques and keeping abreast always.

Working in multidisciplinary units composed of clinicians, surgeons, oncologists, imaging specialists, and so forth, is essential to allow progress in breast cancer treatment and diagnosis.

Conflict of Interests

The authors declare that they have no conflict of interests.

References

[1] J. Ferlay, P. Autier, M. Boniol, M. Heanue, M. Colombet, and P. Boyle, "Estimates of the cancer incidence and mortality in Europe in 2006," *Annals of Oncology*, vol. 18, no. 3, pp. 581–592, 2007.

[2] "European comission," in *European Guidelines for Quality Assurance in Breast Cancer Screening and Diagnosis*, N. Perry, M. Broeders, C. de Wolf, S. Tornberg, R. Holland, L. Van Karsa et al., Eds., Office for Official Publications of the European Communities, Luxembourg, 4th edition, 2006.

[3] L. T. Niklason, B. T. Christian, L. E. Niklason et al., "Digital tomosynthesis in breast imaging," *Radiology*, vol. 205, no. 2, pp. 399–406, 1997.

[4] C. M. Hakim, D. M. Chough, M. A. Ganott, J. H. Sumkin, M. L. Zuley, and D. Gur, "Digital breast tomosynthesis in the diagnostic environment: a subjective side-by-side review," *American Journal of Roentgenology*, vol. 195, no. 2, pp. W172–W176, 2010.

[5] M. P. Jeong, E. A. Franken Jr., M. Garg, L. L. Fajardo, and L. T. Niklason, "Breast tomosynthesis: present considerations and future applications," *Radiographics*, vol. 27, supplement 1, pp. S231–S240, 2007.

[6] A. Tejerina, *Tomosynthesis: National Experience*, International World Congress of Senology, Valencia, Spain, 2010.

[7] E. Thurfjell, M. G. Thurfjell, E. Egge, and N. Bjurstam, "Sensitivity and specificity of computer-assisted breast cancer detection in mammography screening," *Acta Radiologica*, vol. 39, no. 4, pp. 384–388, 1998.

[8] J. L. Urbain, "Breast cancer screening, diagnostic accuracy and health care policies," *CMAJ*, vol. 172, no. 2, pp. 210–211, 2005.

[9] R. L. Birdwell, D. M. Ikeda, K. O'Shaughnessy, and E. Sickles, "Mammographic characteristics of 115 missed cancers later detected with screening mammography and the potential utility of computer-aided detection," *Radiology*, vol. 219, no. 1, pp. 192–202, 2001.

[10] R. F. Brem and J. Schoonjans, "Radiologist detection of microcalcifications with and without computer-aided detection: a comparative study," *Clinical Radiology*, vol. 56, no. 2, pp. 150–154, 2001.

[11] *American College of Radiology: Breast Imaging Reporting and Data System (BI-RADS)*, Ultrasound, 4th edition, 2003.

[12] T. Greene, A. Estabrook, L. Chinitz et al., "A single institution review of new breast malignancies identified solely by sonography," *Journal of the American College of Surgeons*, vol. 203, no. 6, pp. 894–898, 2006.

[13] M. F. Insana, C. Pellot-Barakat, M. Sridhar, and K. K. Lindfors, "Viscoelastic imaging of breast tumor microenvironment with ultrasound," *Journal of Mammary Gland Biology and Neoplasia*, vol. 9, no. 4, pp. 393–404, 2004.

[14] A. Itoh, E. Ueno, E. Tohno et al., "Breast disease: clinical application of US elastography for diagnosis," *Radiology*, vol. 239, no. 2, pp. 341–350, 2006.

[15] G. Scaperrotta, C. Ferranti, C. Costa et al., "Role of sonoelastography in non-palpable breast lesions," *European Radiology*, vol. 18, no. 11, pp. 2381–2389, 2008.

[16] B. Fisher, S. Anderson, J. Bryant et al., "Twenty-year follow-up of a randomized trial comparing total mastectomy, lumpectomy, and lumpectomy plus irradiation for the treatment of invasive breast cancer," *The New England Journal of Medicine*, vol. 347, no. 16, pp. 1233–1241, 2002.

[17] U. Veronesi, N. Cascinelli, L. Mariani et al., "Twenty-year follow-up of a randomized study comparing breast-conserving surgery with radical mastectomy for early breast cancer," *The New England Journal of Medicine*, vol. 347, no. 16, pp. 1227–1232, 2002.

[18] N. Houssami and D. F. Hayes, "Review of preoperative Magnetic Resonance Imaging (MRI) in breast cancer: should MRI be performed on all women with newly diagnosed, early stage breast cancer?" *CA Cancer Journal for Clinicians*, vol. 59, no. 5, pp. 290–302, 2009.

[19] F. Sardanelli and F. Podo, "Breast MR imaging in women at high-risk of breast cancer. Is something changing in early breast cancer detection?" *European Radiology*, vol. 17, no. 4, pp. 873–887, 2007.

[20] N. Avril, C. A. Rosé, M. Schelling et al., "Breast imaging with positron emission tomography and fluorine-18 fluorodeoxyglucose: use and limitations," *Journal of Clinical Oncology*, vol. 18, no. 20, pp. 3495–3502, 2000.

[21] K. Schilling, M. S. Narayanan, and J. E. Kalinyak, "Multimodality effect of breast density, menopausal status and hormone use in high resolution Positron Emission Mammography," in *Proceedings of the 94th Annual Meeting of the Radiological Society of North America (RSNA '08)*, November 2008.

[22] W. A. Berg, I. N. Weinberg, D. Narayanan et al., "High-resolution fluorodeoxyglucose positron emission tomography with compression ("positron emission mammography") is highly accurate in depicting primary breast cancer," *The Breast Journal*, vol. 12, no. 4, pp. 309–323, 2006.